

---

# Methods<sup>1</sup>

---

## Expedition 336 Scientists<sup>2</sup>

### Chapter contents

Core recovery and depths . . . . .	1
Lithostratigraphy . . . . .	4
Petrology, alteration, structural geology, and hard rock geochemistry . . . . .	5
Inorganic geochemistry . . . . .	15
Organic geochemistry . . . . .	17
Microbiology . . . . .	17
Physical properties . . . . .	23
Downhole logging . . . . .	30
References . . . . .	34
Figures . . . . .	39
Tables . . . . .	83

### Core recovery and depths

This chapter presents the methods for our shipboard observations. It also enables the interested investigator to identify data and select samples for further analysis. The information presented here concerns only shipboard operations and analyses described in the site chapters. Methods used by various investigators for shore-based analyses of Integrated Ocean Drilling Program (IODP) Expedition 336 data will be described in individual publications in various professional journals and the “**Expedition research results**” chapters of this *Proceedings* volume. This introductory section provides an overview of operations, curatorial conventions, and general core handling and analysis.

### Site locations

At all Expedition 336 sites, GPS coordinates from a precruise site survey ([Schmidt-Schierhorn et al., 2012](#)) were used to position the R/V *JOIDES Resolution* on site. The only seismic system used during the cruise was the Syquest Bathy 2010 CHIRP subbottom profiler, which was monitored on the approach to each site to confirm the seafloor depth agreed with that from the precruise survey. Once the vessel was positioned at a site, the thrusters were lowered and a positioning beacon was dropped to the seafloor. The dynamic positioning control of the vessel uses navigational input from the GPS and triangulation to the seafloor beacon, weighted by the estimated positional accuracy (Fig. [F1](#)). The final hole position was the mean position calculated from the GPS data collected over the time that the hole was occupied.

### Drilling operations

The advanced piston corer (APC), extended core barrel (XCB), and rotary core barrel (RCB) systems were used during Expedition 336. These standard coring systems and their characteristics are summarized in Graber et al. (2002). The APC system cuts soft sediment cores with minimal coring disturbance relative to other IODP coring systems. After the APC core barrel is lowered through the drill pipe and lands near the bit, the drill pipe is pressured up until the two shear pins that hold the inner barrel attached to the outer barrel fail. The inner barrel then advances into the formation and cuts the core. The driller can detect a successful cut, or “full stroke,” from the pressure gauge on the rig floor. The XCB system is deployed when the formation becomes too stiff for the

<sup>1</sup>Expedition 336 Scientists, 2012. Methods. In Edwards, K.J., Bach, W., Klaus, A., and the Expedition 336 Scientists, *Proc. IODP, 336*: Tokyo (Integrated Ocean Drilling Program Management International, Inc.).  
doi:10.2204/iodp.proc.336.102.2012  
<sup>2</sup>[Expedition 336 Scientists' addresses.](#)



APC system or when drilling harder substrate, such as chert.

APC refusal is conventionally defined in two ways: (1) the piston fails to achieve a complete stroke (as determined from the pump pressure reading) because the formation is too hard or (2) excessive force (>60,000 lb; ~267 kN) is required to pull the core barrel out of the formation. When full or partial stroke can be achieved but excessive force cannot retrieve the barrel, the core barrel can be “drilled over,” that is, after the inner core barrel is successfully shot into the formation, the drill bit is advanced to total depth to free the APC barrel. When an APC core barrel achieves only a partial stroke, the lowermost portion of the core could be material that is “sucked” into the core barrel. Only standard steel core barrels were used during Expedition 336 coring operations. Most APC/XCB cored intervals were ~9.5 m long, which is the length of a standard core barrel. Core recovery information is provided in the “Operations” section of each site chapter (Expedition 336 Scientists, 2012a, 2012b, 2012c, 2012d). APC cores were not oriented during Expedition 336 coring. Formation temperature measurements were only attempted in IODP Hole U1382B. Downhole logging was conducted in Ocean Drilling Program (ODP) Hole 395A and IODP Holes U1382A and U1383C.

The XCB system was used to advance the hole when APC refusal occurred at the sediment/basement contact. The XCB is a rotary system with a small cutting shoe extending below the large rotary APC/XCB bit. The smaller bit can cut a semi-indurated core with less torque and fluid circulation than the main bit and thus optimizes recovery. The XCB cutting shoe (bit) extends up to ~30.5 cm ahead of the main bit in soft sediments but retracts into the main bit if hard formations are encountered.

The RCB system was deployed to core basement rocks. The RCB is a conventional rotary drilling system and requires a dedicated RCB bottom-hole assembly and a dedicated RCB drilling bit (outer diameter of 9 $\frac{7}{8}$  inch).

### IODP depth conventions

Deep Sea Drilling Project, ODP, and IODP Phase 1 reports, diagrams, and publications used three primary designations to reference depth: meters below rig floor (mbrf), meters below seafloor (mbsf), and meters composite depth (mcd). These designations are combinations of origin of depth (rig floor or seafloor), measurement units (m), and method of construction (composite). The designations evolved over many years to meet the needs of individual science parties.

Over the course of ODP and IODP scientific drilling, issues with existing depth scale designations and the

lack of a consistent framework became apparent. For example, application of the same designation to scales created with distinctly different tools and methods was common (e.g., mbsf for scales measured by drill string tally and those measured with the wireline). Consequently, new scale-type designations were created ad hoc to differentiate the wireline logging scale from the core depth scale so that depth-mapping procedures and products could be adequately described. Management and use of multiple maps, composite scales, or splices for a hole or a site were problematic, and the requirement to integrate scientific procedures among three IODP implementing organizations amplified the need to establish a standardized and versatile depth framework.

A new classification and nomenclature for depth scale types was defined in 2006–2007 (see IODP Depth Scales Terminology version 2 at [www.iodp.org/program-policies/](http://www.iodp.org/program-policies/)) (Table T1). This framework provided the implementing organizations with a basis to address more specific issues of how to manage depth scales, depth maps, and splices. This new depth framework has been implemented in the context of the Laboratory Information Management System (LIMS) database aboard the *JOIDES Resolution*.

The methods and nomenclature for calculating sample depth in a hole have changed to be method-specific, which will ensure that data acquisition, scale mapping, and composite-scale and splice construction are unequivocal.

The primary scales are measured by the length of drill string (e.g., drilling depth below rig floor [DRF] and drilling depth below seafloor [DSF]), length of core recovered (e.g., core depth below seafloor [CSF] and core composite depth below seafloor [CCSF]), and logging wireline (e.g., wireline log depth below rig floor [WRF] and wireline log depth below seafloor [WSF]). All units are in meters. Relationships between scales are either defined by protocol (such as the rules for computation of CSF from DSF), or they are defined on the basis of user-defined correlations (such as stratigraphic correlation of cores between holes to create a common CCSF scale from the CSF scale of each hole or for core-to-log correlation). The distinction in nomenclature should keep the user aware that a nominal depth value at two different scales usually does not refer to the exact same stratigraphic interval.

Unless otherwise noted, all Expedition 336 core depths have been calculated as CSF Method A (CSF-A), and all downhole wireline depths have been calculated as WSF Method A (WSF-A) (see Table T1). To more easily communicate shipboard results in this volume, all depths are reported as mbsf, except where otherwise noted.

## Core handling and analysis

Core handling and flow were adjusted to best meet the microbiological priorities of the expedition, which are described in more detail in other sections of this chapter and volume. Fluorescent microspheres were deployed in the core catcher for all cores taken during Expedition 336 (except the mudline core). Hard rock cores were immediately split into ~1.5 m long sections and taken to the splitting room, where they were emptied into sterilized split liners. Immediate review by microbiologists and petrologists allowed hard rock microbiology samples to be selected and taken. These samples were photographed and then removed to the microbiology laboratory for processing. The normal hard rock core flow was then resumed, with the exception that the outer surfaces of whole-round core pieces of sufficient length were also digitally scanned. For sediment cores, the core liner was marked on the catwalk to identify core sections and intensive whole-round samples for microbiology and interstitial water samples. Syringe samples were taken for headspace and microbiological analyses. The core sections remaining after whole-round sampling were taken inside, labeled, and moved to the core refrigerator, where oxygen concentration measurements were made with optodes and interstitial water samples were taken using Rhizon samplers.

At the end of the expedition, the cores were transferred from the ship into refrigerated containers and sent to the IODP Bremen Coast Repository in Bremen, Germany.

### Drilling-induced core deformation

Cores may be significantly disturbed and contain extraneous material as a result of the coring and core-handling process. In formations with loose sand layers or rocks, the loose pieces from intervals higher in the hole may be washed down by drilling circulation and accumulate at the bottom of the hole, to be sampled with the next core. The top 10–50 cm of each core must therefore be examined critically for potential “fall-in” during description. Common coring-induced deformation includes concave-downward appearance of originally horizontal bedding. In APC cores, the motion of the piston may result in fluidization (flow-in) at the bottom of the cores. Retrieval from depth to the surface may result in elastic rebound. Gas that is in solution at depth may become free and drive core segments within the liner apart. When gas content is high, pressure must be relieved for safety reasons before the cores are cut into segments. This is accomplished by drilling holes into the liner, which forces some sediment, along with gas, out

of the liner. Holes may also be drilled in the liner to allow water-filled sections of core to drain. Observed core disturbances are described in “[Lithostratigraphy](#)” in the “Sediment and basement contact coring” chapter (Expedition 336 Scientists, 2012a) and graphically indicated on the core summary graphic reports (barrel sheets) (see “[Core descriptions](#)”).

### Curatorial procedures and sample-depth calculations

Site, hole, core, and sample numbering followed standard IODP procedure. A full curatorial identifier for a sample consists of the following information: expedition, site, hole, core number, core type, section number, and interval in centimeters measured from the top of the core section, along with the sampling tools and volumes taken. For example, a sample identification of “336-U1382B-1H-2, 10–12 cm” represents a sample taken from the interval between 10 and 12 cm below the top of Section 2 of Core 1 (“H” designates that this core was taken with the APC system) of Hole B of Site U1382 during Expedition 336 (Fig. [F1](#)). The “U” preceding hole number indicates the hole was drilled by the United States Implementing Organization (USIO) platform, the *JOIDES Resolution*.

Core intervals are defined by the length of drill string, the seafloor depth, and the amount the driller advances the core barrel, reported in DSF. Once a core is recovered on board, the length of core is measured, and this is the “curated” length. The depth of a sample below seafloor (CSF) is calculated by adding the depth of the sample below the section top and the lengths of all higher sections in the core to the core-top depth measured with the drill string (DSF). A soft- to semisoft-sediment core from less than a few hundred meters below seafloor expands upon recovery (typically a few percent to as much as 15%), so the recovered interval does not match the cored interval. In addition, a coring gap typically occurs between cores, as shown by composite depth construction. Thus, a discrepancy can exist between the DSF depth and the CSF depth.

For instance, when a recovered core measures >100% of the cored interval, the CSF depth of a sample taken from the bottom of that core will be deeper than that from a sample from the top of the subsequent core. For this expedition we report all results in the core depth below seafloor method allowing these overlaps (Table [T1](#)), chiefly to avoid confusion during core description and sampling.

If a core has incomplete recovery, all cored material is assumed to originate from the top of the drilled interval as a continuous section for curation purposes. The

true depth interval in the cored interval is not known and should be considered a sampling uncertainty in age-depth analysis and correlation of core data with downhole logging data.

## Lithostratigraphy

Sediment cores recovered during Expedition 336 were split into archive and working halves. The cores were oriented (top and bottom) and referenced, and the archive halves underwent several stages of analyses and measurements, including density, susceptibility, and velocity measurements and natural gamma radiation (NGR) measurements. The archive halves were also imaged, run through the Section Half Multisensor Logger (SHMSL), and measured for physical properties (wet mass and dry mass), velocity, and thermal conductivity. The archive halves were then described.

Lithostratigraphy was determined with the help of some of the analytical and descriptive techniques listed above; for sedimentologic observation, visual (macroscopic) core description and thin section and smear slide description were also used. These procedures are outlined below.

### Visual (macroscopic) core description

Descriptive data were entered using the DESClogik program (see DESClogik user guide in Technical Documentation [[iodp.tamu.edu/tasapps/](http://iodp.tamu.edu/tasapps/)]) and uploaded to the LIMS database. Spreadsheet templates were customized for Expedition 336 in DESClogik prior to the arrival of the first core. The spreadsheet templates were used to record macroscopic core descriptions, as well as smear slide and thin section data, which allowed quantification of the texture and relative abundance of biogenic and nonbiogenic components. The locations of all smear slide and thin section samples taken from each core were uploaded in the IODP-USIO Sample Master program. The descriptive data were used to produce visual core description (VCD) graphic reports. Symbols used in sedimentary VCDs are shown in Figure F2.

Sediment colors were determined qualitatively using the Munsell soil color charts (Munsell Color Company, Inc., 2000).

Sediment components and percentages in the core were determined using a hand lens, binocular microscope, smear slide examination, or thin section.

### Core imaging

Core section imaging included both whole- and half-core scanning on the Section Half Imaging Logger

(SHIL) (see SHIL quick start guide in Technical Documentation [[iodp.tamu.edu/tasapps/](http://iodp.tamu.edu/tasapps/)]). The SHIL incorporates a line-scan camera that uses three pairs of advanced-illumination high-current focused light emitting diode (LED) line lights to illuminate large cracks and blocks in the core surface and sidewalls. Each LED pair has a color temperature of 6500 K and emits 90,000 lx at 3 inches. The line-scan camera imaged 10 lines/mm to create a high-resolution TIFF file (see “Raw TIF image” in the LIMS database). The camera height was adjusted so that each pixel imaged a 0.1 mm<sup>2</sup> section of the core. However, actual core width per pixel varied because of differences in section-half surface height. High- and low-resolution JPG files were subsequently created from the high-resolution TIFF file (an uncropped and lightened JPG [see “Uncropped image” in the LIMS database], and a cropped and lightened JPG [see “Cropped image” in the LIMS database]). The system generates a ruler according to curated lengths of the cropped version.

Whole-core sections were wetted before being scanned to improve image quality. Half-core sections (flat face of split cores) were imaged as soon as possible after splitting to minimize color changes that occur through oxidation. These half-core sections were scanned dry to preserve the quality and accuracy of the pictures. Before scanning soft-sediment half-core sections, the split surfaces of the archive halves were scraped lightly with a glass slide to create an even surface. All images were uploaded to the LIMS database.

### Smear slides

Smear slides were prepared using standard preparation techniques, as outlined in Myrbo (2007) and Bown (1998). Samples were treated with kerosene to disaggregate the grains, as outlined in Riedel and Sanfilippo (1977).

A sample was broken into small pieces, dried thoroughly in an oven or on a hot plate at ~80°–100°C, and then covered with kerosene while still warm. When the sediment was saturated (usually within a few minutes), the excess liquid was decanted and the sample was immediately covered with water. The sample was then allowed to stand with occasional stirring until it was judged that no further disaggregation would occur, ~5–30 min.

### Thin sections

Thin sections were created on board when representative lithified sediments were encountered. Thin sections generally provide less biased samples of whole rock than do smear slides, and they allow for more accurate identification of the minerals present.

## Sediment and hard rock classification

Sediment names indicate the degree of sediment induration (e.g., sand versus sandstone, silt versus siltstone, mud versus mudstone, ooze versus chalk, or limestone). One or two modifiers precede the principal name.

### Sediment lithology

Sediments that contain more than ~70% calcareous components, the majority of which are secreted by pelagic organisms (planktonic foraminifers and calcareous nannofossils), are called ooze if they are soft, chalk if they are firm, and limestone if they are hard. The term “ooze” is used to describe <2 mm calcareous unlithified sediments containing >90% carbonate.

When clasts of hard rock were encountered within unlithified lithologies, grain size was described using the classification of Wentworth (1922). Sand clast sizes include very fine sand (63–125  $\mu\text{m}$ ), fine sand (125–250  $\mu\text{m}$ ), medium sand (250–500  $\mu\text{m}$ ), coarse sand (500  $\mu\text{m}$  to 1 mm), and very coarse sand (1–2 mm). Granules are between 2 and 4 mm, pebbles are between 4 and 64 mm, and cobbles are between 64 and 256 mm. The degree of rounding of the clasts or grains and the degree of sorting were also determined. In unlithified lithologies, when sediment contains hard rock clasts of pebble size (4–64 mm) in a matrix of ooze, it is named “muddy gravel.”

### Indurated lithologies

The classification of Dunham (1962) was used for limestones, typically when thin sections were described. When mud (micrite) is absent and the texture is grain supported, the limestone is called “grainstone”; when carbonate mud is present and the texture is grain supported, the limestone is named “packstone”; when carbonate mud is present and the texture is mud supported, with at least 10% grains, the limestone is “wackestone,” and with <10% grains the limestone is named “mudstone.”

### Modifiers and suffixes

Modifiers added to the principal term “ooze” consist of the names of the major fossil types and may include a suffix such as “-bearing” or “-rich.” The fossil type that is least abundant is named first. For example, “foraminifer-bearing nannofossil-rich ooze” describes an ooze made of a majority of nannofossil tests with foraminifer tests; “nannofossil-rich ooze” means that nannofossils represent the dominant part of the ooze. Biogenic components are not described in textural terms.

## Petrology, alteration, structural geology, and hard rock geochemistry

### Igneous petrology

Rock description procedures during Expedition 336 generally followed those used during previous IODP expeditions (e.g., Expeditions 335, 309/312, and 304/305). The flow of core description during Expedition 336 was done as follows. First, lithologic units and subunits were defined by either visual identification of actual lithologic contacts (e.g., chilled margins) or by inference of the position of such contacts using observed changes in composition (e.g., phenocryst assemblages or volcanic and/or volcanoclastic features). Unit definition was followed by an initial description of the lithologic characteristics, igneous textures, minerals, and vesicle distributions on a piece-by-piece basis. Macroscopic observations were ultimately combined with those from detailed thin section petrographic studies of the key igneous units. Data from X-ray diffraction (XRD) analysis (see “[X-ray diffraction](#)” in “Alteration and metamorphism”) and bulk-rock chemical analyses (see “[Hard rock geochemistry](#)”) were also used to confirm constituent minerals and to interpret igneous units. Data for the macroscopic and microscopic descriptions of recovered cores were entered into the LIMS database using the DESClogik program (see DESClogik user guide in Technical Documentation [[iodp.tamu.edu/tasapps/](http://iodp.tamu.edu/tasapps/)]).

### Igneous units and contact logs

Unit boundaries were identified on the basis of the presence of contacts, chilled margins, changes in primary mineralogy, color, grain size, and structural or textural variations. Lithologically and texturally similar pieces from consecutive core sections were logged as belonging to the same unit. In order to preserve important information about igneous stratigraphy without defining an unreasonable number of units in a single core, subunits were designated when there were noticeable changes in texture, color, and grain size without accompanying changes in mineralogy. Where contacts deviated from horizontal within the core reference frame, their depths were logged at their midpoints. Igneous unit and contact logs provide information about unit boundaries and a brief description of each unit. For each unit, the table lists unit number, core number, depth interval (in meters below seafloor), a description of the upper and lower boundaries, and a unit description. In addition, VCD reports (including an alteration summary) were

produced for each core section. Symbols used in hard rock VCDs are shown in Figure F3.

## Macroscopic core description

### Lithology

Volcanic rocks were classified according to the following two definitions:

- Basalt: all igneous rocks of basaltic composition having a groundmass with a modal grain size from glassy to fine grained.
- Dolerite: holocrystalline fine- to medium-grained rocks of basaltic composition with well-developed subophitic or ophitic textures.

Basalts were further divided according phenocryst content, using the following conventions:

Aphyric = <1% phenocrysts.

Sparsely phyric = 1%–5% phenocrysts.

Moderately phyric = >5%–10% phenocrysts.

Highly phyric = >10% phenocrysts.

For phyric basalts, phenocryst phases were included as hyphenated modifiers preceding the rock name. If phenocryst abundances are <1%, however, the modifier “aphyric” precedes the rock name.

Mafic and ultramafic plutonic rocks were classified on the basis of abundance, grain size, and texture of their primary minerals (as inferred prior to alteration) using the International Union of Geological Sciences (IUGS) system (Fig. F4) (Streckeisen, 1974; Le Maitre, 1989; Le Maitre et al., 2002). This classification defines the following mafic and ultramafic rock lithologies:

- Troctolite: olivine + plagioclase > 95%, olivine > 10%, and plagioclase > 10%.
- Olivine gabbro: olivine + plagioclase + clinopyroxene, none of which are <5%.
- Gabbro or diorite: plagioclase + clinopyroxene > 95%, plagioclase > 10%, clinopyroxene > 10%, and quartz < 5%.
- Gabbronorite: plagioclase + clinopyroxene + orthopyroxene, none of which are <5%.
- Quartz diorite: quartz + alkali feldspar + plagioclase (QAP), where quartz is 5%–20% and alkali feldspar is <10%.
- Tonalite: QAP, where quartz is 20%–60% and alkali feldspar is <10%.
- Trondhjemite: tonalite with total mafic mineral content < 10%.
- Dunite: olivine > 90%.
- Harzburgite: olivine > 40% and clinopyroxene < 10%.

- Lherzolite: olivine > 40%, orthopyroxene > 10%, and clinopyroxene > 10%.
- Wehrlite: olivine > 40% and orthopyroxene < 10%.
- Olivine orthopyroxenite: olivine = 10%–40% and clinopyroxene < 10%.
- Olivine websterite: olivine = 10%–40%, orthopyroxene > 10%, and clinopyroxene > 10%.
- Olivine clinopyroxenite: olivine = 10%–40% and orthopyroxene < 10%.
- Orthopyroxenite: orthopyroxene > 90%.
- Websterite: olivine < 10%, orthopyroxene > 10%, and clinopyroxene > 10%.
- Clinopyroxenite: clinopyroxene > 90%.

In the IUGS classification, diorite is distinguished from gabbro by the anorthite content of plagioclase, with diorites having <50 mol% An. Because anorthite content cannot be observed during macroscopic description, we used the convention followed during Expedition 335: if a gabbroic rock contained quartz (<5%) or primary amphibole, indicating a high degree of fractionation, the rock was classified as diorite. If no quartz or primary amphibole was observed, the rock was classified as gabbro.

Minor modifications to the IUGS system were made as follows so that rock types could be more accurately subdivided on the basis of significant differences rather than arbitrary cutoffs based on the abundance of a single mineral.

For gabbroic rocks, the following modifiers based on modal mineralogy were used:

- Disseminated oxide: Fe-Ti oxide = 1%–2%.
- Oxide: Fe-Ti oxide > 2%.
- Olivine-bearing: olivine = 1%–5%.
- Orthopyroxene-bearing: orthopyroxene = 1%–5%.
- Troctolitic: clinopyroxene = 5%–15% and olivine > 20%.
- Olivine-rich: olivine > 70%.
- Anorthositic: plagioclase > 80%.

Additional descriptive modifiers are defined as follows:

- Leucocratic: light colored with high proportions of plagioclase.
- Micro: dominant grain size < 1 mm.
- Doleritic: fine- or medium-grained gabbroic rocks with dominant ophitic or subophitic textures.

Where alteration in ultramafic rocks is so extensive that estimation of the primary mineral assemblages is impossible, the rock is called “serpentinite.” If primary assemblages can be inferred from pseudomorphs and

textures in ultramafic rocks, even though they are partially or completely replaced, the rock name is based on the reconstructed primary assemblage, preceded by the modifier “serpentinized” (e.g., serpentinized dunite).

### Mineralogy

Volcanic rocks were described according to groundmass, phenocrysts (if any), and vesicles. Phenocryst abundance (in percent), shape, and maximum, minimum, and median grain size (in millimeters) were recorded for each phase. Vesicle abundance (in percent); vesicularity; size distribution; minimum, maximum, and modal size (in millimeters); roundness (rounded, subrounded, or well rounded); and sphericity (highly spherical, moderately spherical, slightly spherical, or elongate) were also recorded. Fill (in percent) and fill composition were documented in the alteration log, together with another estimation of vesicle abundance, either on a piece-by-piece basis or for a set of pieces having similar alteration characteristics. The following data for each primary silicate were recorded in the LIMS database using the DESClogik program:

- Visually estimated modal percent. Note that this estimation represents the modal mineralogy as observed in fresh rocks, whereas in altered rocks it represents the estimated igneous modes prior to alteration. Where a mineral occurs in trace quantities (i.e., it is too scarce to assign a meaningful percentage), 0.1% was recorded. Accessory phases were also noted where observed.
- Minimum, average, and maximum grain size for each mineral phase.
- Mineral shape (euhedral, subhedral, or anhedral).
- Mineral habit, defined as
  - Equant = aspect ratio < 1:2,
  - Subequant = aspect ratio 1:2 to 1:3,
  - Tabular = aspect ratio 1:3 to 1:5,
  - Elongate = aspect ratio > 1:5, or
  - Interstitial, poikilitic, vermicular, skeletal, acicular, aggregates, columnar, fibrous aggregates, granular, isometric, lath-shaped, lath, oikocryst, prismatic, radial aggregates, subparallel aggregates, or vericular.

### Contacts

Contacts between units were described according to contact type, definition, morphology, geometry, and interpretation. Where the contact was not recovered, this was noted as “contact not recovered.”

Contact types are defined as follows:

- Grain-size contact: units on either side have markedly different grain sizes.

- Modal contact: units on either side have markedly different mineral proportions.
- Color contact: units on either side have markedly different primary (i.e., not alteration related) color.
- Magmatic vein: thin, discontinuous intrusions of igneous material are present.
- Chilled margins: sharp gradients in grain size occur near igneous contacts.
- Dike: greater than centimeter-scale tabular intrusions of igneous material occur.

Where contacts are obscured by deformation and metamorphism, the following classification is applied:

- Sheared contact: interval with deformation fabric is in contact with an undeformed interval.
- Foliated contact: both intervals have deformation fabrics.
- Tectonic contact: contact appears to be the result of faulting.

Contacts having magmatic, crystal-plastic, or brittle deformation structures are further reported in the structure log.

### Texture

The textures of volcanic rocks are defined on the basis of groundmass modal grain size, grain-size distribution, and the relationships between different grains.

Grain size was defined as follows:

- Glassy.
- Cryptocrystalline = <0.1 mm.
- Microcrystalline = 0.1–0.2 mm.
- Fine grained = 0.2–1 mm.
- Medium grained = 1–5 mm.
- Coarse grained = 5–30 mm.
- Pegmatitic = >30 mm.

Volcanic rock grain-size distribution (applied to phenocrysts only) was described using the following terms:

- Unimodal: all phenocrysts are of similar size.
- Bimodal: phenocrysts define two size populations.
- Seriate: phenocrysts form a continuous range of sizes.

To describe the textural relationships between different silicate grains, the following terms were used:

- Ophitic: total inclusion of plagioclase in clinopyroxene.
- Subophitic: partial inclusion of plagioclase in clinopyroxene.

- Intergranular: coarser touching grains form a framework of the rock with interstices filled by crystalline material.
- Intersertal: coarser touching grains form a framework of the rock with interstices filled by glass.
- Hyalophitic: predominantly glassy groundmass with little interstitial texture.

Textures of plutonic rocks were also defined according to grain size, grain-size distribution, and the relationships between different grains. Grain sizes were defined using the same terms as those for volcanic rocks. Grain-size distributions for plutonic rocks are classified as follows:

- Equigranular: all minerals are of similar size.
- Inequigranular: grain size varies significantly. Inequigranular textures are further divided using following terms:
  - Seriate: a continuous range of crystal sizes is present.
  - Varitextured: domains with contrasting grain size occur.
  - Poikilitic: relatively large oikocrysts enclose smaller crystals, termed “chadacrysts,” of one or more other minerals.

The following terms were used for plutonic rocks to describe the textural relationships between different silicate grains: intergranular, intersertal, subophitic, ophitic, granular (i.e., aggregation of grains of approximately equal size), dendritic (branching arrangement of elongate crystal), and comb structure (a comblike arrangement of crystals growing inward from a contact).

The textures of oxide and sulfide minerals were also described in terms of grain size and their relationship to adjacent minerals. In plutonic rocks, oxides commonly occur as aggregates, and for grain size determination an aggregate is counted as a single grain.

### Thin section description

Thin section observations were performed to confirm macroscopic observations and to add microscopic characteristics of core samples. Thin section description closely followed the procedure for macroscopic core description. The following data were recorded and entered into the LIMS database using separate tabs in the thin section workbook in DESClogik.

#### *Lithology and texture*

- Rock name (based on thin section observation), using the same definitions as those used for macroscopic descriptions.

- Grain size modal name (glassy, cryptocrystalline, microcrystalline, fine grained, medium grained, coarse grained, or pegmatitic).
- Grain-size distribution (equigranular, seriate, vari-textured, or poikilitic).
- Texture (granular, subophitic, ophitic, granophyric, porphyritic, intergranular, intersertal, variolitic, or granoblastic).

#### *Mineralogy*

- Present abundance (in percent) of primary minerals preserved.
- Estimated abundance (in percent) of primary minerals prior to alteration.
- Estimated value of mineral replacement by alteration.
- Individual comments for primary minerals.

For primary mineral grains, the following data were recorded using the same conventions as those used during macroscopic description:

- Minimum, maximum, and median size.
- Mineral shape and habit.
- Special features of primary minerals.

### Alteration and metamorphism

The characteristics of alteration and metamorphism of volcanic and plutonic rocks recovered during Expedition 336 were determined using visual inspection of the core, microscopic thin section descriptions, and XRD analyses.

Visual observations of the core were recorded in the (1) alteration log (plutonic-mantle rocks and volcanic rocks), (2) vein/halo log, and (3) breccia log. Shipboard observations of alteration and metamorphism were recorded using the DESClogik worksheet interface and uploaded to the LIMS database. Where basalt and gabbro and/or serpentinite were found in the same section, the appropriate alteration log sheet was used for intervals of each rock type. Alteration and metamorphism of rocks were described in terms of general intensity of background (groundmass and phenocrysts) alteration. The presence of localized alteration patches (zones of more intense alteration), also referred to as alteration halos when lining open cracks or veins, was also recorded. Vein and vesicle filling and breccia clasts and matrix filling were also reported together with the abundance of secondary minerals. Description of alteration of the archive half of the core also provides information on secondary mineral replacement of primary igneous features including phenocrysts and groundmass. Information on the extent of replacement of igneous minerals and groundmass by secondary minerals and, where possible, the nature and approximate modes of sec-

ondary mineral assemblages was recorded using DESClogik. The presence, description, and mineralogy of veins or vesicle infill were also recorded. Each logged interval may represent multiple pieces, core sections, or local alteration features within a piece.

The vein/halo log contains all data (e.g., shape, texture, orientation, etc.) related to vein features. The breccia log also contains data on breccia type (e.g., magmatic, hydrothermal, tectonic, and sedimentary), clast features (e.g., abundance, shape, lithology, and alteration), matrix, and cement properties. If the breccia clasts have any magmatic, crystal-plastic, or brittle structures, these features are described on the structure log (see below). Magmatic, crystal-plastic, and brittle deformation structures were also logged in the structure log.

### Macroscopic core description

All volcanic, mafic, and ultramafic rocks recovered during Expedition 336 are described as follows.

#### Unit and subunit alteration summary

Alteration intensity plotted on the VCD reports corresponds to the background/groundmass alteration intensity. On the lithologic unit logs (volcanic and plutonic/mantle rocks), rocks were graded according to alteration intensity as follows based on volume of alteration products:

- Fresh = <1%.
- Rare = 1%–3%.
- Slight = >3%–10%.
- Moderate = >10%–30%.
- Abundant = >30%–50%.
- High = >50%–90%.
- Complete = >90%–100%.

Alteration textures were described using the following terms in order to document variations and heterogeneities in alteration style and intensity:

- Pervasive: uniform alteration style and intensity throughout the rock.
- Patchy: pervasive background alteration with local alteration patches.
- Pseudomorph: complete replacement of primary mineral with characteristic shape.
- Corona: primary mineral crystal surrounded by an alteration rim.
- Recrystallized: pervasive background alteration, where the rocks are recrystallized to granoblastic contact metamorphic assemblages.
- Clasts: breccia clasts enclosed in a matrix of secondary minerals.

- Clasts with halos: breccia clasts that contain alteration halos and are enclosed in a matrix of secondary minerals.

The following information is displayed on the VCD forms:

- Vein summary: approximate frequency (rare = 0–5 veins/m, several = >5–15 veins/m, common = >15–30 veins/m, and very common = >30 veins/m) and average vein thickness, along with minerals in order of abundance.
- Vesicle summary: abundance and major minerals filling vesicles, together with general comments.
- Alteration summary: groundmass and phenocrysts (also recorded in lithology logs).

#### Volcanic rock alteration

The volcanic rock alteration log was used to record bulk volcanic rock alteration, either piece by piece or for a given group of pieces. Each entry records identifiers for core, section, piece(s), and interval (in centimeters); length of each piece or group of pieces; depth below seafloor (in meters) at the top of the piece or group of pieces; and igneous unit. Information on alteration type (as represented by rock color and secondary mineral abundances) for groundmass, alteration patches, halos, and phenocrysts is provided. A column for comments is also included.

The following features were observed and recorded for groundmass alteration, as well as for any patchy textural intervals, large alteration halos, and phenocrysts:

- Color.
- Percentage of rock altered to secondary phases.
- Percentage of each primary mineral replaced.
- Secondary minerals replacing primary minerals.

#### Plutonic and mantle rock alteration

The plutonic and mantle rock alteration log was used to record bulk rock alteration of gabbro and other coarse-grained holocrystalline rocks and ultramafic rocks. Total modal percentage of secondary minerals was estimated in hand specimen, as were proportions of major primary igneous minerals (olivine, clinopyroxene, plagioclase, orthopyroxene, and oxides) and the secondary minerals by which they were replaced. A column for comments is included. The following data were recorded for patchy textural intervals: pervasive background alteration information for the rock hosting the patches (as above), size (<1 cm, 1–3 cm, or >3 cm), shape (round, irregular, elongate, or network), area percentage of patch in the rock or interval, total percentage of alteration (secondary phases) in the patches, and primary

mineral alteration and secondary phases present (as in background alteration).

### **Veins and halos**

Description of veins and alteration halos is recorded in the vein/halo log using the DESClogik worksheet interface. Vein and halo descriptions were reported on a piece-by-piece and vein-by-vein scale. All tabulated information was recorded from the archive halves. Alteration halos, either associated to observed veins or along-piece edges, were tabulated to provide a consistent characterization of the extent of alteration halos of the rocks (with respect to fresher basalt) and to quantify the different alteration types. Approximate abundance of secondary minerals in veins was reported, mostly on the basis of color, hardness, HCl reactivity, and crystal habit/morphology. Where additional mineralogical evidence is available from either thin section descriptions or X-ray diffractograms, these identifications are integrated into the summary alteration and the VCDs. Alteration halos representing zones of increased alteration adjacent to veins were described by width, color, and secondary mineral percentages in the halo comments column of the vein/halo log. Vein nets grading into breccia were reported in the breccia log.

For each vein and halo, we recorded the following information in the vein/halo log (e.g., Fig. F5):

- Top and bottom (in centimeters) of the feature and vein width (in millimeters) to estimate the apparent vein area on the cut surface.
- Piece or subpiece number and length (in centimeters) to estimate piece surface area.
- Boundary (diffuse or sharp).
- Vein boundary definition (sharp, diffuse, gradational, sutured, or sharp to gradational).
- Shape (straight, sigmoidal, irregular, pull-apart, or fault vein).
- Attitude (horizontal, subhorizontal, vertical, subvertical, inclined, steeply dipping, nonoriented, planar, planar-linear, linear, or curved).
- Connectivity (anastomosing, isolated, non-branched or single, branched, crosscut, T-shaped, Y-shaped, splayed, wispy, or network).
- Texture (massive, cross-fiber, slip-fiber, vuggy, or polycrystalline).
- Structure (simple, composite, banded, haloed, or intravenous).
- Geometry (en echelon, ribbon, or cross fractures).
- Vein color and filling (smectite, carbonate, Fe oxyhydroxide, zeolite, etc.).
- Presence and color of a related alteration halo and width (in millimeters) of the halo on one side of the vein.
- Alteration halo properties (diffuse or multilayered) and percent of alteration of the background/groundmass and texture.
- Orientation (dip angle and dip direction) of fracture and trend and plunge of associated lineation and slickenlines (with respect to measurement of orientation; see “**Structural measurements**”).
- Comments about veins and halos.

Note that if a vein had any remarkable magmatic, crystal-plastic, or brittle structure (e.g., shear vein, fault, or microfault), we also described these structural features (e.g., sense of shear, etc.) on the structure log and added a comment to the vein/halo log.

### **Breccia**

The descriptions of brecciated units were recorded in the breccia log using the DESClogik worksheet interface. Breccia descriptions were reported on a piece-by-piece scale noting the following:

- Depth interval and piece number.
- Type:
  - Hydrothermal: containing secondary matrix or vein minerals.
  - Magmatic: containing glass or quench textures such as hyaloclastite and pillow breccia and primary matrix minerals.
  - Tectonic: cataclasite and fault-gouge in which the matrix consists of the same material as the host rock.
  - Sedimentary: matrix filling composed entirely of sedimentary materials (clays and carbonate).
- Clasts: abundance (in percent), size (minimum, maximum, and average), shape, composition (monomictic or polymictic), color, internal structures (veining, shearing, crushing, or fracturing), lithology, and alteration (fresh, altered, or devitrification).
- Matrix and cement: abundance, color, grain size, percentage of secondary minerals, and composition.

When the breccia had any orientation, dip angle, or dip direction that could be described with respect to measurement of orientation, we also recorded the structural features on the structure log.

### **Thin section description**

Thin sections of volcanic, mafic, and ultramafic plutonic rocks recovered during Expedition 336 were examined in order to

- Confirm macroscopic identifications of secondary minerals;

- Determine their mode of occurrence in terms of vesicle and void fillings, vein composition, and primary mineral replacement;
- Identify chronological relationships between different secondary minerals;
- Establish distribution, occurrence, and abundance of secondary minerals downhole; and
- Quantify the amount of alteration, especially cryptocrystalline rocks.

Modal estimates of the secondary minerals allowed characterization of alteration intensity. A total alteration percentage was calculated using modal composition of phenocrysts and groundmass minerals and their respective percentage of alteration.

Thin section descriptions were recorded using DESClogik and subsequently uploaded to the LIMS database. A summary description of secondary mineral assemblages and replacement relations to primary phases, as well as mineralogy of veins and vesicles, was entered in DESClogik so it could be added to the thin section report. Digital photomicrographs were taken during the expedition to document features described in thin sections.

### X-ray diffraction

Phase identification of whole rocks, patches, or vein material was aided by XRD analyses using a Bruker D-4 Endeavor diffractometer with a Vantec-1 detector using nickel-filtered  $\text{CuK}\alpha$  radiation. XRD was performed on small amounts of powder (usually ~20 mg) as smear slides or pressed onto sample holders. Instrument conditions were as follows:

- Voltage = 40 kV.
- Current = 40 mA.
- Goniometer scan (bulk samples) =  $4^\circ\text{--}70^\circ 2\theta$ .
- Step size =  $0.0087^\circ$ .
- Scan speed = 0.2 s/step.
- Divergence slit =  $0.3^\circ$ , 0.6 mm.

### Structural geology

The conventions for the techniques used for macroscopic and microscopic description of structural features observed in igneous rocks used during Expedition 336 generally followed those used during Expeditions 304/305, 309/312, and 335. Definitions of structural measurements and descriptive parameters, as well as their corresponding description dictionaries, were further refined as part of the process of configuring the DESClogik core description software for hard rock descriptions.

### Structural measurements

Depth intervals of structures were recorded as the distance from the top of the section to the top and bottom of the structural feature. Depth to the midpoint of structures was recorded for structures with measurable width, such as veins or intervals with magmatic foliation (Fig. F6). Where they occur, crosscutting relationships were described with core section depth. Apparent fault displacements of planar markers were recorded as they appeared on the cut face of the archive half of the core. Displacements observed on the vertical core cut face were treated as dip-slip components of movement and labeled in spreadsheets as either normal or reverse for faults inclined  $<90^\circ$ ; their displacement in millimeters was also recorded. Shear sense indicators were also marked on the spreadsheets. Slickenside or slickenside orientation trends and plunge measurements or the trend and plunge direction of the slip line between offset linear markers were incorporated wherever possible to determine dip-slip, oblique-slip, or strike-slip components.

We measured structures on the archive half relative to the standard IODP core reference frame (Fig. F7). The plane normal to the axis of the borehole is referred to as the apparent horizontal plane. On this plane, a  $360^\circ$  net is used, with pseudo-south ( $180^\circ$ ) at the bottom line of the working half and pseudo-north ( $000^\circ$ ) pointing out of the archive half (Fig. F7B). The cut surface of the split core, therefore, is a vertical plane striking  $090^\circ\text{--}270^\circ$  and dips vertically. Apparent dip angles of planar features were measured on the cut face of the archive half of the core using a protractor, and its sense was indicated, whether toward  $090^\circ$  or  $270^\circ$  (Fig. F7C). A second apparent dip reading was obtained where possible in the  $000^\circ\text{--}180^\circ$  plane section perpendicular to the core face (second apparent orientation) in order to find a true dip value. The two apparent dips and dip directions (or one apparent direction combined with the strike) measured for each planar feature were used to calculate the dip angle and dip direction. Mineral foliations and planar igneous contacts were measured in exactly the same way.

### Macroscopic core description and terminology

The structural geologists oriented the whole cores and marked lines along which the core pieces were cut in half. Cores were marked to maximize dip on planar structures so that the dominant structure dips toward  $270^\circ$  in the core reference frame (i.e., toward the right when looking down at the cut surface of the archive half of the core). Where no obvious structures were present, cores were marked to maximize contiguity with adjacent core pieces.

All material from both the working and archive halves was examined. Sketches of structures and orientation measurements were made from the archive half, but observations on working-half pieces were also made for certain features that were better exposed there than in the archive half. For each section, detailed structural information was entered into the petrology worksheets in DESClogik, as described above. The worksheets contain data on location, types of structures, structural intensity, and orientation. The structural data were separated in two categories:

1. Brittle structures: breccia, faults, joints, drilling-induced fractures, serpentine foliation, cataclastic fabric intensity, and veins.
2. Magmatic and crystal-plastic structures: magmatic foliation, magmatic layering (including compositional and grain-size layering), igneous contacts, crystal-plastic foliation, and sense of shear.

Veins, defined here as fractures filled with secondary minerals, were described in the vein/halo log in the petrology worksheets, along with vein orientations. Breccia was described in the breccia log in the petrology worksheets, along with orientation and type of breccia (magmatic, hydrothermal, tectonic, or sedimentary) (see “[Alteration and metamorphism](#)”).

The most representative or prominent structural features in the cores recovered during Expedition 336 are plotted on the VCD reports. These features include intensity of magmatic and crystal-plastic fabric alignment, density of brittle fractures, and precise locations of observed prominent structures such as igneous contacts, magmatic layering and magmatic veins, vein net and breccia, cataclastic zones, shear veins, faults, joints and fractures (except for horizontal irregular fractures; see “[Brittle deformation](#)”), and folds, where recognizable.

Short explanations of the terms and abbreviations used in the above categories are given below. We followed the terminology of Ramsay and Huber (1987), Twiss and Moores (1992), Davis (1984), and Passchier and Trouw (1996).

### **Brittle deformation**

Brittle deformation features included faults, defined as fractures with shear displacement, and joints, defined as fractures with no shear displacement. We used “fracture” as a general term indicating brittle failure with or without displacement. The term “microfault” was also used to describe faults with <1 mm width of related deformation or faults with displacement measurable at the core scale. “Shear veins,” defined here as fractures with secondary mineralization and shear-sense indicators (such as slickenlines and

fibrose mineral growth), were logged independently in the vein/halo log, along with orientation of slickenlines and sense of shear, where measurable (see “[Alteration and metamorphism](#)”). The orientations of open joints/fractures that occur along the broken surface of veins were recorded in the structure log in the petrology worksheets rather than in the vein/halo log. We also described the intensity of serpentine foliation and commented on the serpentine structural features in the structure log. Descriptions of brittle deformation include the following:

- Semibrittle vs. brittle: any feature involving both brittle and crystal-plastic deformation (i.e., melt-filled fractures).
- Type of fault rock: fault gouge, cataclasite, or pseudotachylite. Microfaults were also identified here. The type of fault rock may be accompanied by identifiers describing fabric alignment such as foliation and lineation.
- Clast/matrix ratio (in percent).
- Sense of shear: normal (n), reverse (r), dextral (d), sinistral (s), or a combination of nd, ns, rd, and rs.
- Fault offset (in millimeters), where measurable.
- Trend and plunge of slickensides, slickenlines, and slickenfibers.
- Intensity of cataclastic deformation and intensity rank (Fig. F6):
  - 0 = undeformed.
  - 1 = minor fracturing with no significant grain-size reduction (GSR).
  - 2 = moderate fracturing without GSR.
  - 3 = dense aastomosing fracturing with incipient GSR.
  - 4 = well-developed GSR with evidence for clast rotation (independent particulate flow).
  - 5 = cataclastic.
- Intensity of serpentine foliation and intensity rank (Fig. F6):
  - 0 = massive.
  - 1 = weakly foliated.
  - 2 = moderately foliated.
  - 3 = strongly foliated.
- Density of subhorizontal irregular fractures, identified as irregular or concave, horizontal to subhorizontal (<20°) fractures without secondary mineralization, occurring at piece ends or confined in a piece and perhaps related to drilling-induced fracturing or preexisting anisotropy of the rocks:
  - 0 = no fractures.
  - 1 = <1 fracture/10 cm.
  - 2 = 15 fractures/10 cm.
  - 3 = >5 fractures/10 cm, or rubble.

- Density of joints/fractures other than subhorizontal irregular fractures (Fig. F6):
  - 0 = no open fractures.
  - 1 = <1 fracture/10 cm.
  - 2 = 1–5 fractures/10 cm.
  - 3 = >5 fractures/10 cm.
- Fracture morphology: planar, curved, concave, irregular, stepped, splayed, anastomosing, or Riedel array (Fig. F5).
- Fracture thickness (in millimeters). By definition, a closed fracture/joint has 0 mm thickness.
- Comments: serpentine structural features, cross-cutting relationships, and morphology of fracture termination.
- Orientation (dip angle and dip direction) of fracture and trend and plunge of associated lineation.

### ***Magmatic and crystal-plastic structures***

Magmatic fabrics were defined macroscopically by magmatic layering, including compositional and grain-size layering, and shape-preferred orientation (SPO) of primary minerals where there is no evidence of crystal-plastic deformation. Descriptions of magmatic fabric include the following:

- Symmetry of magmatic fabric: linear (L), planar (S), planar-linear (L-S), or not detectable.
- Layering: grain size or compositional.
- Names of consistent layering minerals.
- Magmatic foliation, accompanied by intensity rank (Fig. F6).
- Sense of shear: normal (n), reverse (r), dextral (d), sinistral (s), or a combination of nd, ns, rd, and rs.
- Comments: name and general shape of fabric elements, together with crosscutting relationship, shape, boundary features (i.e., planar, curved, or irregular), and anything else of interest.
- SPO of mineral phases or groups of mineral phases, along with modal percent of measured mineral phases, shape ratio, and orientation of SPO long axis. Specimens were ranked according to SPO ratio:
  - 0 = macroscopically isotropic (<1.05 SPO ratio).
  - 1 = weak (1.05 to <1.2 SPO ratio).
  - 2 = moderate (1.2 to <2.0 SPO ratio).
  - 3 = strong ( $\geq 2.0$  SPO ratio).
- Orientation of magmatic fabrics: dip angle and dip direction of planar fabric and trend and plunge of lineation, where measurable.

Crystal-plastic fabrics are lineations or foliations defined by grains exhibiting plastic strain. The textural criterion used for gabbroic rocks, on which this was

based, was modified slightly for peridotites. Descriptions for crystal-plastic fabric include the following:

- Symmetry: linear (L), planar (S), planar-linear (L-S), or not detectable.
- Intensity, accompanied by intensity rank (Fig. F6):
  - 0 = undeformed.
  - 1 = weakly foliated/lineated.
  - 2 = strongly foliated/lineated.
  - 3 = porphyroclastic/protomylonitic.
  - 4 = mylonitic.
  - 5 = ultramylonitic.
- Boundary geometry (i.e., shear zone boundary): planar, irregular, curved, concordant, or discordant.
- Boundary sharpness: sharp or diffused.
- Sense of shear: normal (n), reverse (r), dextral (d), sinistral (s), or a combination of nd, ns, rd, and rs.
- Comments: name and general shape of minerals that define crystal-plastic fabrics, together with crosscutting relationships, spacing, shape features, and anything else of interest.
- SPO of mineral phases or groups of mineral phases, with modal percent of measured mineral phases, shape ratio, and orientation of SPO long axis. SPO was ranked as follows:
  - 0 = macroscopically isotropic (<1.05 SPO ratio).
  - 1 = weak (1.05 to <1.2 SPO ratio).
  - 2 = moderate (1.2 to <2.0 SPO ratio).
  - 3 = strong ( $\geq 2.0$  SPO ratio).
- Orientation: dip angle and dip direction of planar fabric and trend and plunge of lineation, where measurable.

### **Microstructures**

To better characterize different types of deformation, we studied the microstructural features of interesting or prominent mesoscopic structures. Thin sections of recovered material were examined in order to

- Confirm macroscopic descriptions of structures,
- Characterize the microstructure of the rocks,
- Document crystal-plastic overprints of magmatic fabrics and brittle overprints of crystal-plastic fabrics,
- Provide information on the kinematics of brittle and brittle-ductile deformation,
- Identify temporal relationships between magmatic deformation and alteration processes, and
- Document major structural zones and downhole variations.

Microstructure descriptions followed the terminology of Passchier and Trouw (1996). Where possible, shipboard thin sections were oriented with respect to the core reference frame, and samples were cut

perpendicular to the foliation and parallel to any extensional lineation, because this is the plane that best displays both shear-sense indicators and the preferred dimensional orientation of minerals. The orientation of structures measured during macroscopic core description was confirmed, and macroscopic observations were refined by microscopic description. Digital photomicrographs (available in the LIMS database) were taken and annotated to document features described in thin sections.

We generally followed the terminology used during Expedition 335. Structural domains were recorded in the structure log in the thin section description worksheet. Additional classifications and terminology were incorporated from Expeditions 304 and 305 (Expedition 304/305 Scientists, 2006). The following microscopic features were recorded for each structural domain:

- Type of microstructure: magmatic, submagmatic, crystal-plastic, cataclastic, or metamorphic.
- Morphology of grain boundary: straight, curved, serrate, polygonal, complex, or varied.
- Intensity of magmatic fabric: isotropic, weak, moderate, or strong.
- Intensity of static recrystallization: absent, weak, strong, partial, or complete.
- Presence of submagmatic fractures: absent, rare, or common.
- Intensity of crystal-plastic undulose extinction: absent, weak, moderate, strong, complete, patchy, or subgrains.
- Morphology of crystal-plastic subgrain boundaries: straight, curved, serrate, or polygonal.
- Presence of crystal-plastic deformation twinning: absent, rare, or common.
- Intensity of crystal-plastic dynamic recrystallization: absent, weak, strong, or complete.
- Intensity of overall crystal-plastic fabric:
  - 0 = absent.
  - 1 = weakly foliated/lineated.
  - 2 = strongly foliated/lineated.
  - 3 = porphyroclastic/protomylonitic.
  - 4 = mylonitic.
  - 5 = ultramylonitic.
- Sense of shear estimated from crystal-plastic fabric, described as normal (n), reverse (r), dextral (d), or sinistral (s).
- Clast/matrix ratio (in percent) of cataclasite/brittle fracture.
- Size (in millimeters) of clasts in cataclasite/brittle fracture.
- Intensity of cataclastic fabric and intensity rank:

0 = undeformed.

1 = minor fracturing with no significant GSR.

2 = moderate fracturing without GSR.

3 = dense anastomosing fracturing with incipient GSR.

4 = well-developed GSR with evidence for clast rotation (independent particulate flow).

5 = cataclastic.

## Hard rock geochemistry

### Sampling and analysis of igneous rocks

#### Sample preparation

Representative samples of igneous rocks were analyzed for major and trace element concentrations during Expedition 336 using inductively coupled plasma–atomic emission spectroscopy (ICP-AES). Approximately 10 cm<sup>3</sup> samples were cut from the core with a diamond saw blade. During this expedition, both the geochemistry sample and the thin section billet were taken from a quarter-cut core sample in the same interval. All outer surfaces were polished with a diamond-impregnated disk to remove surface contamination by saw marks and altered rinds resulting from drilling. Each sample was then placed in a beaker containing trace-metal-grade methanol and ultrasonicated for 15 min. After the methanol was decanted, the samples were washed in deionized water for 10 min in an ultrasonic bath and then were further ultrasonicated for 10 min in Barnstead deionized water (~18 M $\Omega$ -cm). The cleaned pieces were dried for 10–12 h at 110°C.

The cleaned, dried samples were crushed to <1 cm chips between two disks of Delrin plastic in a hydraulic press. The chips were ground to a fine powder in a tungsten carbide SPEX 8000M mixer/mill or, for larger samples, a SPEX 8515 shatterbox. According to Expedition 304/305 Scientists (2006), contamination from the tungsten carbide mills is negligible for the elements analyzed during this cruise. After the chips were ground, a ~1 g aliquot of the sample powder was weighed on a Mettler Toledo dual balance system and ignited at 1025°C for 4 h to determine weight loss on ignition (LOI). The estimated uncertainty of LOI values is ~0.2 mg (0.02 wt%).

The following protocol essentially follows the shipboard procedure described in ODP *Technical Note 29* (Murray et al., 2000). After determination of LOI, 100.0  $\pm$  0.2 mg aliquots of the ignited whole-rock powders were weighed and mixed with 400.0  $\pm$  0.5 mg of LiBO<sub>2</sub> flux that had been preweighed on shore. Standard rock powders and full procedural blanks were included with unknowns in each ICP-AES run. All samples and standards were weighed on the Cahn C-31 microbalance (designed to measure

on board), with weighing errors estimated to be  $\pm 0.05$  mg under relatively smooth sea-surface conditions. After that, 10 mL of 0.172 mM aqueous LiBr solution was added to the mixture of flux and rock powder as a nonwetting agent to prevent the cooled bead from sticking to the crucible. Samples were then fused individually in Pt-Au (95:5) crucibles for  $\sim 12$  min at a maximum temperature of 1050°C in an internal-rotating induction furnace (Bead Sampler NT-2100). After cooling, beads were transferred to 125 mL high-density polypropylene (HDPE) bottles and dissolved in 50 mL 10% HNO<sub>3</sub>, aided by shaking with a Burrell wrist-action bottle shaker for 1 h. Following digestion of the bead, the solution was passed through a 0.45  $\mu$ m filter into a clean 60 mL wide-mouth HDPE bottle. Next, 2.5 mL of this solution was transferred to a plastic vial and diluted with 17.5 mL of 10% HNO<sub>3</sub> to bring the total volume to 20 mL. The final solution-to-sample dilution factor was  $\sim 4000$ . For standards, the stock solutions were placed in an ultrasonic bath for 1 h prior to final dilution to ensure a homogeneous solution.

### Analyses

Major (Si, Ti, Al, Fe, Mn, Mg, Ca, Na, K, and P) and trace (Ba, Sr, Zr, Y, V, Sc, Cu, Zn, Co, Cr, and Ni) element concentrations of standard and unknown samples were determined with a Teledyne Leeman Labs Prodigy ICP-AES instrument. Wavelengths used for sample analysis during Expedition 336 are provided in Table T2. These wavelengths were selected on the basis of the quality of calibration lines, including signal (sample)-to-noise (blank) ratios. The plasma was ignited at least 30 min before each run of samples to allow the instrument to warm up and stabilize. A zero-order search was then performed to check the mechanical zero of the diffraction grating. After the zero-order search, the mechanical step positions of emission lines were tuned by automatically searching with a 0.002 nm window across each emission peak using basalt laboratory standards BAS-140 (Sparks and Zuleger, 1995) or BAS-206 (Shipboard Scientific Party, 2003) in 10% HNO<sub>3</sub>. During the initial setup, BAS-140 was used to select an emission profile for each peak to determine peak-to-background intensities and set the locations of background levels for each element. The Prodigy software uses these background locations to calculate the net intensity for each emission line. Photomultiplier (PMT) voltage was optimized by automatically adjusting the gain for each element using BAS-140.

The ICP-AES data presented in the site chapters were acquired using the Gaussian mode of the Prodigy software. This mode fits a curve to points across a peak and integrates the area under the curve for each

element measured. Each sample was analyzed four times from the same dilute solution (i.e., in quadruplicate) within a given sample run. For elements measured at more than two wavelengths, we either used the wavelength giving the better calibration line in a given run or, if the calibration lines for both wavelengths were of similar quality, used the data from both and reported the average concentration.

### Data reduction

Following each run of the instrument, the measured raw-intensity values were transferred to a data file and corrected for instrument drift and procedural blank. Drift correction was applied to each element by linear interpolation between the drift-monitoring solutions run every fourth analysis. After drift correction and blank subtraction, a calibration line for each element was calculated using the results for the certified rock standards. Element concentrations in the samples were then calculated from the relevant calibration lines.

Estimates of the accuracy and precision of major and trace element analyses during Expedition 336 are based on replicate analyses of check standards (BAS-140 and MRG-1), the results of which are presented and compared with published data in Table T3. Run-to-run relative standard deviation by ICP-AES was generally  $\pm 3\%$  for major elements and  $\pm 10\%$  for trace elements. Exceptions typically occurred when the element in question was near background levels.

### Total carbon and nitrogen analysis

Total carbon and nitrogen contents were also obtained for the rock samples. Contents of these elements were determined using a Thermo Finnigan Flash EA 1112 carbon-hydrogen-nitrogen-sulfur (CHNS) analyzer. Aliquots of 10 mg of rock powder samples were weighed and placed in a tin container and then combusted at 900°C in a stream of oxygen. Nitrogen oxides were reduced to N<sub>2</sub>, and the mixture of CO<sub>2</sub> and N<sub>2</sub> was separated by gas chromatography (GC3) and detected by a thermal conductivity detector. The gas chromatograph (GC) oven temperature was set at 65°C. Calibration was based on the synthetic standard sulfanilamide, which contains 41.81 wt% C, 16.27 wt% N, and 18.62 wt% S. The standard deviation of carbon, nitrogen, and sulfur concentrations was less than  $\pm 0.1\%$ .

## Inorganic geochemistry

Pore water dissolved ion and gas samples and data were collected using three different methods to maximize the analytical program, minimize possible

sample handling and contaminations sources, and measure ephemeral dissolved gas data. These methods include standard sediment squeezing, pore water extraction using Rhizon samplers, and measurements using oxygen optodes.

### Sediment squeezing

Shipboard interstitial water samples were obtained from 10–20 cm long whole-round samples cut on the catwalk. Samples were capped and taken to the laboratory for immediate processing. Sampling resolution ranged from 1–2 per core to 1 per section to obtain a high-resolution data set. When there were too many interstitial water samples to process immediately, the capped whole-round samples were stored temporarily in a nitrogen-filled glove bag at 4°C. Samples sat for no more than 3 h before processing. Sediment processing for interstitial water sampling in the laboratory was carried out in a nitrogen-flushed and pressurized glove bag. After extrusion from the core liner, the outer layer of each whole-round sample was carefully scraped with a spatula to remove potential contamination from drill water (surface seawater). The remaining sediment was placed in a titanium squeezer modified after the standard stainless steel squeezer of Manheim and Sayles (1974). The piston was positioned on top of the squeezer, and the entire unit was removed from the glove bag and placed on the hydraulic press. Pressures as high as 76 MPa were applied in the squeezer, calculated from the measured hydraulic press pressure and the ratio of the piston areas of the hydraulic press and the squeezer.

Interstitial water was passed through a prewashed Whatman Number 1 filter above a titanium screen and subsequently extruded into an acid washed or sterile 50 mL plastic syringe. Fluids were then filtered through a 0.45 µm Gelman polysulfone disposable filter into appropriate sample containers. Aliquots for shore-based trace metal and elemental analyses were placed in HDPE plastic bottles. These bottles were cleaned by soaking them in 10% HCl for 24 h at 60°C and rinsing them repeatedly with 18.2 MΩ water. Some of these aliquots were acidified with 4 mL of subboiled 6N HCl per liter of sample for shore-based trace element analysis. Samples for <sup>14</sup>C analysis were placed in evacuated glass serum bottles (60 mL). These bottles contained 20 µL of saturated mercuric chloride that was evaporated before the bottle was filled with sample. Samples for isotopic analysis (H, O, and dissolved inorganic carbon) were stored at 4°C without headspace in glass vials with Teflon-lined screw cap lids.

Squeezed pore water samples were analyzed according to standard procedures (Gieskes et al., 1991).

Only two measurements were conducted at sea (pH and alkalinity). The pH was determined by ion-selective electrode. Alkalinity was determined by Gran titration with a Metrohm autotitrator. Shore-based analyses included chlorinity measurements, conducted using a potentiometric titration with silver nitrate and a Mettler Toledo DL25 titrator equipped with a silver ring electrode (Mettler/Toledo ME 89599) filled with a 2M KNO<sub>3</sub> solution. Chlorinity measurements were standardized with International Association for the Physical Sciences of the Ocean (IAPSO) standard seawater. Other shore-based analyses include Na calculated by difference, major and minor ions measured using inductively coupled plasma–optical emission spectroscopy (Na, Mg, Ca, K, Sr, Li, B, Mn, Fe, Li, Si, and Ba), and some trace elements measured using inductively coupled plasma–mass spectroscopy with a sample dilution of 1:75 (U, V, Co, Rb, Mo, Cs, and Ba).

### Extraction using Rhizon samplers and dissolved oxygen measurements

Following removal of whole round core and syringe samples on the catwalk for microbiological sampling and pore water squeezing, all remaining core sections were capped and immediately transferred to the ship Hold Deck refrigerated storage area for oxygen profiling and pore water extraction with Rhizon samplers (Rhizosphere Research Products, Wageningen, The Netherlands), in a similar manner as was conducted during IODP Expedition 329 (Expedition 329 Scientists, 2011b). The cold storage area was roughly 6°C throughout the sampling period, and cores were delivered to cold storage typically within 45 min of receiving core on deck. As soon as possible after delivery of core sections to the sampling area, Rhizon samplers were inserted through holes drilled in the core liner to collect pore water for nutrient and isotopic analyses in shore-based laboratories. The first 1 mL of fluid collected was wasted to ensure that any possible contaminants in the Rhizon filter were removed. Up to 10 mL of pore water was collected in each sample for a period of up to 24 h, depending on sediment porosity. Fluids for nutrient analysis were stored frozen (–20°C) in acid-cleaned HDPE vials. These samples were analyzed using standard colorimetric methods (flow injection analysis) for nutrient analysis (ammonium, nitrate, and phosphate). Additional fluids for isotopic analysis were stored at 4°C without headspace in glass vials with Teflon-lined screw cap lids.

After the core sections had equilibrated to cold storage temperatures (as measured with a PreSens PT 1000 temperature sensor inserted into the interior of the core, PreSens, Regensburg, Germany), oxygen

concentrations were determined. Core temperatures were as high as 18°C when the cores arrived in the cold room, in response to time spent on the catwalk. Oxygen was measured using needle-type fiber-optic oxygen microsensors (optodes; PreSens, Regensburg, Germany; Fischer et al. 2009) inserted manually into sediments through holes drilled in the core liners. Temperature was measured within 2 cm of the oxygen sample location. Both optode and temperature sensors were connected to a MICROX TX3 single channel fiber-optic oxygen meter (PreSens) graciously loaned by Dr. Lars Ottosen (Danish Technological University, Aarhus, Denmark). Signals were recorded using the OxiView software provided by the manufacturer. Prior to sample measurement, optodes were calibrated using water-saturated air (100% air saturation) and sodium sulfite-saturated solution (0% air saturation), according to manufacturer protocols. Optodes frequently had to be replaced due to wear or breakage. The signal for oxygen measurements was allowed to equilibrate to a steady value, ~3–10 min depending on sediment porosity. Roughly 1–2 oxygen measurements were made per core section delivered to the cold storage area, with higher frequency near the sediment/water and sediment/basement interfaces, resulting in a resolution of roughly 20–100 cm. Some sections could not be analyzed in this fashion because of high sediment disturbance or inclusion of rocks within the sediment matrix. Optode measurements were conducted at random depths within a core section to prevent bias.

## Organic geochemistry

The organic geochemistry program comprised characterization of volatiles and sedimentary inorganic geochemistry, including inorganic carbon. These analyses were carried out as part of routine shipboard safety and pollution prevention requirements, to characterize the interstitial waters and sediment geochemistry for shipboard interpretation, and to provide sampling frameworks for shore-based research.

### Sediment gas sampling and analysis

The organic geochemistry program monitored the compositions and concentrations of volatile hydrocarbons (C<sub>1</sub>–C<sub>6</sub>) and other gases (i.e., O<sub>2</sub>, N<sub>2</sub>, and H<sub>2</sub>S) in the void gas samples and in the sediments from headspace gas samples at typical intervals of one per core. The IODP gas sampling protocol for pollution prevention and safety, required by IODP safety regulations, was modified to better constrain the concentrations of dissolved hydrocarbon gases. The routine headspace procedure involved placing ~5 cm<sup>3</sup> of sediment sample in a 20 cm<sup>3</sup> glass serum

vial that was sealed with a septum and metal crimp cap and heated at 70°C for 30 min. A 5 cm<sup>3</sup> volume of gas from the headspace in the vial was removed with a glass syringe for analysis by GC3. Detailed procedures are those described in Kvenvolden and McDonald (1986).

The headspace gas samples were analyzed using an Agilent 6890 Series II gas chromatograph (GC) equipped with a 2.4 m × 3.2 mm stainless steel column packed with 80/100 mesh HayeSep R and a flame ionization detector (FID). This instrument quickly measures the concentrations of methane (C<sub>1</sub>), ethane (C<sub>2</sub>), ethene (C<sub>2=</sub>), propane (C<sub>3</sub>), and propene (C<sub>3=</sub>). The gas syringe was directly connected to the GC via a 0.25 cm<sup>3</sup> sample loop. Helium was used as the carrier gas, and the GC oven temperature was programmed to ramp 90°–100°C at 30°C/min, ramp 100°–110°C at 15°C/min, remain at 110°C for 4.5 min, and then ramp to 150°C at 50°C/min, with a final holding time of 1.8 min. Data were collected and evaluated with an Agilent Chemstation data-handling program. Chromatographic response was calibrated against preanalyzed standards.

### Bulk sediment geochemistry: sedimentary inorganic and organic carbon

Inorganic carbon concentrations were determined using a Coulometrics 5011 carbon dioxide coulometer. One carbonate determination was performed typically for each 1.5 m section of core. Samples of ~10–15 mg of freeze-dried, ground sediment were reacted with 2N HCl. The liberated CO<sub>2</sub> was titrated to a colorimetric end point. Calcium carbonate content, as weight percent, was calculated from the inorganic carbon (IC) content with the assumption that all inorganic carbon was present as calcium carbonate:

$$\%CaCO_3 = \%IC \times 8.33.$$

The coulometer was calibrated with pure CaCO<sub>3</sub> powder during the expedition, and the analytical precision was determined.

## Microbiology

The primary microbiology objectives for Expedition 336 were to determine the microbial community composition and activity of the deep biosphere harbored in the buried basaltic oceanic crust at Sites 395A, U1382 (~50 m west of Hole 395A), and U1383 (prospectus Site NP-2) and near the sediment/basement interface in Holes U1383D and U1383E (near the new deep Hole U1383C seafloor borehole observatory [CORK]), U1382B (near Hole 395A), and

U1384A (prospectus site NP-1) at the North Pond site on the western Mid-Atlantic Ridge flank. Strategies to reach these objectives included deployment of novel microbial colonization devices within CORK observatories (see [Edwards et al., 2012](#); Orcutt et al., 2010, 2011), opportunistic sampling of biofilms on an old CORK recovered from Site 395, and collection of fresh crustal rocks by drilling in oceanic crust along the presumed flow path of formation fluids. These studies complement and expand upon similar work conducted on the eastern flank of the Juan de Fuca Ridge (Cowen et al., 2003; Engelen et al., 2008; Fisher et al., 2005, 2011; Nakagawa et al., 2006; Orcutt et al., 2010, 2011; Steinsbu et al., 2010), although the Juan de Fuca sites represent a reduced and warm hydrothermal setting as compared to the cool hydrothermal conditions within North Pond oceanic crust. These studies also build upon previous decades of work studying fluid flow in basement at North Pond and a recent site survey cruise with the R/V *Merian* (Ziebis et al., 2012).

A secondary microbiology objective of this expedition was to collect sediment from multiple sites around North Pond, including prospectus Sites NP-1 (Hole U1384A) and NP-2 (Holes U1382D and U1382E) and Site 395 (Hole U1382B), to examine the phylogenetic and functional connection between sediment microbial communities and those harbored within oceanic crust and the overlying seawater and to examine how these relationships may vary vertically (i.e., with distance from the sediment/basement interface) and horizontally (i.e., along the presumed flow path of fluids within oceanic crust). Of interest was the evaluation of basement fluid flow on basal sediment biogeochemistry and microbial ecology, as has been evaluated elsewhere (Engelen et al., 2008; Lever et al., 2010).

This section focuses on the shipboard methods used for rock and sediment sample collection and handling for microbiological analyses; CORK-related microbiology experiments are described in [Edwards et al., 2012](#). Briefly, samples of oceanic crust collected for microbiology were subsampled for environmental DNA and RNA extraction and analysis, cell counts, fluorescent in situ hybridization (FISH) studies, contamination tests, evaluation with the new deep ultraviolet (UV) fluorescence scanner for biofilm biomass (Bhartia et al., 2010), and several enrichment and culturing experiments. Sediment samples were also collected for DNA and RNA extraction and analysis, cell counts, FISH studies, contamination tests, lipid analysis, and several enrichment and culturing experiments to be conducted on shore.

## Core handling and sampling

To examine potential contamination of hard rock and sediment core samples, slurries of yellow-green fluorescent microspheres (Fluoresbrite Carboxylate Microspheres; Polysciences, Inc., 15700) were sealed in plastic bags and placed inside the core catcher prior to deployment of the core barrel according to standard protocol (Smith et al., 2000). Microspheres were used in every RCB core during hard rock coring and also in every APC and XCB core during coring in sediments and across the sediment/basement interface. Perfluorocarbon tracer contamination checks (Lever et al., 2006) were not conducted during this expedition.

### Hard rock cores

Hard rock samples for microbiology originated from RCB coring in Holes U1382A and U1383C and from ACP and XCB coring in Holes U1383D, U1383E, U1382B, and U1384A. Priority was given to large (>10 cm in length) intact pieces or samples with interesting lithology. Nominally one sample was collected per section during RCB coring. Immediately following delivery of core on deck and cutting of the core liner into 1.5 m sections, rocks were exposed for subsampling in the core splitting room by shaking the recovered rocks into another split core liner (which, because of frequent splitting blade breakage, was much faster than trying to split the recovered core liner). Rocks for microbiological sampling were identified immediately, photographed in place, and then collected using combusted aluminum foil for transport to the microbiology laboratory. During ACP and XCB coring, some rocks were handled in the above manner, when appropriate; otherwise, rock and sediment matrix material was transferred via sterile spatula on the catwalk into a sterile Whirl-Pak bag for subsequent subsampling. All sample handlers wore gloves to reduce contamination. In the laboratory, whole-round rock pieces were transferred to sterile Whirl-Pak bags containing 10 mL of sterile filtered seawater for gentle rinsing and removal of any microspheres and other contaminants. The rinse was collected into a 15 mL conical vial and stored at 4°C until processing. The rinsing process was repeated three times. Next, the rock was transferred to a flame-sterilized rock processing box (Expedition 327 Scientists, 2011) and broken into smaller pieces using flame-sterilized chisels and forceps. Subsampling was done as rapidly as possible (5–15 min) to minimize oxygen exposure and cell degradation. Rock fragments were then split into aliquots for the following analyses, depending on available sample volume:

1. Fixed for shore-based FISH or Raman confocal microscopy assays:
  - a. Fixed in cold 3.7% [w/v] paraformaldehyde in 1× phosphate-buffered saline (PBS; 150 mM NaCl per liter of 10 mM sodium phosphate, pH 7.2) for 1–4 h, washed in 1× PBS, and then stored at –20°C in 1:1 1× PBS:ethanol;
  - b. Rinsed in 5% sodium hypochlorite and sterile seawater (to remove any exterior contaminants), fixed in 2% [v/v] formaldehyde (methanol free, Ultra Pure; Polysciences, Inc.) in 1× PBS, and then rinsed and stored as above; or
  - c. Rinsed in 5% sodium hypochlorite and sterile seawater and then fixed and stored in cold 50% [v/v] ethanol in double-deionized water.
2. Preserved for shore-based DNA and RNA analysis and archival either by immediately freezing at –80°C in sterile sample bags or by first rinsing the exterior in 2%–3% sodium hypochlorite and sterile seawater prior to freezing.
3. Transferred to baked aluminum foil (450°C to remove organics) and stored at 4°C for deep UV fluorescence scanning.
4. Transferred to baked aluminum foil (450°C) and frozen at –20°C for stable isotopic analysis of carbonate-<sup>13</sup>C and oxygen isotopes.
5. Rinsed in 5% sodium hypochlorite solution and sterile seawater.
6. Prepared for enrichment and culturing experiments (described below).

Leftover rock material was washed in deionized water, dried, and returned to shore-based laboratories for use as substrate in future colonization experiments.

### Sediment cores

Sediments for microbiological analysis were collected from four holes as whole-round core or syringe samples. APC and XCB cores were cut on the catwalk using sterilized tools (autoclaved spatulas and bleach-cleaned end caps). Everyone assisting in the core cutting and sediment sampling wore gloves to minimize contamination. Each core was inspected before being cut to determine the integrity of the sediment and the potential for disturbance during drilling or recovery. A predetermined sampling plan was followed for each core and section to maximize sampling efficiency and accuracy. Samples were collected from almost every section recovered provided the section was of sufficient quality. A general sampling plan is described below; the full sampling plan is included as Figures F8, F9, F10, and F11.

1. Whole-round samples were cut from the bottom of each section and then capped and stored according to submitted sample requests. A portion

of the sediment was dedicated to pore water geochemistry (see “**Inorganic geochemistry**”). Samples were collected for the following microbiology procedures:

- a. Culture independent analysis: whole-round samples for shore-based DNA and RNA were cut from each core. In upper and middle cores, three 10 cm whole-round cores were collected for both DNA and RNA analysis. In the deepest cores, a whole-round core sample was collected from each section for both DNA and RNA analysis. Additional samples were collected for polar lipid fatty acid and metagenome analysis at a frequency of one per core. All whole-round cores for culture independent analysis were stored at –80°C in a sterile sample bag.
  - b. Culturing: whole-round samples were collected for multiple ship- and shore-based culturing projects. Higher resolution sampling occurred in shallow and deep cores, with fewer samples collected in mid-depth cores. Enrichment cultures were established for nitrogen, iron, sulfur, and carbon-cycling functional groups. Additional culture assays will be constructed on shore to target heterotrophs, fermenters, phosphate cycling, and acetate turnover. Anaerobic and aerobic strategies were employed for both ship- and shore-based samples, with anaerobic samples being stored in silver Mylar bags under nitrogen headspace. Temperatures for incubations ranged from 8°–20°C, and whole rounds were stored at 9°C.
2. Multiple syringe samples were collected from the tops of each core section, focusing on the interior of the core. A syringe sampling diagram is included in Figure F12 and follows the above sediment sampling plan (Figs. F8, F9, F10, F11). One set of 10 mL syringe samples was collected for shore-based DNA characterizations of *Bacteria* and *Archaea* populations. In addition, 2 cm<sup>3</sup> of sediment was collected via syringe and transferred to 20 mL glass serum vials with crimp caps for onboard methane concentration analysis. Sediment was also collected via toothpick from the edge and center of the top of the core section for microsphere contamination analysis. These samples were mixed with sterile filtered PBS solution and stored for shore-based analysis.

### Storage and shipment conditions

All samples for shore-based DNA/RNA extraction and analysis were stored and shipped frozen (–80°C), whereas samples for shore-based FISH and enrichment studies were stored and shipped cold (–20°–4°C).

## Analytical methods

### Cell counts, FISH, and spectroscopy of hard rock materials

Sample fixation for FISH is described above. Washed samples will be used for shore-based FISH analyses, whereas unwashed samples will be used for cell counting with either SYBR Green I or acridine orange fluorescent dye using previously described methods (Morono et al., 2009). On the basis of results from DNA extraction and analysis, microbial groups of interest will be investigated using group-specific FISH primers according to published protocols (Biddle et al., 2006).

Dried samples for micro- and nano-imaging (with X-ray, electron, and UV-visible spectroscopies) were transferred for shore-based analysis with flame-sterilized pliers to sterile centrifuge tubes without any treatment. Manually polished sections (using gloves and absolute ethanol) or freshly broken fragments will be characterized for mineralogical and organic matter content using Fourier transform infrared spectroscopy and Raman microspectroscopy (Beysac et al., 2003; van Zuilen et al., 2007; Marshall et al., 2010) and scanning electron microscopy with energy dispersive spectrometry and X-ray microscopy (Rommevaux-Jestin and Menéz, 2010; Ménez et al., 2007). Ultrathin sections will be prepared using a focused ion beam as described by Benzerara et al. (2005) for observations using scanning X-ray microscopy and transmission electron microscopy (Benzerara et al., 2006).

### Nucleic acid extraction and analysis

DNA will be extracted in shore-based laboratories using a variety of methods, depending on sample type and analytical laboratory, to maximize cross-comparison of methods. Genes of interest, including the 16S rRNA gene as well as functional genes, will be amplified using multiple amplification strategies.

In one shore-based laboratory, DNA will be extracted from hard rock samples using the MO BIO DNA extraction kit for soil (MO BIO Laboratories, Inc.), following the manufacturer's protocol with minor modification. An archaeal 16S rRNA gene amplicon library will be prepared, and the resulting library will be sequenced using the 454 GS FLX Titanium pyrosequencing platform (454 Life Sciences, Roche). The taxonomic affiliation of each read will be resolved as described elsewhere (Lanzén et al., 2011). In addition, archaeal and bacterial 16S rRNA genes will be quantified by quantitative polymerase chain reaction (qPCR) following a previously described protocol (Roalkvam et al., 2011). Specific archaeal groups such as Marine Benthic Group B and Marine Group I may

be quantified by qPCR with group-specific primers, depending on results from the amplicon library.

In another shore-based laboratory, DNA will be extracted from hard rock samples using a "homemade" DNA extraction protocol utilizing phenol-chloroform extraction following published protocols (Lever et al., 2010; Orcutt et al., 2011). In addition, 16S rRNA genes will be amplified with published primer sets using Ion Torrent semiconductor sequencing (Rothburg et al., 2011) coupled with Sanger-style sequencing.

In another shore-based laboratory, DNA and RNA will be extracted from hard rock samples using the MO BIO PowerSoil DNA extraction kit (MO BIO Laboratories, Inc.) following the manufacturer's protocol with minor modifications, as described in Gérard et al. (2009). Genes of interest, including the 16S rRNA gene and some functional genes, will be amplified using PCR with published protocols.

Total RNA will be extracted from sediment and crushed basalt in another shore-based laboratory using a method previously described in Mills et al. (2008) with modifications noted in Mills et al. (2012). Extracts will be treated with deoxyribonuclease (DNase) to remove residual DNA prior to reverse-transcription PCR. Initial amplifications will target the 16S rRNA gene transcripts using published primers. Amplicons will be sequenced using the 454 GS FLX Titanium pyrosequencing platform (454 Life Sciences, Roche). The metabolically active community structure will be determined by sequence annotation. Functional gene transcripts will be quantified on the basis of results of community structure analysis to determine community function.

To evaluate the preenrichment microbial community in sediments prior to cultivation, a preliminary analysis by PCR amplification will be conducted in a shore-based laboratory to examine the existence of methanogens, sulfate reducers, and methanotrophs. DNA will be extracted from each sediment sample using the PowerMax soil DNA isolation kit (MO BIO Laboratories, Inc.) following the manufacturer's protocol. The gene encoding methyl coenzyme M reductase (*mcrA*) of methanogens will be amplified using a PCR method, as described by Nunoura et al. (2008). The gene encoding dissimilatory sulfite reductase (*dsrA*) of sulfate reducers will be amplified using a PCR method, as described previously (Kondo et al., 2004). The gene encoding particulate methane monooxygenase (*pmoA*) will be amplified using a PCR method, as described previously by Tavormina et al. (2008).

### Deep UV fluorescence scanning

To evaluate the presence of cells and organics on the surfaces of hard rock materials using deep UV

fluorescence (Bhartia et al., 2008, 2010), rock fragments (1–2 cm<sup>3</sup>) were scanned with the new Deep Exploration Biosphere Investigative portable tool (DEBI-pt) similar to the Deep Exploration Biosphere Investigative tool (DEBI-t) downhole logging tool described in “[Downhole logging](#).” The DEBI-pt combines a targeted ultraviolet chemical sensor (TUCS) (Photon Systems, Inc.) with an X-Y scanning stage. A 224.3 nm HeAg hollow-cathode laser induces fluorescence of organics and microbes. Detection uses six discrete, laser-gated PMT-based bands at 280, 300, 320, 340, 360, and 380 nm. The laser focuses on a 200 μm spot translated over the sample at a rate that satisfies Nyquist sampling. Using the motor encoders, the maps are displayed in millimeters and provide spatial coordinates from a registered set of points.

Samples for DEBI-pt analysis were carefully collected during rock subsampling to preserve the interior and exterior orientation of the material. Pieces were photo-documented before being wrapped in baked foil and stored at 4°C to enable detailed correlation of DEBI-pt scans with sample orientation. Samples collected from coring operations were placed on a stage below the TUCS. Care was taken to minimize exposure of the samples to potential contaminants. A charged-coupled device camera was used for targeting and focus. Once the sample was in focus, the *x* and *y* sample dimensions and the desired degree of overlap were input in the control software. When the scanning run was complete, the data were transferred to interpolation software that created a multidimensional array that was then viewed with a custom analysis package, which represented the data as a fluorescence map indicating the location and intensity of fluorescence for each of the bands. The scanned samples were then stored for shore-based thin sectioning for petrology to correlate fluorescence regions with the mineralogy of each sample.

DEBI-pt experiments were also conducted with smears of the microsphere solutions, pipe dopes, and drilling fluids used during coring to generate background spectra profiles for these materials that could be used for comparison with natural samples.

### Culturing and enrichment

Several types of metabolic groups will be targeted by enrichment and cultivation using various techniques, as outlined below.

#### Target 1

- Metabolic group: hydrogen-utilizing microorganisms from basement (specifically from peridotite, gabbro, veins, and basalt glass), including hydrogenotrophic methanogens, anaerobic nitrate reducers, anaerobic sulfate reducers, and microaerobic and aerobic hydrogen oxidizers.

- Procedure: on board, rock fragments (20–30 cm<sup>3</sup>) were crushed inside a stainless cylinder mortar in the anaerobic chamber. The small rock fragments were transferred into a 100 mL glass bottle that was sealed tightly with a butyl rubber stopper and stored at 4°C until processing in the shore-based laboratory. The targeted microbial groups will be cultivated in a basic medium composition described elsewhere (Takai et al., 2003, 2008) and outlined in Table T4.
  - For cultivation of methanogens, the basic medium will be supplemented with 0.2% (w/v) NaHCO<sub>3</sub>, 0.03% (w/v) NH<sub>4</sub>Cl, 0.5 mg/L of resazurin, 0.05% (w/v) sodium sulfide, 2% (w/v) metallic iron powder, and 1% (v/v) vitamin mix solution, and the pH will be adjusted to 6.5. The cultivation will be conducted in the test tube with the gas phase of H<sub>2</sub> (80%) + CO<sub>2</sub> (20%) (3 atm).
  - For cultivation of other H<sub>2</sub>-oxidizers, the basic medium will be supplemented with 0.1% (w/v) NaHCO<sub>3</sub>, 0.025% (w/v) NH<sub>4</sub>Cl, 0.025% (w/v) NaNO<sub>3</sub>, and 0.1% (v/v) vitamin mix solution.
  - For anaerobic H<sub>2</sub>-oxidizers, 0.05% (w/v) NaNO<sub>3</sub> will also be added. The pH will be adjusted to ~7. The cultivation will be conducted in the test tubes with the gas phase of
    1. H<sub>2</sub> (80%) + CO<sub>2</sub> (20%) (3 atm),
    2. H<sub>2</sub> (79.5%) + CO<sub>2</sub> (20%) + O<sub>2</sub> (0.5%) (3 atm), and
    3. H<sub>2</sub> (78%) + CO<sub>2</sub> (20%) + O<sub>2</sub> (2%) (3 atm). The incubation temperatures will be 4°–15°C.

#### Target 2

- Metabolic group: high pressure–adapted heterotrophs from Hole 395A CORK rust and thermistor cable.
- Procedure: rust samples (~100 μL) were mixed with 25 mL of Difco 2216 marine media or 1:10 diluted Difco 2216 marine media (for oligotrophic heterotrophs) in glass bottles. Samples were stored at 4°C until shore-based manipulation. Thermistor cable samples were stored at 4°C in sterile Whirl-Pak bags for shore-based manipulation. In the shore-based laboratory, high-pressure incubation will be used to enrich and select for high pressure–adapted microorganisms using pin-closure pressure vessels (Wang et al., 2009a). Isolated high pressure–adapted microorganisms will then be characterized and compared with other deep-sea high-pressure microorganisms isolated from different ocean provinces.

#### Target 3

- Metabolic group: aerobic and anaerobic CO<sub>2</sub>, CH<sub>4</sub>, acetate, NH<sub>4</sub>, and NO<sub>3</sub>-cycling microorganisms from hard rocks.

- Procedure: rock fragments were broken into smaller pieces using sterile Xpress hydraulic press devices. Smaller rock fragments (~50 cm<sup>3</sup>) were transferred to sterile 250 mL screw-cap Pyrex bottles with thick rubber stoppers and mixed with 50 mL of artificial seawater. A variety of aerobic and anaerobic enrichments were then created with mixtures of stable isotope-labeled substrates, with the labeled substrate used at 1–2 mM or 20% [v/v] headspace.
  - Aerobic combinations included <sup>13</sup>C-labeled sodium bicarbonate + <sup>15</sup>N-labeled NH<sub>4</sub>Cl, <sup>13</sup>C-labeled sodium bicarbonate + <sup>15</sup>N-labeled sodium nitrate, <sup>13</sup>C-labeled methane + <sup>15</sup>N-labeled ammonium chloride, and <sup>13</sup>C-labeled sodium acetate + <sup>15</sup>N-labeled ammonium chloride.
  - Anaerobic combinations included <sup>13</sup>C-labeled sodium bicarbonate + <sup>15</sup>N-labeled NH<sub>4</sub>Cl, <sup>13</sup>C-labeled methane + <sup>15</sup>N-labeled ammonium chloride, <sup>13</sup>C-labeled methane + <sup>15</sup>N-labeled sodium nitrate, and <sup>13</sup>C-labeled sodium acetate + <sup>15</sup>N-labeled ammonium chloride.

After enrichment at ambient temperature in the dark for 6 weeks or more, the enrichments will be checked by microscopy to evaluate growth in the shore-based laboratory. Headspace gas in the enrichments will be analyzed by gas chromatography–mass spectrometry to evaluate the production or consumption of <sup>13</sup>C-compounds. Enriched samples will be evaluated in the shore-based laboratory using taxonomic, metagenomic, or transcriptomic analyses of extracted DNA or RNA (Wang et al., 2009b; Xie et al., 2011). Based on the genetic results, oligonucleotide probes may be designed to target specific microbial groups using FISH (Pernthaler et al., 2002). Subsequently, FISH-targeted isotopically labeled cells may be evaluated by nanoscale secondary-ion mass spectrometry to link taxonomic groups with functional processes (Orphan et al., 2001). Further enrichment to isolation may be conducted, and single-cell capture with micromanipulator or flow cytometry followed by single-cell sequencing may also be performed (Zhang et al., 2006).

#### Target 4

- Metabolic group: aerobic autotrophic carbon fixers from basement rocks.
- Procedure: rock fragments were broken into smaller pieces using sterile Xpress hydraulic press devices. Smaller rock fragments (~5 cm<sup>3</sup>) were transferred to glass serum vials, covered with sterile filtered aerobic surface seawater amended with <sup>13</sup>C-labeled sodium bicarbonate at a concentration

of 1–2 mM, and sealed without headspace. Enrichments will be incubated for various time periods (up to 6 months) following methods described previously (Expedition 330 Scientists, 2012). At the end of each time period, samples will be collected for determining <sup>13</sup>C incorporation into bulk organic matter. Samples exhibiting significant incorporation will subsequently be analyzed by molecular methods (density gradient centrifugation of extracted DNA) to identify active microbial populations.

#### Target 5

- Metabolic group(s): methanogens, sulfate reducers, sulfide oxidizers, and nitrate-reducing iron-oxidizing bacteria from basement.
- Procedure: rock fragments were broken into smaller pieces using a flame-sterilized metal rock crusher. Smaller rock fragments (~3 g) were transferred to 160 mL glass serum vials, covered with 60 mL of media, sealed with a butyl rubber stopper, and incubated in the dark at 10°C. Cultures were inoculated in the anaerobic chamber.
  - Media for methanogenic enrichments consisted of 500 mL of autoclaved surface seawater (from Site 395) amended with 5 mL Wolfe's mineral solution, 5 mL Wolfe's vitamin solution, 10 mL methanol, and 5 mg resazurin.
  - Media for sulfate reducers was the same, with the substitution of 1 g sodium acetate for the methanol. Media was boiled and then transferred to an anaerobic glove box to purge with O<sub>2</sub>-free nitrogen gas.
  - Media for sulfide oxidizers consisted of autoclaved seawater amended with potassium nitrate (0.5 g/L) and potassium phosphate (0.5 g/L), which was filter-sterilized and added to 160 mL serum vials containing a 20 mL sulfide-rich (1 mM) agar plug.
  - Media for nitrate-reducing iron-oxidizing bacteria was similar to the base media for sulfide oxidizers (without the agar plug), with the addition of 0.5 g steel wool (as an iron source).

#### Target 6

- Metabolic group(s): aerobic iron-oxidizing bacteria and anaerobic heterotrophs from Hole 395A CORK rust and thermistor cable.
- Procedure: six 150 mL serum bottles were filled with 60 mL autoclaved and filter-sterilized seawater. Each was stoppered, brought to a semirapid boil, and maintained at boiling for 5 min with a 22.5 gauge needle as a pressure outlet. After 5 min another needle was inserted, from which flowed nitrogen gas at 2–4 psi. The bottle was then

flushed with nitrogen while boiling for 5 min. At this point, both needles were removed and the bottles were sealed and allowed to cool on the bench top. In an anaerobic chamber, a “tip of spatula” amount of material from the CORK remotely operated vehicle platform Area 9D and Packer 1 samples (see Tables T5, T7, both in the “Site 395” chapter [Expedition 336 Scientists, 2012b]) were added into two bottles each. Additionally, the ThermStr-5 sample, representing a mid-depth string sample, was shaken in a Whirl-Pak bag with 50 mL of autoclaved seawater. The bag was then vortexed for 90 s to shake loose any colonizing microbes on the external polyethylene rope. One milliliter of this water was used as inoculum in one bottle. After inoculation, 0.25 g of steel wool was added to all bottles, and 15% of headspace was replaced with pure O<sub>2</sub>. One bottle was treated as a negative control.

#### Target 7

- Metabolic group(s): aerobic and anaerobic heterotrophic groups from sediment and basement.
- Procedure: basement material and sediment were used as inoculum for enrichment assays for heterotrophy. Prior to addition, basement samples were crushed inside a flame-sterilized stainless steel cylinder mortar to coarse grain size. A total of 2 g sediment or 2.5 g basement material was transferred in duplicate to 30 mL serum vials containing one of three autoclaved media types: 1× Difco 2216 marine media, 1/100× Difco 2216 marine media, or 1/100× Difco 2216 marine media with 0.5 g pyrite. An additional set of the pyrite-enriched media was made and autoclaved to provide a kill control to differentiate abiotic and biotic effects on the pyrite. A representative vial from each media type remained basalt free to provide a negative control. All vials were incubated in the dark at 4°C.

#### Target 8

- Metabolic group: methanogens, sulfate reducers, sulfur oxidizers, and methanotrophs in sediments.
- Procedure: two syringes of sediment were subsampled from each whole-round core (10 cm long). One syringe was used for cultivation and the other was used for DNA analysis as an advance inspection for cultivation. Before subsampling took place, the sectional surface was cut off. The syringe samples were taken from the central part of the core. A syringe sample (10 cm<sup>3</sup>) for cultivation was put into a 100 mL glass bottle and immediately flashed with nitrogen gas to remove oxygen. After the bottle was sealed tightly with a

butyl rubber stopper, it was stored at 4°C until processing in the shore-based laboratory. The other syringe sample (5 cm<sup>3</sup>) for a DNA analysis was put into a 15 mL plastic tube and frozen at –80°C. Target microbial groups will be cultivated using the same methods as those used for the rock samples. The additional cultivation targets for sediment are aerobic methanotrophs, which will be cultivated as described elsewhere (Hirayama et al., 2007). The basic medium outlined in Table T4 will be used for methanotrophs, and the gas phase in the tubes will be prepared as CH<sub>4</sub> (45%) + N<sub>2</sub> (40%) + CO<sub>2</sub> (10%) + O<sub>2</sub> (5%) (2 atm). The incubation temperatures will be 4°–15°C.

#### Onshore sample requests

Sediment samples were collected for multiple onshore sample requests. Requests included both molecular and culture-based analysis. These requests were fulfilled when they complemented without overlapping the work being conducted by the onboard science party. These plans included nitrogen-based culturing, colony-forming units, lipid and fatty acid analysis, and phosphorus-cycling measurements. Sediment samples were collected approximately once per core for each of the four requests and preserved at either 4° or –80°C, as instructed (Figs. F8, F9, F10, F11). Additional samples were collected using a syringe from the top of selected sections (Fig. F12).

#### Physical properties

The material recovered during Expedition 336 was characterized by physical properties measurements. Most of the techniques used are noninvasive and allow correlation of the recovered material to the seismic and logging data. The two different types of material (hard rock and sediment) handled during this expedition were processed similarly, except where indicated in this report. A sketch of the core flow is provided for both: hard rock (Fig. F13) and sediment (Fig. F14). Please note that time estimates provided are for individual core sections.

Whole-round cores were placed in the core laboratory for 3 h (hard rock) or 4 h (sediment) to allow thermal equilibration at room temperature. Because oxygen measurements were done first for all sections of sediment recovered, the equilibration time for sediment was sometimes longer. Core sections longer than 8 cm were run through the Whole-Round Multisensor Logger (WRMSL) to measure gamma ray attenuation (GRA) density, magnetic susceptibility (MS), and *P*-wave velocity. During previous expeditions, the WRMSL also included a noncontact resistivity

detector, but this piece of equipment was not on board the ship during Expedition 336. The *P*-wave logger (PWL) was turned off for hard rock cores because poor coupling between the liner and core material made meaningful measurements impossible. Whole-round images were taken of the entire surface of large rock pieces.

Sections longer than 50 cm were logged with the Natural Gamma Radiation Logger (NGRL), and total counts of NGR were obtained. Absolute concentrations of  $^{40}\text{K}$  were obtained for both sediment and hard rock cores by calibrating the instrument using standards for this element.

Measurements of thermal conductivity were taken with the TK04 thermal conductivity meter on the archive halves of hard rock cores. This measurement was not performed on sediment cores because the high water content made it impossible to register values with the probe.

Sediment and hard rock cores were split into archive and working halves after measurements were taken on the WRMSL and NGRL. The archive halves of sediment cores were then scanned on the SHIL and run through the Section Half Multisensor Logger (SHMSL) to measure point magnetic susceptibility (MSP) and color reflectance. MSP was measured with a Bartington MS2E1 contact sensor probe. Color reflectance was also measured on this logger with an Ocean Optics photospectrometer. A laser on the SHMSL recorded piece heights and located gaps and cracks in the cores. Hard rock pieces were accommodated for this track with pieces of foam that helped the sensors land, avoiding piece tilting in most cases. The instrument software uses the laser estimations to avoid gaps between rocks. The data were also filtered for gaps not detected by the laser (see [“Data processing and filtering”](#)). Additionally, formation factor was calculated; however, this was only done on sediment working halves.

Discrete samples of both sediment and hard rock were processed for moisture and density (MAD). Hard rock samples were selected on the basis of lithology and degree of alteration to be representative of the lithologic units. Sediment samples were taken at a rate of one per section in representative areas. MAD measurements included bulk density, dry density, grain density, water content, void ratio, and porosity. Compressional *P*-wave measurements were taken for the three axes of the cube sample (hard rock) or the core half (sediment) on the Gantry system. Sediment working half samples were measured for *P*-wave velocity using the caliper and occasionally the bayonets (Hole U1383D). A more comprehensive description of the physical properties procedure can be found in *Technical Note 26* (Blum, 1997).

All of the physical properties data recovered were uploaded to the LIMS database. The data were visually double-checked at the end of the process using LIMSpeak beta version.

### Whole-Round Multisensor Logger measurements

MS, GRA density, and *P*-wave velocity (sediment only) were measured simultaneously with the three sensors at sampling intervals of 1 cm, with a time integration of 5 s for each measurement. A freshwater-filled section standard was run after each core for quality control to verify the calibration of the GRA densitometer and the PWL. Calibration for the GRA densitometer was performed with aluminum and water standards. GRA and MS measurements on hard rock underestimate the real value because the method assumes that cores fill the entire volume of the core liner, which never occurs in hard rock cores. However, this underestimation can be corrected if the diameter of the core is taken into account. Hard rock cores have in general a smaller diameter (~58 mm) than the internal diameter of the core liner (66 mm), which can be corrected by multiplying the system output by  $^{66}_{58} = 1.138$  (Jarrard and Kerneklian, 2007). MS and GRA data were filtered with a MATLAB code written during Expedition 336 to eliminate poor-quality data originating from cracks and gaps in recovery. A correction for the diameter of the samples was also included in the data process. The diameter of sediment cores was considered to be 66 mm, whereas the diameter of hard rock cores was considered to be 58 mm.

### GRA bulk density

The bulk density of a material is defined as its mass divided by the volume it occupies. This measurement depends on the compaction of the material and therefore is susceptible to changes due to handling. GRA density is measured on the WRMSL with a beam of collimated gamma rays from a 10 mCi  $^{137}\text{Cs}$  source with a gamma photopeak at 662 KeV. The gamma rays pass through the core sample and are detected on the opposite side of the liner. The Compton scattering experienced by the gamma rays attenuates their energy as they pass through the sample. The number of photons that travel through the sample without attenuation can be detected and used to calculate the bulk density of the sediment. The instrument has a 3 mm collimator that focuses the area of incidence of the gamma ray beam on the core. The detector of the system is a 3 inch diameter  $\times$  3 inch thick NaI(Tl) crystal scintillator with an integrated PMT tube. During Expedition 336 this instrument was used to take measurements of the whole-round core at a rate of one per centimeter.

The bulk density of a sample was calculated as

$$\rho = (1/\mu d)\ln(I_0/I),$$

where

- $\rho$  = the bulk density of the sample,
- $\mu$  = the Compton attenuation coefficient,
- $d$  = the sample diameter (assumed to be ~66 mm for sediment and ~58 mm for hard rock),
- $I_0$  = the gamma source intensity, and
- $I$  = the measured intensity received by the detection system.

Bulk density was calculated on the basis of intensities measured through GRA calibration. Hard rock measurements were corrected afterward for the difference in sample diameter (e.g., Jarrard and Kernekian, 2007).

A core liner filled with distilled water and an aluminum standard was used to calibrate this instrument before each hole and when needed (e.g., if the data obtained for the freshwater standard run after each core presented an error >1%–2%). Bulk density was registered in grams per cubic centimeter.

### Magnetic susceptibility

Magnetic susceptibility indicates the response of a material to a known external magnetic field:

$$K = M/H,$$

where

- $K$  = magnetic susceptibility,
- $M$  = the magnetization induced in the material, and
- $H$  = the magnetic field strength.

Based on its response to the magnetic field, a material can be paramagnetic, ferromagnetic, ferrimagnetic, antiferromagnetic, or diamagnetic. Magnetic susceptibility measurements are useful in identifying a material's composition.

A Bartington loop sensor (MS2C) on the WRMSL track measured the magnetic susceptibility of both sediment and hard rock cores. In this system a low-intensity (~80 A/m root mean square [RMS]) magnetic field operating at 0.565 kHz is applied to the material in the core. The magnetic susceptibility of the sample is then calculated and corrected on the basis of an empirical relation for the difference in diameter of the core (66 mm) versus the loop sensor (88 mm) (see MS2 Magnetic Susceptibility System operation manual, [www.bartington.com/operation-manuals.html](http://www.bartington.com/operation-manuals.html)).

The magnetic susceptibility of core pieces shorter than 8 cm cannot be accurately determined because the resolution of this method is  $\pm 4$  cm. Data from

samples with gaps or fractures were filtered from the data set.

The MS2C coil is calibrated by the manufacturer; hence, no calibrations were done on this equipment offshore. The results are expressed in  $10^{-5}$  SI units. The MS2 recorder attached to the SHMSL has an output threshold of 9999 SI and truncates the most significant digit for higher measurements. Data were filtered for both sediment and hard rock cores (see “Data processing and filtering”).

### P-wave logger

The PWL was used only for sediment cores and was deactivated during the processing of hard rock whole rounds because of the inaccuracy that the separation between the rock and liner creates. The system uses Olympus-NDT Microscan delay line transducers that transmit at 0.5 MHz. The system is automatized to take the value of the peak of first arrival of the *P*-wave. However, 10,000 measurements of amplitude versus time of the wave are taken and stored in case reanalysis is needed. The distance between transducers was measured with a built-in linear voltage displacement transformer (LDVT).

Calibration was done when necessary by using a standard acrylic cylinder with different diameters to take measurements. The values for the different diameters should present a known *P*-wave velocity of  $2750 \pm 20$  m/s and a linear relation between measurements of the different diameters. After each core (or each section of hard rock core), a water-filled standard was used to push the last section and a measurement was taken on it to crosscheck the calibration. When the value for this water standard differed by >2% of 1500 m/s, recalibration was performed.

The time delay from calibration is subtracted from the measured arrival time to give a traveltime of the *P*-wave through the sample. The thickness of the sample is automatically divided by the traveltime to calculate *P*-wave velocity in meters per second.

### Natural Gamma Radiation Logger

NGR from sediment and hard rock cores is the result of the decay of  $^{238}\text{U}$ ,  $^{232}\text{Th}$ , and  $^{40}\text{K}$  isotopes. The NGR detector used during Expedition 336 was designed by Texas A&M (Vasiliev et al., 2011) and installed on board the *JOIDES Resolution* in 2009. Eight 4 inch NaI (TI) custom-shaped detectors simultaneously measure adjacent sections of the recovered material. Each detector center is separated by 20 cm from the next. Each detector PMT is attached to an ORTEC ScintiPack-296, which maximizes counting times and minimizes error in the limited time available

during core flow for this instrument (~10 min per core section). Two types of shielding are used in this instrument to reduce background noise. Low-activity passive lead spacers act as shields in between detectors. Lead plugs are also placed between each PMT and the Scintipack to reduce the  $^{40}\text{K}$  gamma background from the internal parts of the Scintipack. The passive shielding above and around the detectors also reduces the electromagnetic showers generated by cosmic rays and environmental gamma rays. Active shielding can reduce the background created by the high-energy part of cosmic rays and cosmic muons. Because of the implemented energy threshold, the NaI scintillators do not detect gamma rays with energy below 100 keV and thus are not affected by X-rays created by the cosmic rays in the passive lead shielding. The data acquisition and readout systems were assembled from commercial modules produced by ORTEC, Phillips Scientific, and CAEN. The data acquisition logic was adapted for low counting rates on the basis of empirical data (Vasiliev et al., 2011).

The interface allows users to set experimental parameters. The data collected are comparable with previous data from IODP and logging data. The detector counts were summed for the range (100–3000 keV). Background counts were done on an empty core liner for 5 h after our arrival at each site. NGR measurements were taken every 20 cm on the recovered material for both sediment and hard rock cores. The system averages the NGR over 46 cm (23 cm on each side of the detector), making more intense coverage too time-intensive and not extremely scientifically beneficial. Longer detection periods give more accurate values than shorter measurements at higher spatial resolution. The counting time was set to 2 h per section for hard rock cores and 30 min per section for sediment. These detection periods were chosen to balance good counting statistics with optimal core flow.

Sample location accuracy, as with other physical properties systems, is determined within millimeters and averaged over 46 cm surrounding the detector. The detector has enough resolution to identify the energy contributions of  $^{238}\text{U}$ ,  $^{232}\text{Th}$ , and  $^{40}\text{K}$  in marine sediments and rocks, even with low count records. NGR measurements can be related to geological strata and the geochemistry of the recovered material. NGR measurements can also help to correlate the core material recovered with the downhole logs and adjacent boreholes (Michibayashi et al., 2008).

The NGR detector unit was energy-calibrated using  $^{137}\text{Cs}$  and  $^{60}\text{Co}$  sources and identifying the peaks at 662 and 1330 keV, respectively (calibration materials are from Eckert and Ziegler Isotope Products, USA). Calibration standards of  $^{40}\text{K}$  and  $^{232}\text{Th}$  were run for

each detector so that quantitative spectral analysis could be performed. Obtaining quantitative values for  $^{40}\text{K}$ ,  $^{232}\text{Th}$ , and  $^{238}\text{U}$  can help with future quantification of the radionuclide daughters (International Atomic Energy Agency, 2003).

Edge effects due to the geometry of the core and the geometry of the system are unavoidable. Corrections were applied when the core edge was between 0 and 18 cm away from the center of the detector. Initial data reduction is automatically performed by the system's software. A density function based on NGR detection for the instrument's geometry was used to calculate the potassium values. The GRA density data were used as an indicator of the distribution of the core pieces. This is particularly useful in hard rock cores.

### Thermal conductivity

Thermal conductivity is the rate at which heat flows through a material and depends on the material temperature, pressure, composition, porosity, structure, and type of saturating fluid. Thermal conductivity is calculated on the basis of a heating curve, which is temperature versus time of the probe. The thermal conductivity calculation for steady state is

$$k_a(t) = (q/4\pi) \{[\ln(t_2) - \ln(t_1)]/[T(t_2) - T(t_1)]\},$$

where

$k_a(t)$  = apparent thermal conductivity for long time intervals,

$q$  = heat flux downgradient,

$t$  = time, and

$T$  = temperature corresponding to time intervals.

Because the correct time intervals are difficult to choose, the system analyzes the heating curve data by using the "special approximation method (SAM) algorithm" (see TK04 Thermal Conductivity Meter User's Manual, [www.te-ka.de/de/pdf/TK04-Manual.pdf](http://www.te-ka.de/de/pdf/TK04-Manual.pdf)). This algorithm divides the heating curve into several thousand time intervals and determines the thermal conductivity for each one. Finally, the software automatically chooses the least disturbed of the solutions.

Thermal conductivity measurements were performed on split samples of hard rock cores with a TK04 system. No measurements were taken for sediment cores because they contained excessive fluid and this measurement can be strongly affected by convection in sediment cores. Measurement attempts in nearly all sections of the first sediment core were unsuccessful.

The archive halves of hard rock cores were used for thermal conductivity measurements. The probe was used in half-space mode, where a needle probe is embedded in the surface of an acrylic glass block with

low thermal conductivity (0.184 W/[m·K]). Samples were polished before use. After the samples were saturated in seawater under vacuum at room temperature over 24 h, both the sample and probe were isolated in an extruded polystyrene foam-covered seawater bath for at least 15 min prior to measurement in order to eliminate the effect of drafts in the laboratory. Before each measurement, the temperature of the core was monitored to ensure that the drift was  $<0.04^{\circ}\text{C}/\text{min}$ . The different probes have specific configurations and calibrations that are integrated into the software. Heating power and time were input by the user so that the heating power was approximately twice the value of the expected thermal conductivity. Measuring time was set to 80 s. The manufacturer suggests smoothing the split surface with 120–320 gauge silicon carbide powder to improve the contact of the probe. For preservation reasons, no silicon gel can be used to improve contact when this measurement is taken in archive samples.

Thermal conductivity was measured at least once per core section when the pieces recovered had sufficient length ( $>6$  cm) to avoid edge effects. When time and sample constraints allowed, several measurements per section were taken. Three repeated measurements were done per sample and the mean and standard deviation was calculated. The measurements were not mathematically corrected for subseafloor conditions.

### Section Half Multisensor Logger measurements

The SHMSL is the next step in the core flow after splitting the core. In this part of the process the archive halves are scanned on the SHIL to produce a high-resolution image. Color reflectance spectra and MSP are measured on the SHMSL every centimeter. A laser sensor detects the height of the sample and locates the end of the section.

#### Color reflectance spectrometry

An Ocean Optics, Inc., system was used to measure UV to near-infrared light using a halogen light source. Measurements were taken every centimeter, and each measurement took  $\sim 5$  s. Resolution was one measurement per 1 cm on hard rock cores and at least one measurement per 2 cm on sediment cores.

In general, the results from this instrument are given as luminescence ( $L^*$ ) and color indexes  $a^*$  (green to red; green being negative and red being positive) and  $b^*$  (blue to yellow; blue being negative and yellow being positive). The ratio  $a^*/b^*$  was also calculated for all boreholes because it can be used as a better proxy to identify changes in sediment characteristics than the independent  $a^*$  and  $b^*$  values. Although

this is the most general output of results, the system also records spectral data at a 2 nm resolution in the range of 380–900 nm wavelengths and tristimulus values for  $x$ -,  $y$ -, and  $z$ -axes. All of the raw data were uploaded to the database.

Calibration was performed with two main sources, black and white, every  $\sim 12$  h. When sediment cores were processed, the material was covered with plastic film to avoid fouling the sensor with sediment. Hard rock cores were not covered.

#### Point magnetic susceptibility

A Bartington MS2E contact probe was used to take MSP measurements. The probe has a flat 15 mm diameter sensor operating at a frequency of 0.580 kHz. Measurements were taken every centimeter at a rate of one per second. Three measurements were taken and averaged to obtain a final value with an accuracy of 5%. Point measurements are more accurate than those obtained from whole-round cores. The area of response of the MS2E sensor is 3.8 mm  $\times$  10.5 mm, with a depth response of 50% at 1 mm and 10% at 3.5 mm (see MS2 Magnetic Susceptibility System operation manual, [www.bartington.com/operation-manuals.html](http://www.bartington.com/operation-manuals.html)). This response makes the system capable of measuring core fragments smaller than 8 cm, which cannot be done with the whole-round system.

The probe takes a measurement in air before each actual measurement, and from this the software performs an automatic correction.

The instrument is calibrated so that the value output is measured assuming the probe is buried in the sample; however, because the probe is only in contact with the upper, flat surface, a correction factor of 2 is automatically applied by the software. No other corrections are needed for this system.

SI dimensionless units are used for the results, making them comparable to the ones obtained in the first part of the core flow. The system was calibrated every  $\sim 12$  h for MSP. No calibration was done for the loop in the WRMSL because this sensor is master calibrated by the manufacturer.

The MS2 recorder attached to the SHMSL has an output threshold of 9999 SI and truncates the most significant digit for higher measurements. Data for this system were filtered on the basis of the color reflectance spectra calculated on the same track.

#### Formation factor measurements

Measurements of electrical conductivity were taken approximately every 10 cm on sediment cores from Sites U1382B, U1383D, and U1384A. The formation factor of the sediment was calculated based on electrical resistivity measurements. Two platinum electrodes

~1 cm long in a nonconductive Teflon piece connected to a Metrohm 712 system were used for this measurement. This system was successfully used for the same type of measurements during Expedition 329 (Expedition 329 Scientists, 2011a). Temperature was also measured at each location. A standard of IAPSO seawater was used before and after measurements had been taken on each section to detrend the wasting of the electrodes. Temperature was also measured on the IAPSO standard. Areas of the core with disturbed sediment, gravel, or sandy textures were avoided because the electrodes could be damaged and the measurements would not give reliable values. All the electrical conductivity values (inverse of electrical resistivity) were adjusted to a standard temperature of 20°C by a fifth-order polynomial (Janz and Singer, 1975),

$$\chi = a + bT + cT^2 + dT^3 + eT^4 + fT^5,$$

where

$$\begin{aligned} a &= 29.05128, \\ b &= 0.88082, \\ c &= -0.000198312, \\ d &= 0.00033363, \\ e &= -0.000010776, \text{ and} \\ f &= 0.000000112518. \end{aligned}$$

Both seawater and sediment measurements were corrected for the effect of temperature. The formation factor was calculated as

$$F = \chi_{\text{IAPSO}} / \chi_{\text{sed}}.$$

This method is useful as a proxy for tortuosity in high-porosity sediments where surface conductivity effects are not a major component.

### Discrete sample measurements

Cubic samples (~7 cm<sup>3</sup>) were cut from the working halves of hard rock cores at an approximate frequency of one per lithologic unit. Alteration of the sample was taken into account when selecting samples. The different lithologies were sampled in order to obtain a good representation of the entire borehole. Hard rock samples were selected on the basis of the amount of material recovered and the prioritization of other sample types. Samples taken for physical properties were used for both *P*-wave discrete measurements on the three axes of the sample and for MAD measurements. No paleomagnetism measurements were conducted during Expedition 336, so the discrete samples taken were used solely for physical properties data acquisition.

MAD sediment samples were taken with a syringe at a rate of one per core section. The samples were care-

fully chosen to be representative of the stratigraphy of the core.

### Compressional *P*-wave velocity discrete measurements

Sediment samples can be measured with three sensors, one in each of the three-dimensional axes; however, because of time constraints, only the caliper was used for the recovered cores.

*P*-wave velocity measurements of hard rock were performed during the MAD process, which saved time during the physical properties processing. Seawater-saturated samples were used for wet mass determinations immediately before *P*-wave measurements. The rest of the MAD process took place after *P*-wave measurement. *P*-wave velocities for the three axes were measured by changing the orientation of the samples in the *x*-axis caliper contact transducers on the *P*-wave velocity gantry.

The transducers used by this system are the same as those used for the whole rounds; however, the software and optimizations used to calculate the *P*-wave are different. The discrete measuring system has an amplifier that provides an improved signal-to-noise ratio compared to that provided by the whole-round system. The discrete measurements register the wave preinverted (and therefore are more accurate). To maximize contact with the transducers, deionized water was applied to the sample surfaces and water-saturated hard rock samples were used.

Velocity measurements on calibration standard cylinders were taken as often as necessary. The calibration was made with acrylic cylinders of differing thicknesses and a known *P*-wave velocity of 2750 ± 20 m/s. The distance between transducers was measured with a built-in LDVT. The wave was automatically processed to find the first arrival value, but all of the wave amplitude measurements over time were recorded in case reprocessing was needed.

As in the whole-round system, the *P*-wave velocity is directly output by the system in meters per second. Each measurement was repeated three times for data consistency on hard rock samples and only once for sediment samples to avoid disturbance effects.

### Moisture and density measurements

Intergranular water content, bulk density, dry density, porosity, and void ratio were determined on discrete samples. A vacuum water saturator, a dual balance system, and a hexapycnometer were used for these measurements.

The vacuum pump system was used to keep the hard rock samples completely saturated. The samples were kept in a vacuum bath of seawater for at least 24 h.

During this time the system was checked every 4 h to make sure the vacuum was maintained. After this, the samples were kept in sample containers with water to avoid desiccation. Immediately before the measurement was taken, the samples were carefully patted with a paper towel to remove excess water. They were then weighed on the dual balance system to obtain their wet mass.

The dual balance system is composed of two analytical balances (Mettler-Toledo XS204) that compensate for ship motion. One balance acts as a reference, in which a known weight close to the weight of the sample is placed. The sample is placed in the other balance. The balance takes 300 measurements of the sample over a period of 1.5 min (default).

After wet weight was measured on the dual balance system, the sample was placed in a convection oven at  $105^\circ \pm 5^\circ\text{C}$  for >24 h. Once the sample was dried, it was cooled in a desiccator for 30–60 min before dry mass was measured. The sample was placed in the hexapycnometer system to measure dry volume. For sediment samples, premeasured vials were used during the process; the weight of the vial was subtracted from the wet and dry mass of the sample.

The hexapycnometer measures dry sample volume with a nominal precision of  $\pm 0.04\text{ cm}^3$ . The pycnometer increases the amount of helium gas required to maintain a target pressure in the sample chamber. The calculation of dry volume is made by comparing the pressure in the chamber with a known volume reference.

Calibrations of this instrument were done in an adjacent chamber with two stainless steel spheres every time a measurement was taken. Four measurements and a standard were measured simultaneously when possible. A fifth measurement was not performed simultaneously because one of the chambers was defective. The chamber used for the measurement of the standard was different each time in order to test each chamber.

MAD calculations are directly implemented by the software and described in detail in Blum (1997). However, the basic equations are presented here.

Salt correction for mass is defined as

$$M_s = s[(M_w - M_d)/(1 - s)],$$

where

$M_s$  = mass corrected for salinity,

$s$  = salinity,

$M_w$  = wet mass, and

$M_d$  = dry mass.

Grain density is defined as

$$\rho_g = (M_d - M_s)/[V_d - (M_s - \rho_s)],$$

where

$\rho_g$  = grain density,

$V_d$  = dry volume, and

$\rho_s$  = density of salt ( $2.257\text{ g/cm}^3$ ).

The salt-corrected mass of pore water ( $M_{pw}$ ) is defined as

$$M_{pw} = (1/s)M_s.$$

Pore water volume ( $V_{pw}$ ) is defined as

$$V_{pw} = M_{pw}/\rho_{pw},$$

where the density of pore water ( $\rho_{pw}$ ) is assumed to be  $1.024\text{ g/cm}^3$ .

Bulk density ( $\rho_b$ ) is defined as

$$\rho_b = M_w/(V_d + V_{pw}),$$

and porosity ( $\phi$ ) is defined as

$$\phi = V_{pw}/(V_d + V_{pw}).$$

## Data processing and filtering

The physical properties measurements are mainly automatized, making it necessary to filter and discard (“clean”) poor measurements. In order to perform all of the necessary filtering for this expedition, MATLAB codes were written to handle each step of the physical properties process.

### Gamma ray attenuation, magnetic susceptibility, and P-wave filters

The GRA data, particularly for hard rock cores, contain a high number of measurements that are not representative of the real bulk density of the material because of underfilled liners and unsaturated samples. As mentioned previously, a correction was done for the diameter of the core. This correction assumed a ~58 mm diameter for hard rock cores and a ~66 mm diameter for sediment cores. Hard rock cores contain multiple pieces, with gaps in between them. In order to exclude the data from these gaps and cracks, a filter was designed using MATLAB to compare each point with three adjacent points and check if the value obtained for them differs by a small amount (0.15 for hard rock cores and 0.05 for sediment cores). This value was determined by comparing the values obtained from MAD samples. When the points present a higher difference than the aforementioned values, they are filtered out of the data. The filter does this in three steps, initially checking the points farthest away and ending with

the adjacent ones. Different intensities of gray shading have been used in the graphs presented in this volume to indicate these three steps of filtering. Measurements less than the density of water ( $1 \text{ g/cm}^3$ ) were not included in this report because they relate to empty core liners.

MS and *P*-wave velocity data were filtered using the same procedure. Because MS and *P*-wave velocity are measured on the same logger as GRA density, the depths at which data points eliminated (as bad data) by filtering the GRA are likely unreliable in both the MS and *P*-wave velocity data sets. All three sensors measure at the same resolution and location, making it easy to filter all of the data on the basis of GRA values.

The *P*-wave sensor on the WRMSL can have poor contact when measuring sediment cores that will not equate to the site of a poor GRA measurement. Therefore, an extra filtering step was implemented for *P*-wave velocity to eliminate all values less than the velocity of water (1500 m/s).

### Color reflectance and point magnetic susceptibility filters

A MATLAB filter was implemented for the SHMSL on the basis of color reflectance measurements. The color reflectance sensor registers the normalized spectrum of the material. These data are not included in the primary database.

Two different filters were used for hard rock and sediment. When the sensor lands incorrectly on a piece of hard rock, it can tilt the rock, causing light from the surrounding environment to be detected in the spectrum. A filter was implemented that detects peaks at the wavelength of the light in the laboratory where the system is installed. This signal is easily differentiated in hard rock cores but is not as obvious in sediment cores. In sediment cores, therefore, this filter was complemented with an additional filter that checks for unsmooth distributions that indicate poor sensor contact.

MSP was filtered on the basis of the points that were eliminated for color reflectance values, following a similar procedure as that explained for the GRA filters.

## Downhole logging

Downhole logs are used to determine the physical, chemical, and structural properties of the formation penetrated by drilling. The data are rapidly collected, continuous with depth, and measured in situ; they can then be interpreted in terms of stratigraphy, lithology, mineralogy, magnetic characteristics, and geochemical composition of the penetrated forma-

tion. Where core recovery is incomplete or disturbed, log data may provide the only way to characterize the borehole section. Where core recovery is good, log and core data complement one another and may be interpreted jointly.

Downhole logs are sensitive to formation properties on a scale that is intermediate between those obtained from laboratory measurements on core samples and geophysical surveys. They are useful in calibrating the interpretation of geophysical site survey data (e.g., through the use of synthetic seismograms) and provide a necessary link for the integrated understanding of physical properties on all scales.

During Expedition 336, downhole measurements were taken in Holes 395A, U1382A, and U1383C.

### Wireline logging

During wireline logging, measurements were made with a variety of Schlumberger logging tools and the third-party Deep Exploration Biosphere Investigative tool (DEBI-t). These tools were combined into a number tool strings that were run down the hole after coring operations were completed. Five wireline tool strings were used during Expedition 336 (Fig. F15; Table T5):

1. Microbiology combination: gamma ray, temperature, and deep UV-induced fluorescence;
2. Adapted microbiology combination I (AMC I): total gamma ray, density, electrical resistivity, and deep UV-induced fluorescence;
3. Formation MicroScanner (FMS)-Hostile Environment Natural Gamma Ray Sonde (HNGS): spectral and total gamma ray and microresistivity images of the borehole wall;
4. Adapted microbiology combination II (AMC II): total and spectral gamma ray, density, and deep UV-induced fluorescence; and
5. FMS-sonic: spectral and total gamma ray, microresistivity images of the borehole wall, and compressional and shear wave velocities.

Each of these tool strings also contained a telemetry cartridge for communicating through the wireline to the Schlumberger data acquisition system on the drillship. The microbiology tool strings included a number of Lamont telemetry cartridges (MultiFunction Telemetry Module [MFTM], EFTB-Lamont Interface Cartridge [ELIC], and Schlumberger-Lamont Telemetry Adapter [SLTA]; see below), which allow the DEBI-t and Lamont Modular Temperature tool (MTT) to be run in-line with the Schlumberger tools and acquisition system.

In the case of taking downhole measurements in Hole 395A, the hole was not prepared for logging. Here, the

logging string was run immediately after the old CORK was removed. The aim was to log the hole and measure the fluorescence of biomass on the borehole wall; hence, no logging preparation was done because it would have seriously disturbed the borehole.

In preparation for logging at newly drilled sites, the boreholes were cased for CORK installation to 102 and 60.41 m DSF in Holes U1382A and U1383C, respectively. Immediately before logging, the holes were fully prepared for CORK installation; several wiper trips were made until no tight spots were encountered, viscous drilling fluid (sepiolite) was circulated through the drill pipe to the bottom of the hole when significant fill was found, and finally, the hole was displaced with seawater (for detailed information, please see “Operations” in the “Site U1382” and “Site U1383” chapters [Expedition 336 Scientists, 2012c, 2012d]). The tool strings were then lowered downhole by a seven-conductor wireline cable during sequential runs (where applicable). A wireline heave compensator (WHC) was employed when appropriate to minimize the effect of ship heave on tool position in the borehole (see “Wireline heave compensator”). During each logging run, incoming data were recorded and monitored in real time on the MCM MAXIS logging computer. The tool strings were then pulled up at constant speed, typically 200–400 m/h, to provide continuous measurements as a function of depth of several properties simultaneously.

### Logged formation properties and tool measurement principles

The logged properties, and the methods by which the tools measure them, are briefly described below. The main logs taken by the tools are listed in Table T6. More detailed information on individual tools and their geological applications may be found in Serra (1984, 1986, 1989), Schlumberger (1989, 1994), Rider (1996), Goldberg (1997), Lovell et al. (1998), Ellis and Singer (2007), and Robinson et al. (2008). A complete list of acronyms for Schlumberger tools and measurement curves is available at [www.slb.com/modules/mnemonics/index.aspx](http://www.slb.com/modules/mnemonics/index.aspx).

### Borehole temperature

The microbiology tool string included the MTT to measure borehole fluid temperature. The Lamont MTT was designed to be able to resolve centimeter-scale temperature variations at typical logging speeds of 250–300 m/h. It uses a highly accurate resistance-temperature device measurement accuracy of  $\pm 0.5^\circ\text{C}$  over a  $0^\circ\text{--}250^\circ\text{C}$  range and contains an accelerometer for depth correction. The MTT is combined with a specially designed cartridge to allow data transmission through the Schlumberger string and wireline.

One additional temperature measurement was made during some of the logging runs by a sensor included in the logging equipment head-mud temperature (LEH-MT) cablehead and processed by the Enhanced Digital Telemetry Cartridge (EDTC) (see below).

Generally, because logs are recorded shortly after coring, the borehole temperature is highly perturbed by the large amounts of seawater and mud circulated during the drilling process.

### Natural radioactivity

The HNGS, a spectral gamma ray tool, uses two bismuth germanate scintillation detectors and five-window spectroscopy to determine concentrations of  $^{40}\text{K}$ ,  $^{232}\text{Th}$ , and  $^{238}\text{U}$  in the formation. These isotopes and the radioactive decay products of U and Th dominate the natural radiation spectrum. The HNGS filters out gamma ray energies of  $<500$  keV, eliminating sensitivity to bentonite or KCl in the drilling mud and improving measurement accuracy. The computation of the elemental abundances uses a least-squares method of extracting thorium, uranium, and potassium elemental concentrations from the spectral measurements.

The EDTC (see below) used to communicate data to the surface includes a sodium iodide scintillation detector to measure total natural gamma ray emission. It is not a spectral tool, but it provides high-resolution total gamma ray intensities for each pass, which allows for precise depth-match processing between logging runs and passes.

### Density and photoelectric effect

Formation density was determined with the Hostile Environment Litho-Density Sonde (HLDS). The sonde contains a radioactive cesium ( $^{137}\text{Cs}$ ) gamma ray source (622 keV) and far and near gamma ray detectors mounted on a shielded skid, which is pressed against the borehole wall by a hydraulically activated decentralizing arm. Gamma rays emitted by the source undergo Compton scattering, which involves the transfer of energy from the gamma rays to the electrons in the formation via elastic collision. The number of scattered gamma rays that reach the detectors is directly related to the density of electrons in the formation, which is in turn related to bulk density. Porosity may also be derived from this bulk density if the matrix density is known.

The HLDS also measures photoelectric absorption as the photoelectric effect (PEF). Photoelectric absorption of gamma rays occurs when their energy is reduced below 150 keV after being repeatedly scattered by electrons in the formation. Because PEF depends on the atomic number of the elements in the formation,

it also varies according to the chemical composition of the minerals present and therefore can be used to identify some minerals (for example, the PEF of calcite = 5.08 barns per electron [b/e<sup>-</sup>] and quartz = 1.81 b/e<sup>-</sup>). Good contact between the tool and borehole wall is essential for good HLDS logs. Poor contact typically results in underestimation of density values.

### Electrical resistivity

The High-Resolution Laterolog Array (HRLA) tool provides six resistivity measurements with different depths of investigation (including the borehole, or mud resistivity, and five measurements of formation resistivity with increasing penetration into the formation). The sonde sends a focused current into the formation and measures the intensity necessary to maintain a constant drop in voltage across a fixed interval, providing a direct resistivity measurement. The array has one central (source) electrode and six electrodes above and below it, which serve alternatively as focusing and returning current electrodes. By rapidly changing the role of these electrodes, a simultaneous resistivity measurement at six penetration depths is achieved. The tool is designed to ensure that all signals are measured at exactly the same time and tool position and to reduce the sensitivity to “shoulder bed” effects when crossing sharp beds thinner than the electrode spacing. The design of the HRLA, which eliminates the need for a surface reference electrode, improves formation resistivity evaluation compared to the traditional Dual Induction Tool (the sonde conventionally used during IODP expeditions before the first usage of the HRLA during Expedition 335, Hole 1256D).

Typically, silicate minerals found in crustal rocks are electrical insulators, whereas sulfide and oxide minerals as well as ionic solutions like pore water are conductors. In most rocks, electrical conduction occurs primarily by ion transport through pore fluids and thus is strongly dependent on porosity. Electrical resistivity, therefore, can be used to evaluate porosity and fluid salinity.

### Acoustic velocity

The Dipole Shear Sonic Imager (DSI) measures the transit times between sonic transmitters and an array of eight receivers. It combines replicate measurements, thus providing a direct measurement of sound velocity through formations that is relatively free from the effects of formation damage and an enlarged borehole (Schlumberger, 1989). Along with the monopole transmitters found on most sonic tools, it also has two crossed-dipole transmitters, which allow measurement of shear wave velocity in addition to compressional wave velocity. Dipole measurements are

necessary to measure shear velocities in slow formations whose shear velocity is less than the velocity of sound in the borehole fluid. Such slow formations are typically encountered in deep ocean drilling (e.g., the sediments overlying igneous basement at Expedition 336 sites; however, these sediments were in the cased hole section and were not measured).

### Fluorescence

The DEBI-t was designed and built specifically for Expedition 336 to better our understanding of the nature of microbial communities harbored in young ridge flanks, to understand their role in ocean crust weathering, and to elucidate whether these deep-seated microbial communities are acquired or indigenous. The DEBI-t was supported by the University of Southern California and developed by Photon Systems, Inc., Caltech’s Jet Propulsion Laboratory, and Lamont-Doherty Earth Observatory (LDEO). This unique tool is based on deep UV (<250 nm) laser detection of biological material and is designed here to assess the relative bioload of the borehole wall and aid in the effective targeting and deployment of the microbiology observatories. The DEBI-t utilizes a 224 nm excitation source and detects fluorescence between 280 and 380 nm. It is equipped with a pin-hole camera that records video of the borehole in order to provide spatial context to the fluorescence information (see Table T7 for DEBI-t specifications).

The original microbiology combination tool string obtains a number of parameters in addition to native fluorescence, including three-axis downhole acceleration, three-axis magnetic field, temperature, and total and spectral (Th, U, and K) gamma ray measurements. The DEBI-t operates with a “fire and forget” methodology, in which the control software directs the instrument to fire the laser, collect data, and transmit information uphole as soon as power is supplied. Power is supplied via a 24 V power supply in the LDEO MFTM. The MFTM also acts as part of the communications interface between the DEBI-t and the Schlumberger wireline tools. During logging operations, the DEBI-t transmits real-time clock, laser power, and detector status to provide information regarding the health of the system. Transmission of these data is initiated by a request from the MFTM. There is no real-time shipboard control over any of the instrument parameters. However, the ability to monitor instrument status in real time allows us to power cycle the DEBI-t while still in the borehole, should the need arise. The transmitted data are logged against depth and used to depth-match the data recorded to the memory card in the DEBI-t, which is logged against time.

The DEBI-t is rated to operate at a maximum pressure of 10,000 psi, and the electronics and optics in

analogous systems have been operated successfully at temperatures between 0° and >40°C. Standard procedure is to log down through the seafloor to the bottom of the open hole, log back up, log all the way down to total depth, and then finally log all the way back up through the seafloor.

### Formation MicroScanner

The FMS provides high-resolution electrical resistivity-based images of borehole walls. The tool has four orthogonal arms and pads, each containing 16 button electrodes that are pressed against the borehole wall during recording. The electrodes are arranged in two diagonally offset rows of eight electrodes each. A focused current is emitted from the button electrodes into the formation, with a return electrode near the top of the tool. Resistivity of the formation at the button electrodes is derived from the intensity of current passing through the button electrodes. Processing transforms these measurements into oriented high-resolution images that reveal the geologic structures of the borehole wall. Further analysis can provide measurements of dip and direction (azimuth) of planar features in the formation.

The development of the FMS tool has added a new dimension to wireline logging (Luthi, 1990; Salimullah and Stow, 1992; Lovell et al., 1998). Features such as vesicles, veins, fractures, and volcanoclastic breccia can be resolved, and the fact that the images are oriented means that fabric analysis can be carried out and structural feature (e.g., fracture) orientations can be measured. If the same features in these high-resolution electrical images can be identified in the recovered core samples, individual core pieces can be reoriented with respect to true north.

The maximum extension of the caliper arms is 38.1 cm (15 inches). In holes with a diameter of >38.1 cm, the pad contact at the end of the caliper arms will be inconsistent and the FMS images may appear out of focus and too conductive. Irregular (rough) borehole walls will also adversely affect the images if contact with the wall is poor. Standard procedure is to make two full passes up the borehole with the FMS to maximize the chance of getting optimal borehole coverage with the pads.

### Borehole inclination and magnetic field measurement

Three-component acceleration and magnetic field measurements were made with the General Purpose Inclinometry Tool (GPIT). The primary purpose of this tool, which incorporates a three-component accelerometer and a three-component magnetometer, is to determine the acceleration and orientation of

the FMS-sonic tool string during logging. This information allows the FMS images to be corrected for irregular tool motion and the dip and direction (azimuth) of features in the images to be determined. The GPIT can be run with other tools as part of other tool strings that can carry remanent or induced magnetization; therefore, its magnetic measurements can sometimes be affected. However, on the FMS-sonic tool string, the GPIT has greater nonmagnetic insulation from the other tools, which greatly reduces the effects on its magnetic measurements. On the microbiology combination tool string, nonmagnetic knuckle joints were placed either side of the GPIT to improve the tool's insulation.

### Auxiliary logging equipment

#### *Cablehead*

The Schlumberger LEH-MT and logging equipment head-q tension (LEH-QT) measures tension at the very top of the wireline tool string, which helps diagnose difficulties in running the tool string up or down the borehole or when exiting or entering the drill string or casing. Additionally, the LEH-MT cablehead includes a temperature sensor on its outside to measure borehole fluid temperature.

#### *Telemetry cartridges*

Telemetry cartridges are used in each tool string to allow the data to be transmitted from the tools to the surface. In addition, the EDTC includes a sodium iodide scintillation detector to measure the total natural gamma ray emission of the formation. (The EDTC also contains an accelerometer that provides data to optimize the WHC before logging begins and to acquire the best possible downhole data.) The temperature measurements made by the LEH-MT are also processed by the EDTC before being sent to the surface for real-time monitoring. Because non-Schlumberger tools were run during Expedition 336 logging, several telemetry cartridges were required to allow communication with the Schlumberger telemetry and permit wireline transmission of data collected to the Schlumberger acquisition unit. A Lamont MFTM and ELIC were placed above the DEBI-t to provide 24 V power to the tool and to allow this third-party tool to run on Schlumberger telemetry. The SLTA was placed above the Lamont MTT in order to facilitate running this tool in combination with Schlumberger tools.

#### *Joints and adapters*

Because the tool strings combine tools of different generations and with various designs, they include several adapters and isolation joints between individual tools to allow communication, avoid interferences

(mechanical, acoustic, or electrical), or position the tool properly in the borehole. The knuckle joints in particular are used to isolate the GPIT tool from magnetized/potentially magnetic portions of the surrounding tool string (microbiology combination tool string) or to decouple the remainder of the centralized tool string (AMC II) from the overlying HLDS sonde that is pressed against the borehole wall by a caliper arm and bowspring.

All of these additions are included and contribute to the total length of the tool strings in Figure F15.

### Logging data quality

The principal influence on log data quality is the condition of the borehole wall. If the borehole diameter is variable over short intervals (resulting from washouts during drilling or ledges caused by layers of harder material) the logs from some tools (e.g., FMS, density, and porosity tools) may be degraded. Deep (0.23–1.5 m) investigation measurements such as resistivity and sonic velocity, which do not require contact with the borehole wall, are generally less sensitive to borehole conditions. Very narrow bridged sections also cause irregular log results. The quality of the borehole is improved by minimizing the circulation of drilling fluid while drilling, flushing the borehole to remove debris, performing a full wiper trip, and logging as soon as possible after drilling and conditioning are completed.

The quality of the depth determination depends on a series of factors. The depth of the wireline-logged measurement is determined from the length of the logging cable paid out at the winch on the ship. The seafloor is identified on the natural gamma ray log by the abrupt decrease in gamma ray count at the sediment/water interface (“mudline”). Discrepancies between drilling and core depth and wireline log depth occur because of core expansion, incomplete core recovery, incomplete heave compensation, and drill pipe stretch, in the case of drilling depth. In the case of log depth, discrepancies occur because of incomplete heave compensation, incomplete correction for cable stretch, and cable slip. Tidal changes in sea level also have an effect. To minimize the wireline tool motion caused by ship heave, a hydraulic WHC (see below) was used (when appropriate) to adjust the wireline length for rig motion during wireline logging operations.

### Wireline heave compensator

The WHC system, which was first used during Expedition 320T (February 2009), is designed to compensate for the vertical motion of the ship and maintain a steady motion of the logging tools. It uses vertical

acceleration measurements made by a motion reference unit (MRU), located under the rig floor near the center of gravity of the ship, to calculate the vertical motion of the ship. It then adjusts the length of the wireline by varying the distance between two sets of pulleys through which the cable passes. Real-time measurements of uphole (surface) and downhole acceleration are made simultaneously by the MRU and the EDTC, respectively. An LDEO-developed software package allows these data to be analyzed and compared in real time, displaying the actual motion of the logging tool string and enabling the efficiency of the compensator to be monitored. In addition to an improved design and smaller footprint compared to the previous system, the location of the WHC with the winch unit on the starboard side of the derrick contributes to a significant reduction in the time necessary to prepare for logging operations.

### Logging data flow and log depth scales

Data for each wireline logging run were monitored in real time and recorded using the Schlumberger MAXIS 500 system. The initial logging data were referenced to the rig floor (WRF). After logging was completed, the data were shifted to a seafloor reference (WSF), which is based on the step in gamma radiation at the sediment/water interface.

The data were transferred on shore to LDEO, where standardized data processing took place. The main part of the processing is depth matching to remove depth offsets between data from different logging runs. This processing results in a new depth scale, wireline log matched depth below seafloor (WMSF). Also, corrections are made to certain tools and logs (e.g., FMS imagery is corrected for tool acceleration, including sonde “stick and slip”), documentation for the logs (with an assessment of log quality) is prepared, and the data are converted to ASCII for conventional logs and GIF for FMS images. The Schlumberger GeoQuest GeoFrame software package is used for most of the processing of all wireline logging data collected. The data were transferred back to the ship within a few days of logging, and the processed data set was made available to the science party (in ASCII and Digital Log Interchange Standard [DLIS] formats) through the shipboard IODP logging database and shipboard servers. This LDEO depth-matched data were used to depth-shift the fluorescence data written to memory in the DEBI-t on the ship.

## References

- Benzerara, K., Menguy, N., López-García, P., Yoon, T.-H., Kazmierczak, J., Tyliszczak, T., Guyot, F., and Brown, G.E., Jr., 2006. Nanoscale detection of organic signatures

- in carbonate microbialites. *Proc. Natl. Acad. Sci. U. S. A.*, 103(25):9440–9445. doi:10.1073/pnas.0603255103
- Benzerara, K., Yoon, T.H., Menguy, N., Tyliczszak, T., and Brown, G.E., Jr., 2005. Nanoscale environments associated with bioweathering of a Mg-Fe-pyroxene. *Proc. Natl. Acad. Sci. U. S. A.*, 102(4):979–982. doi:10.1073/pnas.0409029102
- Beysac, O., Goffé, B., Petitot, J.-P., Froigneaux, E., Moreau, M., and Rouzaud, J.-N., 2003. On the characterization of disordered and heterogeneous carbonaceous materials by Raman spectroscopy. *Spectrochim. Acta, Part A*, 59(10):2267–2276. doi:10.1016/S1386-1425(03)00070-2
- Bhartia, R., Hug, W.F., Salas, E.C., Reid, R.D., Sijapati, K.K., Tsapin, A., Abbey, W., Neelson, K.H., Lane, A.L., and Conrad, P.G., 2008. Classification of organic and biological materials with deep ultraviolet excitation. *Appl. Spectrosc.*, 62(10):1070–1077. doi:10.1366/000370208786049123
- Bhartia, R., Salas, E.C., Hug, W.F., Reid, R.D., Lane, A.L., Edwards, K.J., and Neelson, K.H., 2010. Label-free bacterial imaging with deep-UV-laser-induced native fluorescence. *Appl. Environ. Microbiol.*, 76(21):7231–7237. doi:10.1128/AEM.00943-10
- Biddle, J.F., Lipp, J.S., Lever, M.A., Lloyd, K.G., Sørensen, K.B., Anderson, R., Fredricks, H.F., Elvert, M., Kelly, T.J., Schrag, D.P., Sogin, M.L., Brenchley, J.E., Teske, A., House, C.H., and Hinrichs, K.-U., 2006. Heterotrophic Archaea dominate sedimentary subsurface ecosystems off Peru. *Proc. Natl. Acad. Sci. U. S. A.*, 103(10):3846–3851. doi:10.1073/pnas.0600035103
- Bown, P.R. (Ed.), 1998. *Calcareous Nannofossil Biostratigraphy*: Dordrecht, The Netherlands (Kluwer Academic Publ.).
- Blum, P., 1997. Physical properties handbook: a guide to the shipboard measurement of physical properties of deep-sea cores. *ODP Tech. Note*, 26. doi:10.2973/odp.tn.26.1997
- Cowen, J.P., Giovannoni, S.J., Kenig, F., Johnson, H.P., Butterfield, D., Rappé, M.S., Hutnak, M., and Lam, P., 2003. Fluids from aging ocean crust that support microbial life. *Science*, 299(5603):120–123. doi:10.1126/science.1075653
- Davis, G.H., 1984. *Structural Geology of Rocks and Regions*: New York (John Wiley and Sons, Inc.).
- Dunham, R.J., 1962. Classification of carbonate rocks according to depositional texture. In Ham, W.E. (Ed.), *Classification of Carbonate Rocks*. AAPG Mem., 1:108–121.
- Edwards, K.J., Wheat, C.G., Orcutt, B.N., Hulme, S., Becker, K., Jannasch, H., Haddad, A., Pettigrew, T., Rhinehart, W., Grigar, K., Bach, W., Kirkwood, W., and Klaus, A., 2012. Design and deployment of borehole observatories and experiments during IODP Expedition 336, Mid-Atlantic Ridge flank at North Pond. In Edwards, K.J., Bach, W., Klaus, A., and the Expedition 336 Scientists, *Proc. IODP*, 336: Tokyo (Integrated Ocean Drilling Program Management International, Inc.). doi:10.2204/iodp.proc.336.109.2012
- Ellis, D.V., and Singer, J.M., 2007. *Well Logging for Earth Scientists* (2nd ed.): New York (Elsevier).
- Engelen, B., Ziegelmeüller, K., Wolf, L., Köpke, B., Gittel, A., Cypionka, H., Treude, T., Nakagawa, S., Inagaki, F., Lever, M.A., and Steinsbu, B.O., 2008. Fluids from the ocean crust support microbial activities within the deep biosphere. *Geomicrobiol. J.*, 25(1):56–66. doi:10.1080/01490450701829006
- Expedition 304/305 Scientists, 2006. Methods. In Blackman, D.K., Idefonse, B., John, B.E., Ohara, Y., Miller, D.J., MacLeod, C.J., and the Expedition 304/305 Scientists, *Proc. IODP*, 304/305: College Station, TX (Integrated Ocean Drilling Program Management International, Inc.). doi:10.2204/iodp.proc.304305.102.2006
- Expedition 309/312 Scientists, 2006. Methods. In Teagle, D.A.H., Alt, J.C., Umino, S., Miyashita, S., Banerjee, N.R., Wilson, D.S., and the Expedition 309/312 Scientists. *Proc. IODP*, 309/312: Washington, DC (Integrated Ocean Drilling Program Management International, Inc.). doi:10.2204/iodp.proc.309312.102.2006
- Expedition 327 Scientists, 2011. Methods. In Fisher, A.T., Tsuji, T., Petronotis, K., and the Expedition 327 Scientists, *Proc. IODP*, 327: Tokyo (Integrated Ocean Drilling Program Management International, Inc.). doi:10.2204/iodp.proc.327.102.2011
- Expedition 329 Scientists, 2011a. Methods. In D'Hondt, S., Inagaki, F., Alvarez Zarikian, C.A., and the Expedition 329 Scientists, *Proc. IODP*, 329: Tokyo (Integrated Ocean Drilling Program Management International, Inc.). doi:10.2204/iodp.proc.329.102.2011
- Expedition 329 Scientists, 2011b. South Pacific Gyre sub-seafloor life. *IODP Prel. Rept.*, 329. doi:10.2204/iodp.pr.329.2011
- Expedition 330 Scientists, 2012. Methods. In Koppers, A.A.P., Yamazaki, T., Geldmacher, J., and the Expedition 330 Scientists, *Proc. IODP*, 330: Tokyo (Integrated Ocean Drilling Program Management International, Inc.). doi:10.2204/iodp.proc.330.102.2012
- Expedition 336 Scientists, 2012a. Sediment and basement contact coring. In Edwards, K.J., Bach, W., Klaus, A., and the Expedition 336 Scientists, *Proc. IODP*, 336: Tokyo (Integrated Ocean Drilling Program Management International, Inc.). doi:10.2204/iodp.proc.336.106.2012
- Expedition 336 Scientists, 2012b. Site 395. In Edwards, K.J., Bach, W., Klaus, A., and the Expedition 336 Scientists, *Proc. IODP*, 336: Tokyo (Integrated Ocean Drilling Program Management International, Inc.). doi:10.2204/iodp.proc.336.103.2012
- Expedition 336 Scientists, 2012c. Site U1382. In Edwards, K.J., Bach, W., Klaus, A., and the Expedition 336 Scientists, *Proc. IODP*, 336: Tokyo (Integrated Ocean Drilling Program Management International, Inc.). doi:10.2204/iodp.proc.336.104.2012
- Expedition 336 Scientists, 2012d. Site U1383. In Edwards, K.J., Bach, W., Klaus, A., and the Expedition 336 Scientists, *Proc. IODP*, 336: Tokyo (Integrated Ocean Drilling Program Management International, Inc.). doi:10.2204/iodp.proc.336.105.2012
- Fischer, J.P., Ferdelman, T.G., D'Hondt, S., Røy, H., and Wenzhöfer, F., 2009. Oxygen penetration deep into the sediment of the South Pacific gyre. *Biogeosciences*, 6(8):1467–1478. doi:10.5194/bg-6-1467-2009

- Fisher, A.T., Wheat, C.G., Becker, K., Cowen, J., Orcutt, B., Hulme, S., Inderbitzen, K., Turner, A., Pettigrew, T.L., Davis, E.E., Jannasch, H., Grigar, K., Adudell, R., Meldrum, R., Macdonald, R., and Edwards, K., 2011. Design, deployment, and status of borehole observatory systems used for single-hole and cross-hole experiments, IODP Expedition 327, eastern flank of Juan de Fuca Ridge. *In* Fisher, A.T., Tsuji, T., Petronotis, K., and the Expedition 327 Scientists, *Proc. IODP, 327*: College Station, TX (Integrated Ocean Drilling Program Management International, Inc.). [doi:10.2204/iodp.proc.327.107.2011](https://doi.org/10.2204/iodp.proc.327.107.2011)
- Fisher, A.T., Wheat, C.G., Becker, K., Davis, E.E., Jannasch, H., Schroeder, D., Dixon, R., Pettigrew, T.L., Meldrum, R., McDonald, R., Nielsen, M., Fisk, M., Cowen, J., Bach, W., and Edwards, K., 2005. Scientific and technical design and deployment of long-term seafloor observatories for hydrogeologic and related experiments, IODP Expedition 301, eastern flank of Juan de Fuca Ridge. *In* Fisher, A.T., Urabe, T., Klaus, A., and the Expedition 301 Scientists, *Proc. IODP, 301*: College Station, TX (Integrated Ocean Drilling Program Management International, Inc.). [doi:10.2204/iodp.proc.301.103.2005](https://doi.org/10.2204/iodp.proc.301.103.2005)
- Gérard, E., Moreira, D., Philippot, P., Van Kranendonk, M.J., and López-García, P., 2009. Modern subsurface bacteria in pristine 2.7 Ga-old fossil stromatolite drillcore samples from the Fortescue Group, Western Australia. *PLoS One*, 4(4):e5298. [doi:10.1371/journal.pone.0005298](https://doi.org/10.1371/journal.pone.0005298)
- Gieskes, J.M., Gamo, T., and Brumsack, H., 1991. Chemical methods for interstitial water analysis aboard *JOIDES Resolution*. *ODP Tech. Note*, 15. [doi:10.2973/odp.tn.15.1991](https://doi.org/10.2973/odp.tn.15.1991)
- Goldberg, D., 1997. The role of downhole measurements in marine geology and geophysics. *Rev. Geophys.*, 35(3):315–342. [doi:10.1029/97RG00221](https://doi.org/10.1029/97RG00221)
- Govindaraju, K., 1989. 1989 compilation of working values and sample description for 272 geostandards. *Geostand. Newsl.*, 13(S1). [doi:10.1111/j.1751-908X.1989.tb00476.x](https://doi.org/10.1111/j.1751-908X.1989.tb00476.x)
- Graber, K.K., Pollard, E., Jonasson, B., and Schulte, E. (Eds.), 2002. Overview of Ocean Drilling Program engineering tools and hardware. *ODP Tech. Note*, 31. [doi:10.2973/odp.tn.31.2002](https://doi.org/10.2973/odp.tn.31.2002)
- Hirayama, H., Sunamura, M., Takai, K., Nunoura, T., Noguchi, T., Oida, H., Furushima, Y., Yamamoto, H., Oomori, T., and Horikoshi, K., 2007. Culture-dependent and -independent characterization of microbial communities associated with a shallow submarine hydrothermal system occurring within a coral reef off Taketomi Island, Japan. *Appl. Environ. Microbiol.*, 73(23):7642–7656. [doi:10.1128/AEM.01258-07](https://doi.org/10.1128/AEM.01258-07)
- International Atomic Energy Agency, 2003. Guidelines for radioelement mapping using gamma ray spectrometry data. *I. A. E. A., [Tech. Doc.], IAEA-TECDOC*, 1363. [http://www-pub.iaea.org/mtcd/publications/pdf/te\\_1363\\_web.pdf](http://www-pub.iaea.org/mtcd/publications/pdf/te_1363_web.pdf)
- Janz, G.J., and Singer, S.K., 1975. Copenhagen Standard Sea Water: conductivity and salinity. *J. Solution Chem.*, 4(12):995–1003. [doi:10.1007/BF01074741](https://doi.org/10.1007/BF01074741)
- Jarrard, R.D., and Kerneklian, M.J., 2007. Data report: physical properties of the upper oceanic crust of ODP Site 1256: multisensor track and moisture and density measurements. *In* Teagle, D.A.H., Wilson, D.S., Acton, G.D., and Vanko, D.A. (Eds.), *Proc. ODP, Sci. Results*, 206: College Station, TX (Ocean Drilling Program), 1–11. [doi:10.2973/odp.proc.sr.206.011.2007](https://doi.org/10.2973/odp.proc.sr.206.011.2007)
- Kondo, R., Nedwell, D.B., Purdy, K.J., and Silva, S.Q., 2004. Detection and enumeration of sulphate-reducing bacteria in estuarine sediments by competitive PCR. *Geomicrobiol. J.*, 21(3):145–157. [doi:10.1080/01490450490275307](https://doi.org/10.1080/01490450490275307)
- Kvenvolden, K.A., and McDonald, T.J., 1986. Organic geochemistry on the *JOIDES Resolution*—an assay. *ODP Tech. Note*, 6: College Station, TX (Ocean Drilling Program). [doi:10.2973/odp.tn.6.1986](https://doi.org/10.2973/odp.tn.6.1986)
- Lanzén, A., Jørgensen, S.L., Bengtsson, M.M., Jonassen, I., Øvreås, L., and Urich, T., 2011. Exploring the composition and diversity of microbial communities at the Jan Mayen hydrothermal vent field using RNA and DNA. *FEMS Microbiol. Ecol.*, 77(3):577–589. [doi:10.1111/j.1574-6941.2011.01138.x](https://doi.org/10.1111/j.1574-6941.2011.01138.x)
- Le Maitre, R.W., 1989. *A Classification of Igneous Rocks and Glossary of Terms*: Oxford (IUGS, Blackwell).
- Le Maitre, R.W., Streckeisen, A., Zanettin, B., Le Bas, M.J., Bonin, B., Bateman, P., Bellieni, G., Dudek, A., Efremova, S., Keller, J., Lameyre, J., Sabine, P.A., Schmid, R., Sorensen, H., and Woolley, A.R. (Eds.), 2002. *Igneous Rocks: A Classification and Glossary of Terms* (2nd ed.): Cambridge (Cambridge Univ. Press).
- Lever, M.A., Alperin, M., Engelen, B., Inagaki, F., Nakagawa, S., Steinsbu, B.O., Teske, A., and IODP Expedition Scientists, 2006. Trends in basalt and sediment core contamination during IODP Expedition 301. *Geomicrobiol. J.*, 23(7):517–530. [doi:10.1080/01490450600897245](https://doi.org/10.1080/01490450600897245)
- Lever, M.A., Heuer, V.B., Morono, Y., Masui, N., Schmidt, F., Alperin, M.J., Inagaki, F., Hinrichs, K.-U., and Teske, A., 2010. Acetogenesis in deep seafloor sediments of the Juan de Fuca Ridge flank: a synthesis of geochemical, thermodynamic, and gene-based evidence. *Geomicrobiol. J.*, 27(2):183–211. [doi:10.1080/01490450903456681](https://doi.org/10.1080/01490450903456681)
- Lovell, M.A., Harvey, P.K., Brewer, T.S., Williams, C., Jackson, P.D., and Williamson, G., 1998. Application of FMS images in the Ocean Drilling Program: an overview. *In* Cramp, A., MacLeod, C.J., Lee, S.V., and Jones, E.J.W. (Eds.), *Geological Evolution of Ocean Basins: Results from the Ocean Drilling Program*. *Geol. Soc. Spec. Publ.*, 131(1):287–303. [doi:10.1144/GSL.SP.1998.131.01.18](https://doi.org/10.1144/GSL.SP.1998.131.01.18)
- Luthi, S.M., 1990. Sedimentary structures of clastic rocks identified from electrical borehole images. *In* Hurst, A., Lovell, M.A., and Morton, A.C. (Eds.), *Geological Applications of Wireline Logs*. *Geol. Soc. Spec. Publ.*, 48(1):3–10. [doi:10.1144/GSL.SP.1990.048.01.02](https://doi.org/10.1144/GSL.SP.1990.048.01.02)
- Manheim, F.T., and Sayles, F.L., 1974. Composition and origin of interstitial waters of marine sediments, based on deep sea drill cores. *In* Goldberg, E.D. (Ed.), *The Sea* (Vol. 5): *Marine Chemistry: The Sedimentary Cycle*: New York (Wiley), 527–568.
- Marshall, C.P., Edwards, H.G.M., and Jehlicka, J., 2010. Understanding the application of Raman spectroscopy to the detection of traces of life. *Astrobiology*, 10(2):229–243. [doi:10.1089/ast.2009.0344](https://doi.org/10.1089/ast.2009.0344)

- Ménez, B., Rommevaux-Jestin, C., Salomé, M., Wang, Y., Philippot, P., Bonneville, A., and Gérard, E., 2007. Detection and phylogenetic identification of labeled prokaryotic cells on mineral surfaces using scanning X-ray microscopy. *Chem. Geol.*, 240(1–2):182–192. doi:10.1016/j.chemgeo.2007.02.009
- Michibayashi, K., Hirose, T., Nozaka, T., Harigane, Y., Escartin, J., Delius, H., Linek, M., and Ohara, Y., 2008. Hydration due to high-T brittle failure within in situ oceanic crust, 30°N Mid-Atlantic Ridge. *Earth Planet. Sci. Lett.*, 275(3–4):348–354. doi:10.1016/j.epsl.2008.08.033
- Mills, H.J., Hunter, E., Humphrys, M., Kerkhof, L., McGuinness, L., Huettel, M., and Kostka, J.E., 2008. Characterization of nitrifying, denitrifying, and overall bacterial communities in permeable marine sediments of the northeastern Gulf of Mexico. *Appl. Environ. Microbiol.*, 74(14):4440–4453. doi:10.1128/AEM.02692-07
- Mills, H.J., Reese, B.K., and St. Peter, C., 2012. Characterization of microbial population shifts during sample storage. *Front. Extreme Microbio.*, 3:49. doi:10.3389/fmicb.2012.00049
- Morono, Y., Terada, T., Masui, N., and Inagaki, F., 2009. Discriminative detection and enumeration of microbial life in marine subsurface sediments. *ISME J.*, 3(5):503–511. doi:10.1038/ismej.2009.1
- Munsell Color Company, Inc., 2000. *Munsell Soil Color Chart*: New York (Gretag-Macbeth).
- Murray, R.W., Miller, D.J., and Kryc, K.A., 2000. Analysis of major and trace elements in rocks, sediments, and interstitial waters by inductively coupled plasma-atomic emission spectrometry (ICP-AES). *ODP Tech. Note*, 29. doi:10.2973/odp.tn.29.2000
- Myrbo, A., 2007. Smear slides. *LRC LacCore SOP Series*. <http://lrc.geo.umn.edu/laccore/assets/pdf/sops/smearslides.pdf>
- Nakagawa, S., Inagaki, F., Suzuki, Y., Steinsbu, B.O., Lever, M.A., Takai, K., Engelen, B., Sako, Y., Wheat, C.G., Horikoshi, K., and Integrated Ocean Drilling Program Expedition 301 Scientists, 2006. Microbial community in black rust exposed to hot ridge-flank crustal fluids. *Appl. Environ. Microbiol.*, 72(10):6789–6799. doi:10.1128/AEM.01238-06
- Nunoura, T., Oida, H., Miyazaki, J., Miyashita, A., Imachi, H., and Takai, K., 2008. Quantification of *mcrA* by fluorescent PCR in methanogenic and methanotrophic microbial communities. *FEMS Microbiol. Ecol.*, 64(2):240–247. doi:10.1111/j.1574-6941.2008.00451.x
- Orcutt, B., Wheat, C.G., and Edwards, K.J., 2010. Subseafloor ocean crust microbial observatories: development of FLOCS (Flow-Through Osmo Colonization System) and evaluation of borehole construction materials. *Geomicrobiol. J.*, 27(2):143–157. doi:10.1080/01490450903456772
- Orcutt, B.N., Bach, W., Becker, K., Fisher, A.T., Hentscher, M., Toner, B.M., Wheat, C.G., and Edwards, K.J., 2011. Colonization of subsurface microbial observatories deployed in young ocean crust. *ISME J.*, 5:692–703. doi:10.1038/ismej.2010.157
- Orphan, V.J., House, C.H., Hinrichs, K.-U., McKeegan, K.D., and DeLong, E.F., 2001. Methane-consuming archaea revealed by directly coupled isotopic and phylogenetic analysis. *Science*, 293(5529):484–487. doi:10.1126/science.1061338
- Passchier, C.W., and Trouw, R.A.J., 1996. *Microtectonics*: Berlin (Springer-Verlag).
- Pernthaler, A., Pernthaler, J., and Amann, R., 2002. Fluorescence in situ hybridization and catalyzed reporter deposition for the identification of marine bacteria. *Appl. Environ. Microbiol.*, 68(6):3094–3101. doi:10.1128/AEM.68.6.3094-3101.2002
- Ramsay, J.G., and Huber, M.I., 1987. *The Techniques of Modern Structural Geology* (Vol. 2): *Folds and Fractures*: New York (Acad. Press).
- Rider, M.H., 1996. *The Geological Interpretation of Well Logs* (2nd ed.): Caithness (Whittles Publ.).
- Riedel, W.R., and Sanfilippo, A., 1977. Cinozoic Radiolaria. In Ramsay, A.T.S. (Ed.), *Oceanic Micropalaeontology* (Vol. 2): (Academic Press), 847–912.
- Roalkvam, I., Jørgensen, S.L., Chen, Y., Stokke, R., Dahle, H., Hocking, W.P., Lanzén, A., Haflidason, H., and Steen, I.H., 2011. New insights into stratification of anaerobic methanotrophs in cold seep sediments. *FEMS Microbiol. Ecol.*, 78(2):233–243. doi:10.1111/j.1574-6941.2011.01153.x
- Robinson, S., Mrozewski, S., Hussein, T., Masterson, W., Meissner, E., Williams, T., Keogh, W., Myers, G., Bartington, G., and Goldberg, D., 2008. A new borehole magnetic susceptibility tool for high-resolution formation evaluation. *SPWLA Annu. Logging Symp.*, 49(2):196–197. (Abstract)
- Rommevaux-Jestin, C., and Menéz, B., 2010. Potential of cathodoluminescence microscopy and spectroscopy for the detection of prokaryotic cells on minerals. *Astrobiology*, 10(9):921–932. doi:10.1089/ast.2010.0490
- Rothburg, J.M., Hinz, W., Rearick, T.M., Schultz, J., Mileski, W., Davey, M., Leamon, J.H., Johnson, K., Milgrew, M.J., Edwards, M., Hoon, J., Simons, J.F., Marran, D., Myers, J.W., Davidson, J.F., Branting, A., Nobile, J.R., Puc, B.P., Light, D., Clark, T.A., Huber, M., Branciforte, J.T., Stoner, I.B., Cawley, S.E., Lyons, M., Fu, Y., Homer, N., Sedova, M., Miao, X., Reed, B., Sabina, J., Feierstein, E., Schorn, M., Alanjary, M., Dimalanta, E., Dressman, D., Kasinskas, R., Sokolsky, T., Fidanza, J.A., Namsaraev, E., McKernan, K.J., Williams, A., Roth, G.T., and Bustillo, J., 2011. An integrated semiconductor device enabling non-optical genome sequencing. *Nature (London, U. K.)*, 475(7356):348–352. doi:10.1038/nature10242
- Salimullah, A.R.M., and Stow, D.A.V., 1992. Application of FMS images in poorly recovered coring intervals: examples from ODP Leg 129. In Hurst, A., Griffiths, C.M., and Worthington, P.F. (Eds.), *Geological Application of Wireline Logs II*. Geol. Soc. Spec. Publ., 65(1):71–86. doi:10.1144/GSL.SP.1992.065.01.06
- Schlumberger, 1989. *Log Interpretation Principles/Applications*: Houston (Schlumberger Educ. Serv.), SMP-7017.
- Schlumberger, 1994. *IPL Integrated Porosity Lithology*: Houston (Schlumberger Wireline Testing), SMP-9270.
- Schmidt-Schierhorn, F., Kaul, N., Stephan, S., and Villinger, H., 2012. Geophysical site survey results from North Pond (Mid-Atlantic Ridge). In Edwards, K.J., Bach, W., Klaus, A., and the Expedition 336 Scientists, *Proc. IODP*, 336: Tokyo

- (Integrated Ocean Drilling Program Management International, Inc.). doi:10.2204/iodp.proc.336.107.2012
- Serra, O., 1984. *Fundamentals of Well-Log Interpretation* (Vol. 1): *The Acquisition of Logging Data*. Amsterdam (Elsevier).
- Serra, O., 1986. *Fundamentals of Well-Log Interpretation* (Vol. 2): *The Interpretation of Logging Data*. Amsterdam (Elsevier).
- Serra, O., 1989. *Formation MicroScanner Image Interpretation*. Houston (Schlumberger Educ. Serv.), SMP-7028.
- Shipboard Scientific Party, 2003. Explanatory notes. In Wilson, D.S., Teagle, D.A.H., Acton, G.D., *Proc. ODP, Init. Repts.*, 206: College Station, TX (Ocean Drilling Program), 1–94. doi:10.2973/odp.proc.ir.206.102.2003
- Smith, D.C., Spivack, A.J., Fisk, M.R., Haveman, S.A., Staudigel, H., and the Leg 185 Shipboard Scientific Party, 2000. Methods for quantifying potential microbial contamination during deep ocean coring. *ODP Tech. Note*, 28. doi:10.2973/odp.tn.28.2000
- Sparks, J.W., and Zuleger, E., 1995. Data report: chemical analyses of the Leg 140 reference sample. In Erzinger, J., Becker, K., Dick, H.J.B., Stokking, L.B. (Eds.), *Proc. ODP, Sci. Results*, 137/140: College Station, TX (Ocean Drilling Program), 353–355. doi:10.2973/odp.proc.sr.137140.041.1995
- Steinsbu, B.O., Thorseth, I.H., Nakagawa, S., Inagaki, F., Lever, M.A., Engelen, B., Øvreås, L., and Pedersen, R.B., 2010. *Archaeoglobus sulfatallidus* sp. nov., a thermophilic and facultatively lithoautotrophic sulfate-reducer isolated from black rust exposed to hot ridge flank crustal fluids. *Int. J. Syst. Evol. Microbiol.*, 60(12):2745–2752. doi:10.1099/ijs.0.016105-0
- Streckeisen, A., 1974. Classification and nomenclature of plutonic rocks recommendations of the IUGS subcommission on the systematics of igneous rocks. *Geol. Rundsch.*, 63(2):773–786. doi:10.1007/BF01820841
- Takai, K., Inagaki, F., Nakagawa, S., Hirayama, H., Nunoura, T., Sako, Y., Nealson, K.H., and Horikoshi, K., 2003. Isolation and phylogenetic diversity of members of previously uncultivated  $\epsilon$ -Proteobacteria in deep-sea hydrothermal fields. *FEMS Microbiol. Lett.*, 218(1):167–174. doi:10.1111/j.1574-6968.2003.tb11514.x
- Takai, K., Nakamura, K., Toki, T., Tsunogai, U., Miyazaki, M., Miyazaki, J., Hirayama, H., Nakagawa, S., Nunoura, T., and Horikoshi, K., 2008. Cell proliferation at 122°C and isotopically heavy CH<sub>4</sub> production by a hyperthermophilic methanogen under high-pressure cultivation. *Proc. Natl. Acad. Sci. U. S. A.*, 105(31):10949–10954. doi:10.1073/pnas.0712334105
- Tavormina, P.L., Ussler, W., III, and Orphan, V.J., 2008. Planktonic and sediment-associated aerobic methanotrophs in two seep systems along the North American margin. *Appl. Environ. Microbiol.*, 74(13):3985–3995. doi:10.1128/AEM.00069-08
- Twiss, R.J., and Moores, E.M., 1992. *Structural Geology*. New York (Freeman).
- van Zuilen, M.A., Chaussidon, M., Rollion-Bard, C., and Marty, B., 2007. Carbonaceous cherts of the Barberton Greenstone Belt, South Africa: isotopic, chemical, and structural characteristics of individual microstructures. *Geochim. Cosmochim. Acta*, 71(3):655–669. doi:10.1016/j.gca.2006.09.029
- Vasiliev, M.A., Blum, P., Chubarian, G., Olsen, R., Bennigh, C., Cobine, T., Fackler, D., Hastedt, M., Houpt, D., Mateo, Z., and Vasilieva, Y.B., 2011. A new natural gamma radiation measurement system for marine sediment and rock analysis. *J. Appl. Geophys.*, 75:455–463. doi:10.1016/j.jappgeo.2011.08.008
- Wang, F., Xiao, X., Ou, H.-Y., Gai, Y., and Wang, F., 2009a. Role and regulation of fatty acid biosynthesis in the response of *Shewanella piezotolerans* WP3 to different temperatures and pressures. *J. Bacteriol.*, 191(8):2574–2584 doi:10.1128/JB.00498-08
- Wang, F., Zhou, H., Meng, J., Peng, X., Jiang, L., Sun, P., Zhang, C., Van Nostrand, J.D., Deng, Y., He, Z., Wu, L., Zhou, J., and Xiao, X., 2009b. GeoChip-based analysis of metabolic diversity of microbial communities at the Juan de Fuca Ridge hydrothermal vent. *Proc. Natl. Acad. Sci. U. S. A.*, 106(12):4840–4845. doi:10.1073/pnas.0810418106
- Wentworth, C.K., 1922. A scale of grade and class terms for clastic sediments. *J. Geol.*, 30(5):377–392. doi:10.1086/622910
- Xie, W., Wang, F., Guo, L., Chen, Z., Sievert, S.M., Meng, J., Huang, G., Li, Y., Yan, Q., Wu, S., Wang, X., Chen, S., He, G., Xiao, X., and Xu, A., 2011. Comparative metagenomics of microbial communities inhabiting deep-sea hydrothermal vent chimneys with contrasting chemistries. *ISME J.*, 5(3):414–426 doi:10.1038/ismej.2010.144
- Zhang, K., Martiny, A.C., Reppas, N.B., Barry, K.W., Malek, J., Chisholm, S.W., and Church, G.M., 2006. Sequencing genomes from single cells by polymerase cloning. *Nat. Biotechnol.*, 24(6):680–686. doi:10.1038/nbt1214
- Ziebis, W., McManus, J., Ferdelman, T., Schmidt-Schierhorn, F., Bach, W., Muratli, J., Edwards, K.J., and Villinger, H., 2012. Interstitial fluid chemistry of sediments underlying the North Atlantic Gyre and the influence of subsurface fluid flow. *Earth Planet. Sci. Lett.*, 323–324:79–91. doi:10.1016/j.epsl.2012.01.018

**Publication:** 16 November 2012  
**MS 336-102**

Figure F1. IODP conventions for naming sites, holes, cores, and samples, Expedition 336. CC = core catcher.

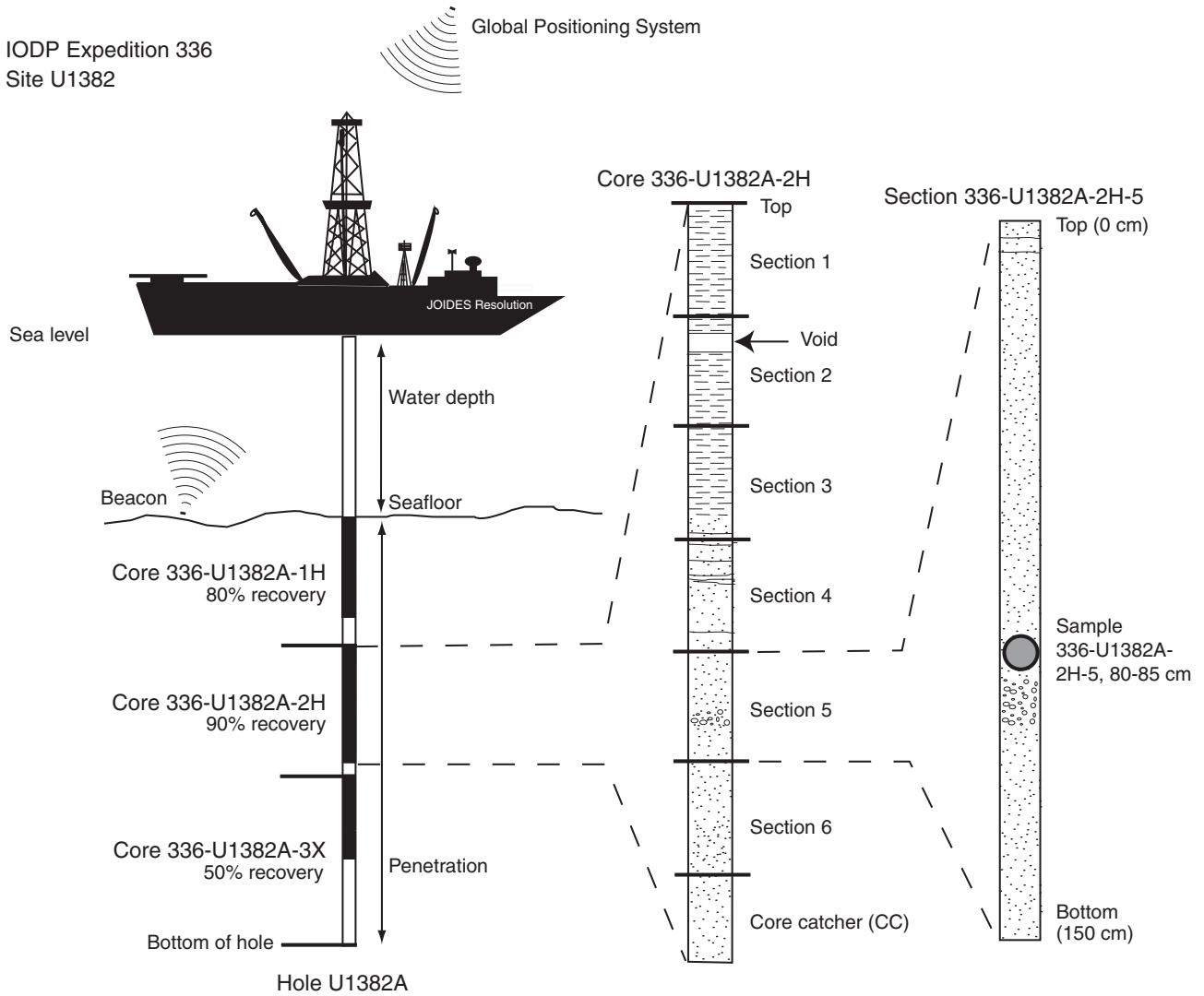
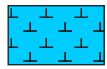


Figure F2. Symbols used in sedimentary VCDs, Expedition 336.

### Lithology

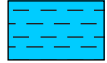
#### Bioclastics



Foraminifer-bearing nannofossil-rich ooze



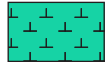
Nannofossil-bearing foraminifer-rich ooze



Foraminifer and nannofossil rich ooze

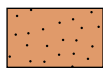


Nannofossil-rich ooze



Foraminifer-rich ooze

#### Siliciclastics



Silty clay

### Coring disturbance



Biscuit



Crack



Fragmented



Flow-in



Soupy

Intensity of disturbance:



Minimally disturbed



Moderately to highly disturbed



Moderately disturbed



Highly disturbed



Destroyed

### Sedimentary structures

Bedding features:



Parallel lamination



Grading (upward fining)



Slump



Contoured bed



Arched lamination

### Shipboard sampling

MADC

Moisture and density, method C

XRD

X-ray diffraction

ICP

ICP-AES analysis

IW

Interstitial water

RMS

Remanence of magnetization

Figure F3. Symbols used in hard rock VCDs, Expedition 336.

### Shipboard studies

TS  
Thin  
section

MBIO  
Microbio

CHNS

SED  
Sediment

IW  
Interstitial  
water

ICP  
ICP-AES  
analysis

Ph  
Close-up  
photo

PMAG  
Paleomagnetic  
analysis

PP  
Physical property  
analysis

TSB  
Petrographic  
thin section

XRD  
X-ray diffraction  
analysis

### Hard rock structures

 Y-shaped vein

 Halo

 Haloed vein

 Vein network

 Veined

### Texture

**G**

Glass

### Alteration

1  
Fresh  
(<2%)

2  
Slight  
(2%-10%)

3  
Moderate  
(10%-50%)

4  
High  
(50%-95%)

5  
Complete  
(95%-100%)

**Figure F4.** Modal classification scheme for mafic-ultramafic plutonic igneous rocks (after Streckeisen, 1974), Expedition 336.

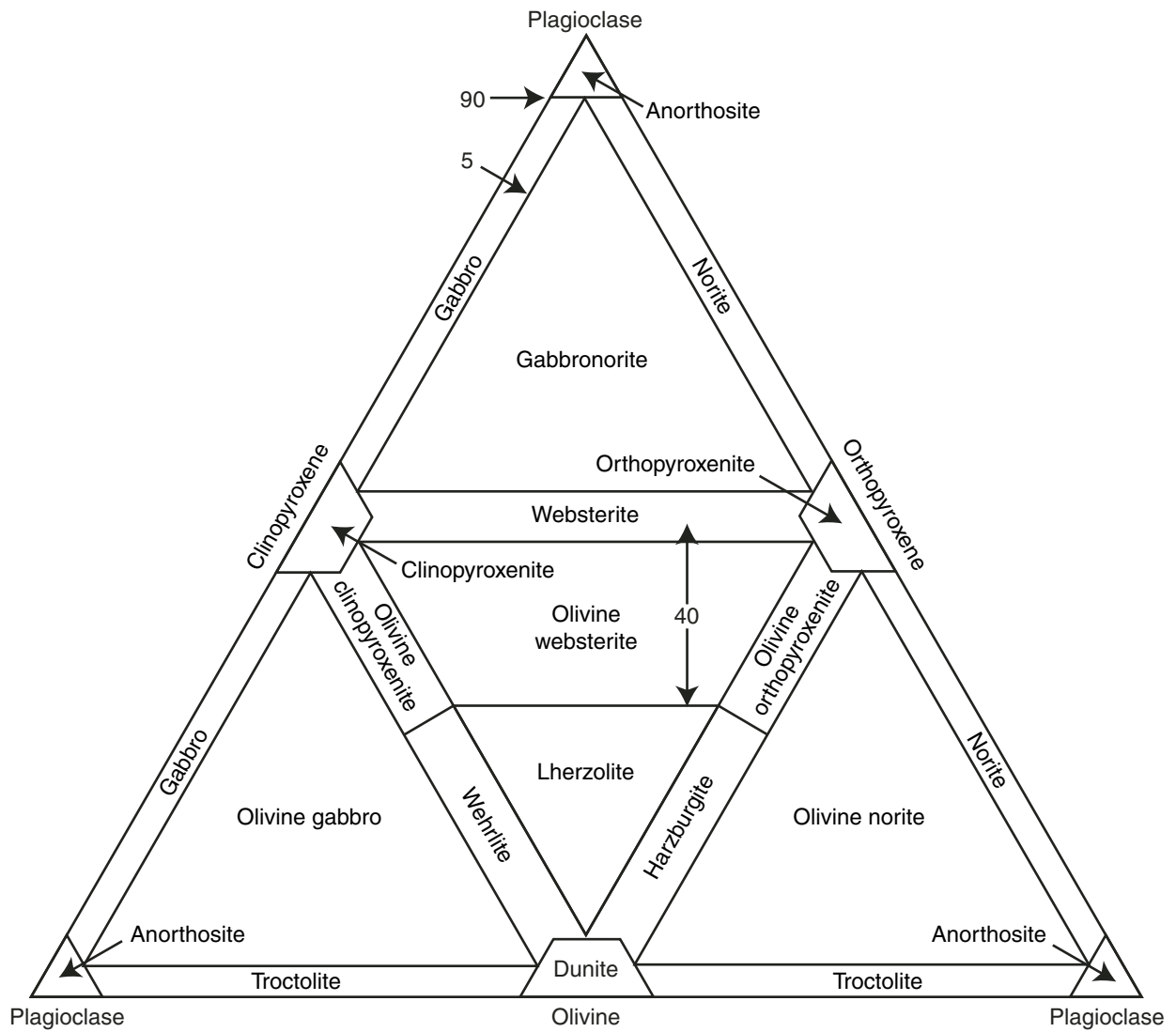


Figure F5. Fracture morphology, Expedition 336.

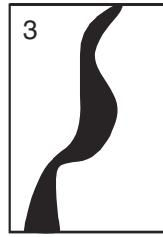
Vein shape



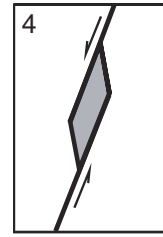
1  
Straight



2  
Sigmoidal



3  
Irregular



4  
Pull-apart

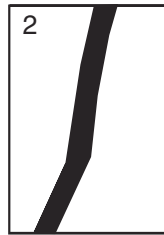


5  
Fault vein

Vein connectivity



1  
Isolated



2  
Single



3  
Branched

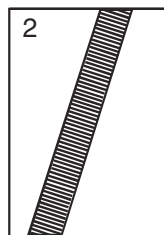


4  
Network

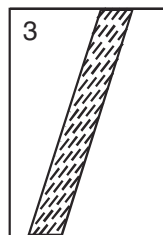
Vein texture



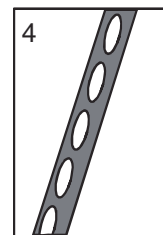
1  
Massive



2  
Cross fiber



3  
Slip fiber

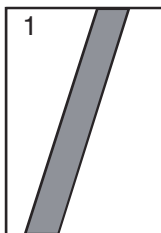


4  
Vuggy

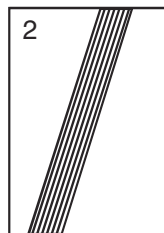


5  
Polycrystalline

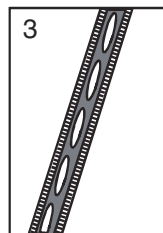
Vein structure



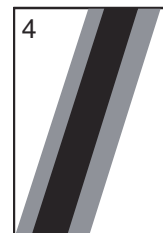
1  
Uniform



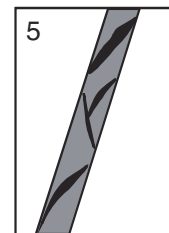
2  
Banded



3  
Composite



4  
Haloed

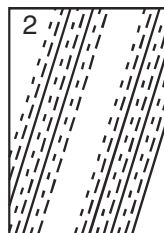


5  
Intravenous

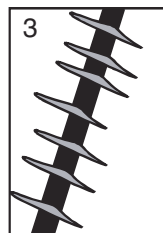
Particular vein geometries



1  
En echelon



2  
Ribbon



3  
Cross fractures

Figure F6. Intensity scales used for structural identification, Expedition 336. See text for detailed explanation.

Feature	0	1	2	3	4	5
Joints/open fractures						
	No open fractures	<1 per 10 cm	1-5 per 10 cm	>5 per 10 cm		
Veins						
	No veins	<1 per 10 cm	1-5 per 10 cm	5-10 per 10 cm	10-20 per 10 cm	>20 per 10 cm
Serpentine foliation						
	Massive	Weakly foliated	Moderately foliated	Strongly foliated		
Cataclastic deformation						
	Undeformed	Minor fracturing No sig. grain size reduction	Moderate fracturing No sig. grain size reduction	Dense anastomosing fracturing and incipient brecciation (<20% matrix)	Well-developed fault brecciation; clast rotation (20%-70% matrix)	Cataclasite (>70% matrix)
Periodotite crystal-plastic deformation						
	Undeformed protogranular	Porphyroclastic weakly foliated	Porphyroclastic strongly foliated	Porphyroclastic (Protomylonite)	Mylonite	Ultramylonite
Gabbro crystal-plastic deformation						
	Undeformed	Weakly foliated	Strongly foliated	Porphyroclastic (Protomylonite)	Mylonite	Ultramylonite
Magmatic foliation						
	Isotropic: no shape fabric	Weak shape fabric	Moderate shape fabric	Strong shape fabric		

**Figure F7.** Core reference frame used to describe orientation of observed structures, Expedition 336. **A.** Cut face of core. **B.** Three-dimensional perspective of core. **C.** Orientation of apparent dip angles and strike.

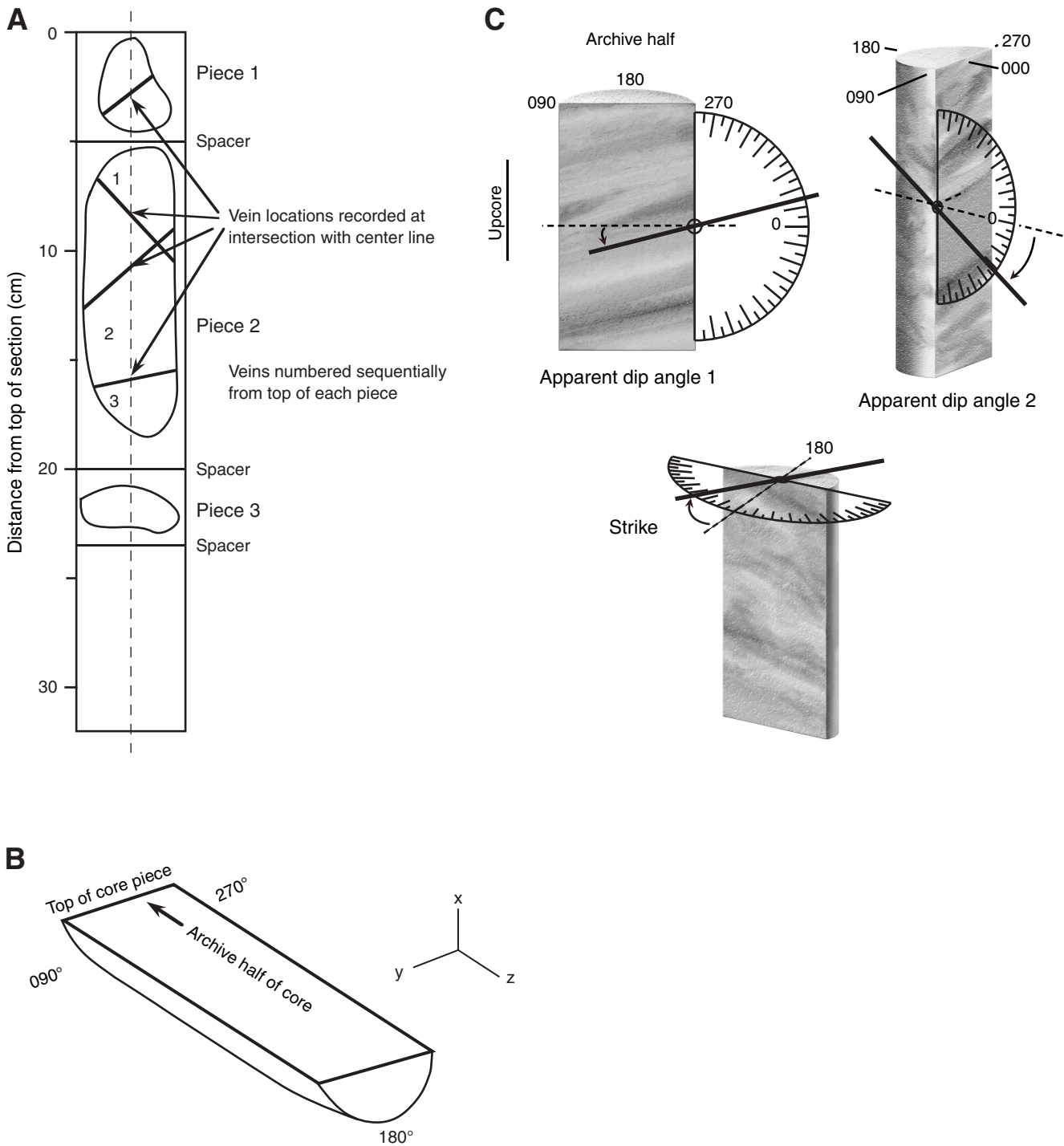




**Figure F8.** Sediment sampling profile, Hole U1382B. All whole-round core sections cut from the core are noted in 10 cm sections. Notes include core disruptions or locations of rock samples collected. (Continued on next nine pages.)

**SITE: 1382B      Core 1      11/8/11      1730**

1H-1		1H-2		1H-3	
0-10		0-10		0-10	A Syringe
10-20		10-20		10-20	
20-30		20-30	B Syringe	20-30	
30-40		30-40		30-40	
40-50		40-50		40-50	
50-60		50-60		50-60	
60-70		60-70		60-70	
70-80		70-80		70-80	
80-90		80-90		80-90	Russell - 4
90-100		90-100		90-100	Wang - 4
100-110		100-110		100-110	Wang - 80
110-120		110-120		110-120	Mills - 80
120-130		120-130	Rennie - 4	120-130	Edwards - 80
130-140		130-140	Wang - 4	130-140	Geochem
140-150		140-150	Archive - 80	140-150	Geochem

1H-4	
0-10	A Syringe
10-20	
20-30	
30-40	
40-50	
50-60	
60-70	Hirayama - 4
70-80	Russell - 4
80-90	Wang - 4
90-100	Wang - 80
100-110	Mills - 4
110-120	Mills - 80
120-130	Edwards - 80
130-140	Geochem
140-150	Geochem

1H-5	
0-10	C Syringe
10-20	
20-30	
30-40	
40-50	
50-60	
60-70	
70-80	
80-90	Rennie - 4
90-100	Wenk - 4
100-110	Wang - 4
110-120	Paytan - 80
120-130	Mamatha - 80
130-140	Zeibis - 4
140-150	Archive - 80

1H-1 = Not sampled; only 50 cm  
1H-2 = 130 cm total



Figure F8 (continued). (Continued on next page.)

**SITE: 1382B      Core 2      11/8/11      1915**

2H-1 = B Syringe

2H-2

0-10	A Syringe
10-20	
20-30	
30-40	
40-50	
50-60	
60-70	
70-80	
80-90	
90-100	
100-110	Russell - 4
110-120	Mills - 80
120-130	Edwards - 80
130-140	Geochem
140-150	Geochem

2H-3

0-10	B Syringe
10-20	
20-30	
30-40	
40-50	
50-60	
60-70	
70-80	
80-90	
90-100	
100-110	
110-120	
120-130	
130-140	
140-150	Rennie - 4

2H-4

0-10	A Syringe
10-20	
20-30	
30-40	
40-50	
50-60	
60-70	
70-80	
80-90	Russell - 4
90-100	Mills - 80
100-110	Edwards - 80
110-120	Geochem
120-130	Geochem
130-140	Geochem
140-150	Geochem

2H-5

0-10	C Syringe
10-20	
20-30	
30-40	
40-50	
50-60	
60-70	
70-80	Rennie - 4
80-90	Wenk - 4
90-100	Paytan - 80
100-110	Mamatha - 80
110-120	Zeibis - 4
120-130	Wang - 4
130-140	Wang - 80
140-150	Archive - 80

2H-6

0-10	A Syringe
10-20	
20-30	
30-40	
40-50	
50-60	
60-70	
70-80	
80-90	Hirayama - 4
90-100	Russell - 4
100-110	Mills - 4
110-120	Mills - 80
120-130	Edwards - 80
130-140	Geochem
140-150	Geochem

2H-7

0-10	B Syringe
10-20	
20-30	
30-40	
40-50	
50-60	
60-70	
70-80	
80-90	
90-100	
100-110	
110-120	
120-130	
130-140	
140-150	Rennie - 4



Figure F8 (continued). (Continued on next page.)

**SITE: 1382B**      Core 3      11/8/11      2045

3H-1	0-10	B Syringe
	10-20	
	20-30	
	30-40	
	40-50	
	50-60	
	60-70	
	70-80	
	80-90	
	90-100	
	100-110	
	110-120	
	120-130	
	130-140	
	140-150	

3H-2	0-10	A Syringe
	10-20	
	20-30	
	30-40	
	40-50	
	50-60	
	60-70	
	70-80	
	80-90	
	90-100	
	100-110	
	110-120	
	120-130	
	130-140	
	140-150	

3H-3	0-10	C Syringe
	10-20	
	20-30	
	30-40	
	40-50	
	50-60	
	60-70	
	70-80	
	80-90	
	90-100	
	100-110	
	110-120	
	120-130	
	130-140	
	140-150	

3H-4	0-10	Geochem
	10-20	Geochem
	20-30	B Syringe
	30-40	
	40-50	
	50-60	
	60-70	
	70-80	
	80-90	
	90-100	
	100-110	
	110-120	
	120-130	
	130-140	
	140-150	

3H-5	0-10	A Syringe
	10-20	
	20-30	
	30-40	
	40-50	
	50-60	
	60-70	
	70-80	
	80-90	
	90-100	
	100-110	
	110-120	
	120-130	
	130-140	
	140-150	

Core was disturbed at the top.  
3H-4 bottom was really wet and mixed.



Figure F8 (continued). (Continued on next page.)

**SITE: 1382B**      Core 4      11/8/11      2230

4H-1	0-10	
	10-20	
	20-30	
	30-40	
	40-50	
	50-60	
	60-70	
	70-80	
	80-90	
	90-100	
	100-110	
	110-120	
	120-130	
	130-140	Mills - 80
	140-150	Edwards - 80

4H-2	0-10	A Syringe
	10-20	
	20-30	
	30-40	
	40-50	
	50-60	
	60-70	
	70-80	
	80-90	Russell - 4
	90-100	Mills - 80
	100-110	Edwards - 80
	110-120	Geochem
	120-130	Geochem
	130-140	Geochem
	140-150	Geochem

4H-3	0-10	B Syringe
	10-20	
	20-30	
	30-40	
	40-50	
	50-60	
	60-70	
	70-80	
	80-90	
	90-100	
	100-110	
	110-120	
	120-130	
	130-140	
	140-150	Rennie - 4

4H-1 = Only 25 cm. Contained Rocks.

4H-4	0-10	C Syringe
	10-20	
	20-30	
	30-40	
	40-50	
	50-60	
	60-70	
	70-80	
	80-90	Hirayama - 4
	90-100	Russell - 4
	100-110	Mills - 4
	110-120	Mills - 80
	120-130	Edwards - 80
	130-140	Geochem
	140-150	Geochem

4H-5	0-10	A Syringe
	10-20	
	20-30	
	30-40	
	40-50	
	50-60	
	60-70	
	70-80	
	80-90	
	90-100	
	100-110	
	110-120	
	120-130	
	130-140	
	140-150	

4H-5 = Bottom half washed out

4H-6	0-10	
	10-20	
	20-30	
	30-40	
	40-50	
	50-60	
	60-70	A Syringe
	70-80	Wenk - 4
	80-90	Paytan - 80
	90-100	Mamatha - 80
	100-110	Zeibis - 4
	110-120	Wang - 4
	120-130	Wang - 80
	130-140	Archive - 80
	140-150	Rennie - 4

Figure F8 (continued). (Continued on next page.)

**SITE: 1382B**      Core 5      11/9/11      0015

5H-1	
0-10	
10-20	
20-30	
30-40	
40-50	
50-60	
60-70	
70-80	
80-90	C Syringe
90-100	Russell - 4
100-110	Mills - 4
110-120	Mills - 80
120-130	Edwards - 80
130-140	Geochem
140-150	Geochem

5H-2	
0-10	
10-20	
20-30	
30-40	
40-50	
50-60	
60-70	A Syringe
70-80	Wenk - 4
80-90	Paytan - 80
90-100	Mamatha - 80
100-110	Zeibis - 4
110-120	Wang - 4
120-130	Wang - 80
130-140	Archive - 80
140-150	Rennie -4

Only 2 sections  
Highly disturbed core.





Figure F8 (continued). (Continued on next page.)

**SITE: 1382B**      Core 6      11/9/11      0245

6H-2	0-10	B Syringe
	10-20	
	20-30	
	30-40	
	40-50	
	50-60	
	60-70	
	70-80	
	80-90	
	90-100	
	100-110	
	110-120	
	120-130	
	130-140	
	140-150	

6H-3	0-10	A Syringe	
	10-20		
	20-30		
	30-40		
	40-50		
	50-60		
	60-70		
	70-80		
	80-90		
	90-100		
	100-110		Russell - 4
	110-120		Mills - 80
	120-130		Edwards - 80
	130-140		Geochem
	140-150		Geochem

6H-6	0-10	B Syringe
	10-20	
	20-30	
	30-40	
	40-50	
	50-60	
	60-70	
	70-80	
	80-90	Russell - 4
	90-100	Mills - 80
	100-110	Edwards - 80
	110-120	Geochem
	120-130	Geochem
	130-140	Geochem
	140-150	Geochem

6H-7	0-10	A Syringe	
	10-20		
	20-30		
	30-40		
	40-50		
	50-60		
	60-70		
	70-80		
	80-90		Hirayama - 4
	90-100		Russell - 4
	100-110		Mills - 4
	110-120		Mills - 80
	120-130		Edwards - 80
	130-140		Geochem
	140-150		Geochem

6H-8	0-10	B Syringe	
	10-20		
	20-30		
	30-40		
	40-50		
	50-60		
	60-70		
	70-80		
	80-90		
	90-100		
	100-110		Rennie - 4
	110-120		Wang - 40
	120-130		Wang - 4
	130-140		Mills - 80
	140-150		Edwards - 80

Sections 1, 2, 4 and 5 = Disturbed  
 Sections 1 and 2 = fell out of top

Small rocks in Mills and Edwards samples

Small rocks in all 6H-8 samples



Figure F8 (continued). (Continued on next page.)

**SITE: 1382B**      Core 7      11/9/11      0445

7H-1 = Part came out top of core. **Sampled for rock samples. Two pieces collected sterily for DNA and RNA.**

7H-2	0-10	B Syringe
	10-20	
	20-30	
	30-40	
	40-50	
	50-60	
	60-70	
	70-80	
	80-90	
	90-100	
	100-110	
	110-120	
	120-130	
	130-140	Mills - 80
	140-150	Edwards - 80

7H-3	0-10	A Syringe
	10-20	
	20-30	
	30-40	
	40-50	
	50-60	
	60-70	
	70-80	
	80-90	
	90-100	
	100-110	
	110-120	
	120-130	
	130-140	Geochem
	140-150	Geochem

7H-4	0-10	A Syringe	
	10-20		
	20-30		
	30-40		
	40-50		
	50-60		
	60-70		
	70-80		
	80-90		Russell - 4
	90-100		Mills - 80
	100-110		Edwards - 80
	110-120		Geochem
	120-130		Geochem
	130-140	Geochem	
	140-150	Geochem	

7H-5	0-10	C Syringe	
	10-20		
	20-30		
	30-40		
	40-50		
	50-60		
	60-70		Wenk - 4
	70-80		Paytan - 80
	80-90		Mamatha - 80
	90-100		Zeibis - 4
	100-110		Wang - 4
	110-120		Wang - 80
	120-130		Archive - 80
	130-140	Geochem	
	140-150	Geochem	

7H-6	0-10	A Syringe	
	10-20		
	20-30		
	30-40		
	40-50		
	50-60		
	60-70		
	70-80		
	80-90		Hirayama - 4
	90-100		Russell - 4
	100-110		Mills - 4
	110-120		Mills - 80
	120-130		Edwards - 80
	130-140	Geochem	
	140-150	Geochem	

7H-7	0-10	B Syringe
	10-20	
	20-30	
	30-40	
	40-50	
	50-60	
	60-70	
	70-80	
	80-90	
	90-100	
	100-110	
	110-120	
	120-130	
	130-140	Rennie - 4
	140-150	Archive - 80



Figure F8 (continued). (Continued on next page.)

SITE: 1382B

Core 8

11/9/11

8H-1 = Rock sampled collected by Edwards

8H-2	0-10	A Syringe
	10-20	
	20-30	
	30-40	
	40-50	
	50-60	
	60-70	
	70-80	
	80-90	
	90-100	
	100-110	Russell - 4
	110-120	Mills - 80
	120-130	Edwards - 80
	130-140	Geochem
140-150	Geochem	

8H-3	0-10	B Syringe
	10-20	
	20-30	
	30-40	
	40-50	
	50-60	
	60-70	
	70-80	
	80-90	
	90-100	
	100-110	
	110-120	
	120-130	
	130-140	
140-150	Rennie - 4	

8H-4	0-10	A Syringe
	10-20	
	20-30	
	30-40	
	40-50	
	50-60	
	60-70	
	70-80	
	80-90	Russell - 4
	90-100	Mills - 80
	100-110	Edwards - 80
	110-120	Geochem
	120-130	Geochem
	130-140	Geochem
140-150	Geochem	

8H-5	0-10	C Syringe
	10-20	
	20-30	
	30-40	
	40-50	
	50-60	
	60-70	
	70-80	Rennie - 4
	80-90	Wenk - 4
	90-100	Paytan - 80
	100-110	Mamatha - 80
	110-120	Zeibis - 4
	120-130	Wang - 4
	130-140	Wang - 80
140-150	Archive - 80	

8H-6	0-10	A Syringe
	10-20	
	20-30	
	30-40	
	40-50	
	50-60	
	60-70	
	70-80	
	80-90	Hirayama - 4
	90-100	Russell - 4
	100-110	Mills - 4
	110-120	Mills - 80
	120-130	Edwards - 80
	130-140	Geochem
140-150	Geochem	

8H-7	0-10	B Syringe
	10-20	
	20-30	
	30-40	
	40-50	
	50-60	
	60-70	
	70-80	
	80-90	
	90-100	
	100-110	
	110-120	
	120-130	
	130-140	Rennie - 4
140-150	Edwards - 4	

2 rock/pebble samples collected for Edwards



Figure F8 (continued). (Continued on next page.)

**SITE: 1382B**      Core 9      11/9/11

Top of core had gravel - Edwards sampled and put at 4C - 15 cm

9H-2

0-10	A Syringe
10-20	
20-30	
30-40	
40-50	
50-60	
60-70	Paytan - 80
70-80	Wang - 4
80-90	Wang - 80
90-100	Mills - 80
100-110	Edwards - 80
110-120	Geochem
120-130	Geochem
130-140	Geochem
140-150	Geochem

9H-3

0-10	B Syringe
10-20	
20-30	
30-40	
40-50	
50-60	
60-70	Russell - 4
70-80	Wang - 4
80-90	Mamatha - 80
90-100	Mills - 80
100-110	Edwards - 80
110-120	Geochem
120-130	Geochem
130-140	Geochem
140-150	Geochem

9H-4

0-10	A Syringe
10-20	
20-30	
30-40	
40-50	
50-60	
60-70	Zeibis - 4
70-80	Wang - 4
80-90	Wang - 80
90-100	Mills - 80
100-110	Edwards - 80
110-120	Geochem
120-130	Geochem
130-140	Geochem
140-150	Geochem

9H-5

0-10	C Syringe
10-20	
20-30	
30-40	
40-50	
50-60	
60-70	
70-80	
80-90	Edwards - 4
90-100	Edwards - 4
100-110	Edwards - 80
110-120	Geochem
120-130	Geochem
130-140	Geochem
140-150	Geochem

9H-6

0-10	A Syringe
10-20	
20-30	
30-40	
40-50	
50-60	
60-70	
70-80	
80-90	Wang - 4
90-100	Russell - 4
100-110	Mills - 4
110-120	Mills - 80
120-130	Edwards - 80
130-140	Geochem
140-150	Geochem

9H-7

0-10	B Syringe
10-20	
20-30	
30-40	
40-50	
50-60	
60-70	Wang - 4
70-80	Wang - 80
80-90	Russell - 4
90-100	Mills - 80
100-110	Edwards - 80
110-120	Geochem
120-130	Geochem
130-140	Geochem
140-150	Geochem

B Syringe



Figure F8 (continued).

**SITE: 1382B**      Core 10      11/9/11

10H-1 = Rocks went to Edwards - 4C

10H-2

0-10	A Syringe
10-20	
20-30	
30-40	
40-50	
50-60	
60-70	Paytan - 80
70-80	Wang - 4
80-90	Wang - 80
90-100	Mills - 80
100-110	Edwards - 80
110-120	Geochem
120-130	Geochem
130-140	Geochem
140-150	Geochem

Microsphere bag found. Edwards 4C

10H-3

0-10	B Syringe
10-20	
20-30	
30-40	
40-50	
50-60	
60-70	Russell - 4
70-80	Wang - 4
80-90	Mamatha - 4
90-100	Mills - 80
100-110	Edwards - 80
110-120	Geochem
120-130	Geochem
130-140	Geochem
140-150	Geochem

10H-4

0-10	A Syringe
10-20	
20-30	
30-40	
40-50	
50-60	
60-70	Zeibis - 4
70-80	Wang - 4
80-90	Wang - 80
90-100	Mills - 80
100-110	Edwards - 80
110-120	Geochem
120-130	Geochem
130-140	Geochem
140-150	Geochem

10H-5

0-10	C Syringe
10-20	
20-30	
30-40	
40-50	
50-60	
60-70	Hirayama - 4
70-80	Wang - 4
80-90	Russell - 4
90-100	Mills - 80
100-110	Edwards - 80
110-120	Geochem
120-130	Geochem
130-140	Geochem
140-150	Geochem

10H-6

0-10	A Syringe
10-20	
20-30	
30-40	
40-50	
50-60	
60-70	Wang - 4
70-80	Russell - 4
80-90	Mills - 4
90-100	Mills - 80
100-110	Edwards - 80
110-120	Geochem
120-130	Geochem
130-140	Geochem
140-150	Geochem

10H-7

0-10	B Syringe
10-20	
20-30	
30-40	
40-50	
50-60	
60-70	Wang - 4
70-80	Wang - 80
80-90	Russell - 4
90-100	Mills - 80
100-110	Edwards - 80
110-120	Geochem
120-130	Geochem
130-140	Geochem
140-150	Geochem

B Syringe

Rocks in Top - Edwards 4C



**Figure F9.** Sediment sampling profile, Hole U1383D. All whole-round core sections cut from the core are noted in 10 cm sections. Notes include core disruptions or locations of rock samples collected. (Continued on next five pages.)

**SITE: 1383D      Core 1      11/7/11      1500**

0-10	A Syringe
10-20	
20-30	
30-40	
40-50	
50-60	
60-70	
70-80	
80-90	
90-100	
100-110	
110-120	
120-130	
130-140	
140-150	

1H-1

0-10	A Syringe
10-20	
20-30	
30-40	
40-50	
50-60	
60-70	Russell - 4
70-80	Wang - 4
80-90	Wang - 80
90-100	Mills - 80
100-110	Edwards - 80
110-120	Geochem
120-130	Geochem
130-140	Geochem
140-150	Geochem

1H-2

0-10	B Syringe
10-20	
20-30	
30-40	
40-50	
50-60	
60-70	Hirayama - 4
70-80	Russell - 4
80-90	Wang - 4
90-100	Wang - 80
100-110	Mills - 4
110-120	Mills - 80
120-130	Edwards - 80
130-140	Geochem
140-150	Geochem

1H-3

0-10	A Syringe
10-20	
20-30	
30-40	
40-50	
50-60	
60-70	
70-80	
80-90	
90-100	Wenk - 4
100-110	Wang - 4
110-120	Paytan - 80
120-130	Mamatha - 80
130-140	Zeibis - 4
140-150	Archive - 80

1H-4



Figure F9 (continued). (Continued on next page.)

**SITE: 1383D**      Core 2      11/7/11      1600

2H-1	0-10	A Syringe
	10-20	
	20-30	
	30-40	
	40-50	
	50-60	
	60-70	
	70-80	
	80-90	
	90-100	
	100-110	Russell - 4
	110-120	Mills - 80
	120-130	Edwards - 80
	130-140	Geochem
	140-150	Geochem

2H-2	0-10	B Syringe
	10-20	
	20-30	
	30-40	
	40-50	
	50-60	
	60-70	
	70-80	
	80-90	
	90-100	
	100-110	
	110-120	
	120-130	
	130-140	
	140-150	Archive - 80

2H-3	0-10	A Syringe	
	10-20		
	20-30		
	30-40		
	40-50		
	50-60		
	60-70		
	70-80		
	80-90		Russell - 4
	90-100		Mills - 80
	100-110	Edwards - 80	
	110-120	Geochem	
	120-130	Geochem	
	130-140	Geochem	
	140-150	Geochem	

2H-4	0-10	C Syringe	
	10-20		
	20-30		
	30-40		
	40-50		
	50-60		
	60-70		
	70-80		
	80-90		Archive - 80
	90-100		Wenk - 4
	100-110	Paytan - 80	
	110-120	Mamatha - 80	
	120-130	Zeibis - 4	
	130-140	Wang - 4	
	140-150	Wang - 80	

2H-5	0-10	A Syringe	
	10-20		
	20-30		
	30-40		
	40-50		
	50-60		
	60-70		
	70-80		
	80-90		Hirayama - 4
	90-100		Russell - 4
	100-110		Mills - 4
	110-120		Mills - 80
	120-130		Edwards - 80
	130-140		Geochem
	140-150	Geochem	

2H-6	0-10	B Syringe
	10-20	
	20-30	
	30-40	
	40-50	
	50-60	
	60-70	
	70-80	
	80-90	
	90-100	
	100-110	
	110-120	
	120-130	
	130-140	
	140-150	Archive - 80



Figure F9 (continued). (Continued on next page.)

**SITE: 1383D**      Core 3      11/7/11      1700

3H-2	0-10	B Syringe
	10-20	
	20-30	
	30-40	
	40-50	
	50-60	
	60-70	
	70-80	
	80-90	
	90-100	
	100-110	Russell - 4
	110-120	Mills - 80
	120-130	Edwards - 80
	130-140	Geochem
	140-150	Geochem

3H-3	0-10	B Syringe
	10-20	
	20-30	
	30-40	
	40-50	
	50-60	
	60-70	
	70-80	
	80-90	
	90-100	
	100-110	
	110-120	
	120-130	
	130-140	
	140-150	Archive - 80

3H-4	0-10	A Syringe
	10-20	
	20-30	
	30-40	
	40-50	
	50-60	
	60-70	
	70-80	
	80-90	Russell - 4
	90-100	Mills - 80
	100-110	Edwards - 80
	110-120	Geochem
	120-130	Geochem
	130-140	Geochem
	140-150	Geochem

3H-5	0-10	C Syringe
	10-20	
	20-30	
	30-40	
	40-50	
	50-60	
	60-70	
	70-80	
	80-90	Archive - 80
	90-100	Wenk - 4
	100-110	Paytan - 80
	110-120	Mamatha - 80
	120-130	Zeibis - 4
	130-140	Wang - 4
	140-150	Wang - 80

3H-6	0-10	A Syringe
	10-20	
	20-30	
	30-40	
	40-50	
	50-60	
	60-70	
	70-80	
	80-90	Hirayama - 4
	90-100	Russell - 4
	100-110	Mills - 4
	110-120	Mills - 80
	120-130	Edwards - 80
	130-140	Geochem
	140-150	Geochem

3H-7	0-10	B Syringe
	10-20	
	20-30	
	30-40	
	40-50	
	50-60	
	60-70	
	70-80	
	80-90	
	90-100	
	100-110	
	110-120	
	120-130	
	130-140	
	140-150	Archive - 80

B Syringe



Figure F9 (continued). (Continued on next page.)

**SITE: 1383D**      Core 4      11/7/11      1800

4H-1 = Syringe B

4H-2

0-10	A Syringe
10-20	
20-30	
30-40	
40-50	
50-60	
60-70	Paytan - 80
70-80	Wang - 4
80-90	Wang - 80
90-100	Mills - 80
100-110	Edwards - 80
110-120	Geochem
120-130	Geochem
130-140	Geochem
140-150	Geochem

4H-3

0-10	B Syringe
10-20	
20-30	
30-40	
40-50	
50-60	
60-70	Russell - 4
70-80	Wang - 4
80-90	Wang - 80
90-100	Mills - 80
100-110	Edwards - 80
110-120	Geochem
120-130	Geochem
130-140	Geochem
140-150	Geochem

4H-4

0-10	A Syringe
10-20	
20-30	
30-40	
40-50	
50-60	
60-70	Zeibis - 4
70-80	Wang - 4
80-90	Wang - 80
90-100	Mills - 80
100-110	Edwards - 80
110-120	Geochem
120-130	Geochem
130-140	Geochem
140-150	Geochem

4H-5

0-10	C Syringe
10-20	
20-30	
30-40	
40-50	
50-60	
60-70	Hirayama - 4
70-80	Wang - 4
80-90	Russell - 4
90-100	Mills - 80
100-110	Edwards - 80
110-120	Geochem
120-130	Geochem
130-140	Geochem
140-150	Geochem

4H-6

0-10	A Syringe
10-20	
20-30	
30-40	
40-50	
50-60	
60-70	Wang - 4
70-80	Russell - 4
80-90	Mills - 4
90-100	Mills - 80
100-110	Edwards - 80
110-120	Geochem
120-130	Geochem
130-140	Geochem
140-150	Geochem

4H-7

0-10	B Syringe
10-20	
20-30	
30-40	
40-50	
50-60	
60-70	Wang - 4
70-80	Wang - 80
80-90	Russell - 4
90-100	Mills - 80
100-110	Edwards - 80
110-120	Geochem
120-130	Geochem
130-140	Geochem
140-150	Geochem



Figure F9 (continued). (Continued on next page.)

**SITE: 1383D**      Core 5      11/7/11      1900

5H-1 = Syringe A

5H-2

0-10	A Syringe
10-20	
20-30	
30-40	
40-50	
50-60	
60-70	Paytan - 80
70-80	Wang - 4
80-90	Wang - 80
90-100	Mills - 80
100-110	Edwards - 80
110-120	Geochem
120-130	Geochem
130-140	Geochem
140-150	Geochem

5H-3

0-10	B Syringe
10-20	
20-30	
30-40	
40-50	
50-60	
60-70	
70-80	
80-90	
90-100	Russell - 4
100-110	Wang - 4
110-120	Geochem
120-130	Geochem
130-140	Geochem
140-150	Geochem

5H-4

0-10	A Syringe
10-20	
20-30	
30-40	
40-50	
50-60	
60-70	Zeibis - 4
70-80	Wang - 4
80-90	Wang - 80
90-100	Mills - 80
100-110	Edwards - 80
110-120	Geochem
120-130	Geochem
130-140	Geochem
140-150	Geochem

5H-5

0-10	C Syringe
10-20	
20-30	
30-40	
40-50	
50-60	
60-70	
70-80	
80-90	
90-100	
100-110	Wang - 4
110-120	Geochem
120-130	Geochem
130-140	Geochem
140-150	Geochem

5H-6

0-10	A Syringe
10-20	
20-30	
30-40	
40-50	
50-60	
60-70	
70-80	Wang - 4
80-90	Mills - 4
90-100	Mills - 80
100-110	Edwards - 80
110-120	Geochem
120-130	Geochem
130-140	Geochem
140-150	Geochem

5H-7

0-10	B Syringe
10-20	
20-30	
30-40	
40-50	
50-60	
60-70	
70-80	
80-90	
90-100	Mamatha - 80
100-110	Wang - 4
110-120	Geochem
120-130	Geochem
130-140	Geochem
140-150	Geochem



Figure F9 (continued).

**SITE: 1383D**      Core 6      11/7/11      2000

6H-1	0-10	B Syringe
	10-20	
	20-30	
	30-40	
	40-50	
	50-60	
	60-70	
	70-80	
	80-90	
	90-100	
	100-110	
	110-120	Geochem
	120-130	Geochem
	130-140	Geochem
140-150	Geochem	

6H-2	0-10	A Syringe + Paytan	
	10-20		
	20-30		
	30-40		
	40-50		
	50-60		
	60-70		
	70-80		Hirayama - 4
	80-90		Russell - 4
	90-100		Mills - 80
	100-110	Edwards - 80	
	110-120	Geochem	
	120-130	Geochem	
	130-140	Geochem	
140-150	Geochem		

6H-3	0-10	A Syringe	
	10-20		
	20-30		
	30-40		
	40-50		
	50-60		
	60-70		Wang - 4
	70-80		Wang - 80
	80-90		Mills - 4
	90-100		Mills - 80
	100-110	Edwards - 80	
	110-120	Geochem	
	120-130	Geochem	
	130-140	Geochem	
140-150	Geochem		

Geochem collected samples but did not squeeze them. Sediment was very mixed and possibly pulled up during coring (not a true core)



**Figure F10.** Sediment sampling profile, Hole U1383E. All whole-round core sections cut from the core are noted in 10 cm sections. Notes include core disruptions or locations of rock samples collected. (Continued on next five pages.)

SITE: 1383E		Core 1	11/8/11	0100		
1H-1	0-10	A Syringe	1H-2	0-10	A Syringe + Paytan	
	10-20			10-20		
	20-30			20-30		
	30-40			30-40		
	40-50			40-50		
	50-60			50-60		Hirayama - 4
	60-70			60-70		Russell - 4
	70-80	70-80		Wang - 4		
	80-90	Russell - 4		80-90	Wang - 80	
	90-100	Wang - 4		90-100	Mills - 4	
	100-110	Wang - 80		100-110	Mills - 80	
	110-120	Mills - 80		110-120	Edwards - 80	
	120-130	Edwards - 80		120-130	Geochem	
	130-140	Geochem		130-140	Geochem	
140-150	Geochem	140-150	Archive			



Figure F10 (continued). (Continued on next page.)

**SITE: 1383E**      Core 2      11/8/11      0230

2H-1 = B Syringe

2H-2

0-10	A Syringe
10-20	
20-30	
30-40	
40-50	
50-60	
60-70	
70-80	
80-90	
90-100	
100-110	Russell - 4
110-120	Mills - 80
120-130	Edwards - 80
130-140	Geochem
140-150	Geochem

2H-3

0-10	B Syringe
10-20	
20-30	
30-40	
40-50	
50-60	
60-70	
70-80	
80-90	
90-100	
100-110	
110-120	
120-130	
130-140	
140-150	Archive - 80

2H-4

0-10	A Syringe
10-20	
20-30	
30-40	
40-50	
50-60	
60-70	
70-80	
80-90	Russell - 4
90-100	Mills - 80
100-110	Edwards - 80
110-120	Geochem
120-130	Geochem
130-140	Geochem
140-150	Geochem

2H-5

0-10	C Syringe
10-20	
20-30	
30-40	
40-50	
50-60	
60-70	
70-80	
80-90	Wenk - 4
90-100	Paytan - 80
100-110	Mamatha - 80
110-120	Zeibis - 4
120-130	Wang - 4
130-140	Wang - 80
140-150	Archive - 80

2H-6

0-10	A Syringe
10-20	
20-30	
30-40	
40-50	
50-60	
60-70	
70-80	
80-90	Hirayama - 4
90-100	Russell - 4
100-110	Mills - 4
110-120	Mills - 80
120-130	Edwards - 80
130-140	Geochem
140-150	Geochem

2H-7

0-10	B Syringe
10-20	
20-30	
30-40	
40-50	
50-60	
60-70	
70-80	
80-90	
90-100	
100-110	
110-120	
120-130	
130-140	
140-150	Archive - 80



Figure F10 (continued). (Continued on next page.)

**SITE: 1383E**      Core 3      11/8/11      0345

1383E = B Syringes

3H-2	0-10	B Syringe
	10-20	
	20-30	
	30-40	
	40-50	
	50-60	
	60-70	
	70-80	
	80-90	
	90-100	
	100-110	Russell - 4
	110-120	Mills - 80
	120-130	Edwards - 80
	130-140	Geochem
	140-150	Geochem

3H-3	0-10	B Syringe
	10-20	
	20-30	
	30-40	
	40-50	
	50-60	
	60-70	
	70-80	
	80-90	
	90-100	
	100-110	
	110-120	
	120-130	
	130-140	
	140-150	Archive - 80

3H-4	0-10	A Syringe
	10-20	
	20-30	
	30-40	
	40-50	
	50-60	
	60-70	
	70-80	
	80-90	Russell - 4
	90-100	Mills - 80
	100-110	Edwards - 80
	110-120	Geochem
	120-130	Geochem
	130-140	Geochem
	140-150	Geochem

3H-5	0-10	C Syringe
	10-20	
	20-30	
	30-40	
	40-50	
	50-60	
	60-70	
	70-80	
	80-90	Wenk - 4
	90-100	Paytan - 80
	100-110	Mamatha - 80
	110-120	Zeibis - 4
	120-130	Wang - 4
	130-140	Wang - 80
	140-150	Archive - 80

3H-6	0-10	A Syringe
	10-20	
	20-30	
	30-40	
	40-50	
	50-60	
	60-70	
	70-80	
	80-90	Hirayama - 4
	90-100	Russell - 4
	100-110	Mills - 4
	110-120	Mills - 80
	120-130	Edwards - 80
	130-140	Geochem
	140-150	Geochem

3H-7	0-10	B Syringe
	10-20	
	20-30	
	30-40	
	40-50	
	50-60	
	60-70	
	70-80	
	80-90	
	90-100	
	100-110	
	110-120	
	120-130	
	130-140	
	140-150	Archive - 80



Figure F10 (continued). (Continued on next page.)

**SITE: 1383E**      Core 4      11/8/11      0500

4H-1 = Syringe B from bottom of section, rest sent for Oxygen

4H-2	0-10	
	10-20	
	20-30	
	30-40	
	40-50	
	50-60	
	60-70	
	70-80	Wang - 80
	80-90	Wang - 4
	90-100	Mills - 80
	100-110	Edwards - 80
	110-120	Geochem
	120-130	Geochem
	130-140	Geochem
	140-150	Geochem

4H-3	0-10	B Syringe
	10-20	
	20-30	
	30-40	
	40-50	
	50-60	
	60-70	Russell - 4
	70-80	Wang - 4
	80-90	Mamatha - 80
	90-100	Mills - 80
	100-110	Edwards - 80
	110-120	Geochem
	120-130	Geochem
	130-140	Geochem
	140-150	Geochem

4H-4	0-10	A Syringe
	10-20	
	20-30	
	30-40	
	40-50	
	50-60	
	60-70	Zeibis - 4
	70-80	Wang - 4
	80-90	Wang - 80
	90-100	Mills - 80
	100-110	Edwards - 80
	110-120	Geochem
	120-130	Geochem
	130-140	Geochem
	140-150	Geochem

4H-5	0-10	C Syringe
	10-20	
	20-30	
	30-40	
	40-50	
	50-60	
	60-70	Hirayama - 4
	70-80	Wang - 4
	80-90	Russell - 4
	90-100	Mills - 80
	100-110	Edwards - 80
	110-120	Geochem
	120-130	Geochem
	130-140	Geochem
	140-150	Geochem

4H-6	0-10	A Syringe
	10-20	
	20-30	
	30-40	
	40-50	
	50-60	
	60-70	Wang - 4
	70-80	Russell - 4
	80-90	Mills - 4
	90-100	Mills - 80
	100-110	Edwards - 80
	110-120	Geochem
	120-130	Geochem
	130-140	Geochem
	140-150	Geochem

4H-7	0-10	B Syringe
	10-20	
	20-30	
	30-40	
	40-50	
	50-60	
	60-70	Wang - 4
	70-80	Wang - 80
	80-90	Russell - 4
	90-100	Mills - 80
	100-110	Edwards - 80
	110-120	Geochem
	120-130	Geochem
	130-140	Geochem
	140-150	Geochem



Figure F10 (continued). (Continued on next page.)

SITE: 1383E Core 5 11/8/11 0630

5H-1 = Syringe A

0-10	
10-20	
20-30	
30-40	A Syringe
40-50	
50-60	
60-70	
70-80	
80-90	
90-100	Mills - 80
100-110	Edwards - 80
110-120	Geochem
120-130	Geochem
130-140	Geochem
140-150	Geochem

0-10	C Syringe
10-20	
20-30	
30-40	
40-50	
50-60	
60-70	Hirayama - 4
70-80	Wang - 4
80-90	Russell - 4
90-100	Mills - 80
100-110	Edwards - 80
110-120	Geochem
120-130	Geochem
130-140	Geochem
140-150	Geochem

0-10	B Syringe
10-20	
20-30	
30-40	
40-50	
50-60	
60-70	Russell - 4
70-80	Wang - 4
80-90	Mamatha - 80
90-100	Mills - 80
100-110	Edwards - 80
110-120	Geochem
120-130	Geochem
130-140	Geochem
140-150	Geochem

0-10	A Syringe
10-20	
20-30	
30-40	
40-50	
50-60	
60-70	Wang - 4
70-80	Russell - 4
80-90	Mills - 4
90-100	Mills - 80
100-110	Edwards - 80
110-120	Geochem
120-130	Geochem
130-140	Geochem
140-150	Geochem

Rock sample at bottom of sample

0-10	A Syringe
10-20	
20-30	
30-40	
40-50	
50-60	
60-70	Zeibis - 4
70-80	Wang - 4
80-90	Wang - 80
90-100	Mills - 80
100-110	Edwards - 80
110-120	Geochem
120-130	Geochem
130-140	Geochem
140-150	Geochem

0-10	B Syringe
10-20	
20-30	
30-40	
40-50	
50-60	
60-70	Wang - 4
70-80	Wang - 80
80-90	Russell - 4
90-100	Mills - 80
100-110	Edwards - 80
110-120	Geochem
120-130	Geochem
130-140	Geochem
140-150	Geochem



Figure F10 (continued).

**SITE: 1383E**      Core 6      11/8/11      0800

6H-2

0-10	A Syringe
10-20	
20-30	
30-40	
40-50	
50-60	
60-70	Paytan - 80
70-80	Wang - 4
80-90	Wang - 80
90-100	Mills - 80
100-110	Edwards - 80
110-120	Geochem
120-130	Geochem
130-140	Geochem
140-150	Geochem

6H-3

0-10	B Syringe
10-20	
20-30	
30-40	
40-50	
50-60	
60-70	Russell - 4
70-80	Wang - 4
80-90	Mamatha - 80
90-100	Mills - 80
100-110	Edwards - 80
110-120	Geochem
120-130	Geochem
130-140	Geochem
140-150	Geochem

6H-4

0-10	A Syringe
10-20	
20-30	
30-40	
40-50	
50-60	
60-70	Zeibis - 4
70-80	Wang - 4
80-90	Wang - 80
90-100	Mills - 80
100-110	Edwards - 80
110-120	Geochem
120-130	Geochem
130-140	Geochem
140-150	Geochem

Rock sample taked from above spot

6H-5

0-10	C Syringe
10-20	
20-30	
30-40	
40-50	
50-60	
60-70	Hirayama - 4
70-80	Wang - 4
80-90	Russell - 4
90-100	Mills - 80
100-110	Edwards - 80
110-120	Geochem
120-130	Geochem
130-140	Geochem
140-150	Geochem

6H-6

0-10	A Syringe
10-20	
20-30	
30-40	
40-50	
50-60	
60-70	Wang - 4
70-80	Russell - 4
80-90	Mills - 4
90-100	Mills - 80
100-110	Edwards - 80
110-120	Geochem
120-130	Geochem
130-140	Geochem
140-150	Geochem

6H-7 = Washed out due to broken core liner  
- not sampled



**Figure F11.** Sediment sampling profile, Hole U1384A. All whole-round core sections cut from the core are noted in 10 cm sections. Notes include core disruptions or locations of rock samples collected. (Continued on next 10 pages.)

SITE: 1384A							
Core 1		11/9/11	2200				
1H-1	0-10	B Syringe	0-10	A Syringe	1H-3	0-10	A Syringe
	10-20		10-20				
	20-30		20-30				
	30-40		30-40				
	40-50		40-50				
	50-60		50-60				
	60-70		60-70				
	70-80	60-70	Hirayama - 4				
	80-90	Russell - 4	70-80	Russell - 4			
	90-100	Wang - 4	80-90	Wang - 4			
	100-110	Wang - 40	90-100	Wang - 40			
	110-120	Mills - 80	100-110	Mills - 4			
	120-130	Edwards - 80	110-120	Mills - 80			
	130-140	Geochem	120-130	Edwards - 80			
	140-150	Geochem	130-140	Geochem			
		140-150	Geochem				
				140-150	Wang - 4		



Figure F11 (continued). (Continued on next page.)

**SITE: 1384A**      Core 2      11/9/11      2315

2H-1

0-10	A Syringe
10-20	
20-30	
30-40	
40-50	
50-60	
60-70	
70-80	
80-90	
90-100	
100-110	Russell - 4
110-120	Mills - 80
120-130	Edwards - 80
130-140	Geochem
140-150	Geochem

2H-2

0-10	B Syringe
10-20	
20-30	
30-40	
40-50	
50-60	
60-70	
70-80	
80-90	
90-100	
100-110	
110-120	
120-130	
130-140	
140-150	

2H-3

0-10	A Syringe
10-20	
20-30	
30-40	
40-50	
50-60	
60-70	
70-80	
80-90	
90-100	
100-110	Russell - 4
110-120	Mills - 80
120-130	Edwards - 80
130-140	Geochem
140-150	Geochem

2H-4

0-10	C Syringe
10-20	
20-30	
30-40	
40-50	
50-60	
60-70	
70-80	
80-90	Wenk - 4
90-100	Paytan - 80
100-110	Mamatha - 80
110-120	Zeibis - 4
120-130	Wang - 4
130-140	Wang - 80
140-150	Archive - 80

2H-5

0-10	A Syringe
10-20	
20-30	
30-40	
40-50	
50-60	
60-70	
70-80	
80-90	Hirayama - 4
90-100	Russell - 4
100-110	Mills - 4
110-120	Mills - 80
120-130	Edwards - 80
130-140	Geochem
140-150	Geochem

2H-6

0-10	B Syringe
10-20	
20-30	
30-40	
40-50	
50-60	
60-70	
70-80	
80-90	
90-100	
100-110	
110-120	
120-130	
130-140	
140-150	



Figure F11 (continued). (Continued on next page.)

**SITE: 1384A      Core 3      11/10/11      0045**

3H-1	0-10	A Syringe
	10-20	
	20-30	
	30-40	
	40-50	
	50-60	
	60-70	
	70-80	
	80-90	
	90-100	
	100-110	
	110-120	
	120-130	
	130-140	
	140-150	

Not sampled - washed out - Broken core liner

3H-2	0-10	B Syringe	
	10-20		
	20-30		
	30-40		
	40-50		
	50-60		
	60-70		
	70-80		
	80-90		
	90-100		
	100-110		Russell - 4
	110-120		Mills - 80
	120-130		Edwards - 80
	130-140		Geochem
	140-150		Geochem

3H-3	0-10	A Syringe
	10-20	
	20-30	
	30-40	
	40-50	
	50-60	
	60-70	
	70-80	
	80-90	
	90-100	
	100-110	
	110-120	
	120-130	
	130-140	
	140-150	

Bottom washed out

3H-4	0-10	C Syringe	
	10-20		
	20-30		
	30-40		
	40-50		
	50-60		
	60-70		Wenk - 4
	70-80		Geochem
	80-90		Geochem
	90-100		Paytan - 80
	100-110		Mamatha - 80
	110-120		Zeibis - 4
	120-130		Wang - 4
	130-140		Wang - 80
	140-150		Archive - 80

3H-5	0-10	A Syringe	
	10-20		
	20-30		
	30-40		
	40-50		
	50-60		
	60-70		
	70-80		
	80-90		Hirayama - 4
	90-100		Russell - 4
	100-110		Mills - 4
	110-120		Mills - 80
	120-130		Edwards - 80
	130-140		Geochem
	140-150		Geochem

3H-6	0-10	B Syringe
	10-20	
	20-30	
	30-40	
	40-50	
	50-60	
	60-70	
	70-80	
	80-90	
	90-100	
	100-110	
	110-120	
	120-130	
	130-140	
	140-150	

Not sampled - washed out - Broken core liner



Figure F11 (continued). (Continued on next page.)

**SITE: 1384A**      Core 4      11/10/11      0200

Microsphere bag found in core catcher - Edwards 4C

4H-2	0-10	A Syringe
	10-20	
	20-30	
	30-40	
	40-50	
	50-60	
	60-70	
	70-80	
	80-90	
	90-100	
	100-110	Russell - 4
	110-120	Mills - 80
	120-130	Edwards - 80
	130-140	Geochem
	140-150	Geochem

4H-3	0-10	B Syringe
	10-20	
	20-30	
	30-40	
	40-50	
	50-60	
	60-70	
	70-80	
	80-90	
	90-100	
	100-110	
	110-120	
	120-130	
	130-140	
	140-150	

4H-4	0-10	A Syringe
	10-20	
	20-30	
	30-40	
	40-50	
	50-60	
	60-70	
	70-80	
	80-90	
	90-100	
	100-110	Russell - 4
	110-120	Mills - 80
	120-130	Edwards - 80
	130-140	Geochem
	140-150	Geochem

4H-5	0-10	C Syringe
	10-20	
	20-30	
	30-40	
	40-50	
	50-60	
	60-70	
	70-80	
	80-90	Wenk - 4
	90-100	Paytan - 80
	100-110	Mamatha - 80
	110-120	Zeibis - 4
	120-130	Wang - 4
	130-140	Wang - 80
	140-150	Archive - 80

4H-6	0-10	A Syringe
	10-20	
	20-30	
	30-40	
	40-50	
	50-60	
	60-70	
	70-80	
	80-90	Hirayama - 4
	90-100	Russell - 4
	100-110	Mills - 4
	110-120	Mills - 80
	120-130	Edwards - 80
	130-140	Geochem
	140-150	Geochem

4H-7	0-10	B Syringe
	10-20	
	20-30	
	30-40	
	40-50	
	50-60	
	60-70	
	70-80	
	80-90	
	90-100	
	100-110	
	110-120	
	120-130	
	130-140	
	140-150	

4H-5 = Bottom half washed out.



Figure F11 (continued). (Continued on next page.)

**SITE: 1384A**      Core 5      11/10/11      0315

0-10	
10-20	
20-30	
30-40	
40-50	
50-60	
60-70	
70-80	
80-90	
90-100	A Syringe
100-110	Russell - 4
110-120	Mills - 80
120-130	Edwards - 80
130-140	Geochem
140-150	Geochem

0-10	B Syringe
10-20	
20-30	
30-40	
40-50	
50-60	
60-70	
70-80	
80-90	
90-100	
100-110	
110-120	
120-130	
130-140	
140-150	

0-10	A Syringe
10-20	
20-30	
30-40	
40-50	
50-60	
60-70	
70-80	
80-90	
90-100	
100-110	Russell - 4
110-120	Mills - 80
120-130	Edwards - 80
130-140	Geochem
140-150	Geochem

0-10	C Syringe
10-20	
20-30	
30-40	
40-50	
50-60	
60-70	
70-80	
80-90	Wenk - 4
90-100	Paytan - 80
100-110	Mamatha - 80
110-120	Zeibis - 4
120-130	Wang - 4
130-140	Wang - 80
140-150	Archive - 80

0-10	A Syringe
10-20	
20-30	
30-40	
40-50	
50-60	
60-70	
70-80	
80-90	Hirayama - 4
90-100	Russell - 4
100-110	Mills - 4
110-120	Mills - 80
120-130	Edwards - 80
130-140	Geochem
140-150	Geochem

0-10	B Syringe
10-20	
20-30	
30-40	
40-50	
50-60	
60-70	
70-80	
80-90	
90-100	
100-110	
110-120	
120-130	
130-140	
140-150	



Figure F11 (continued). (Continued on next page.)

SITE: 1384A Core 6 11/10/11 0430

6H-1	0-10	
	10-20	
	20-30	
	30-40	
	40-50	
	50-60	
	60-70	
	70-80	
	80-90	
	90-100	
	100-110	
	110-120	
	120-130	
	130-140	
	140-150	

Sandy, washed out, not sampled

6H-2	0-10	
	10-20	
	20-30	
	30-40	
	40-50	
	50-60	
	60-70	
	70-80	
	80-90	Russell - 4
	90-100	Wang - 4
	100-110	Mamatha - 20
	110-120	Mills - 80
	120-130	Edwards - 80
	130-140	Geochem
	140-150	Geochem

Some water, but still sampled - No syringe

6H-3	0-10	A Syringe
	10-20	
	20-30	
	30-40	
	40-50	
	50-60	
	60-70	
	70-80	
	80-90	Zeibis - 4
	90-100	Wang - 4
	100-110	Wang - 40
	110-120	Mills - 80
	120-130	Edwards - 80
	130-140	Geochem
	140-150	Geochem

6H-4	0-10	C Syringe
	10-20	
	20-30	
	30-40	
	40-50	
	50-60	
	60-70	
	70-80	
	80-90	Hirayama - 4
	90-100	Wang - 4
	100-110	Russell - 4
	110-120	Mills - 80
	120-130	Edwards - 80
	130-140	Geochem
	140-150	Geochem

6H-5	0-10	A Syringe
	10-20	
	20-30	
	30-40	
	40-50	
	50-60	
	60-70	
	70-80	
	60-70	Wang - 4
	70-80	Russell - 4
	80-90	Mills - 4
	90-100	Mills - 80
	100-110	Edwards - 80
	130-140	Geochem
	140-150	Geochem

6H-6	0-10	B Syringe
	10-20	
	20-30	
	30-40	
	40-50	
	50-60	
	60-70	
	70-80	
	80-90	Wang - 4
	90-100	Wang - 40
	100-110	Russell - 4
	110-120	Mills - 80
	120-130	Edwards - 80
	130-140	Geochem
	140-150	Geochem

B Syringe



Figure F11 (continued). (Continued on next page.)

**SITE: 1384A**      Core 6      11/10/11      0430

6 or 7 H-1

0-10	A Syringe
10-20	
20-30	
30-40	
40-50	
50-60	
60-70	Paytan - 80
70-80	Wang - 4
80-90	Wang - 40
90-100	Mills - 80
100-110	Edwards - 80
110-120	Geochem
120-130	Geochem
130-140	Geochem
140-150	Geochem

6 or 7 H-2

0-10	B Syringe
10-20	
20-30	
30-40	
40-50	
50-60	
60-70	Russell - 4
70-80	Wang - 4
80-90	Mamatha - 20
90-100	Mills - 80
100-110	Edwards - 80
110-120	Geochem
120-130	Geochem
130-140	Geochem
140-150	Geochem

6 or 7 H-3

0-10	A Syringe
10-20	
20-30	
30-40	
40-50	
50-60	
60-70	Zeibis - 4
70-80	Wang - 4
80-90	Wang - 40
90-100	Mills - 80
100-110	Edwards - 80
110-120	Geochem
120-130	Geochem
130-140	Geochem
140-150	Geochem

6 or 7 H-4

0-10	C Syringe
10-20	
20-30	
30-40	
40-50	
50-60	
60-70	Hirayama - 4
70-80	Wang - 4
80-90	Russell - 4
90-100	Mills - 80
100-110	Edwards - 80
110-120	Geochem
120-130	Geochem
130-140	Geochem
140-150	Geochem

6 or 7 H-5

0-10	A Syringe
10-20	
20-30	
30-40	
40-50	
50-60	
60-70	Wang - 4
70-80	Russell - 4
80-90	Mills - 4
90-100	Mills - 80
100-110	Edwards - 80
110-120	Geochem
120-130	Geochem
130-140	Geochem
140-150	Geochem

6 or 7 H-6

0-10	B Syringe
10-20	
20-30	
30-40	
40-50	
50-60	
60-70	Wang - 4
70-80	Wang - 40
80-90	Russell - 4
90-100	Mills - 80
100-110	Edwards - 80
110-120	Geochem
120-130	Geochem
130-140	Geochem
140-150	Geochem

B Syringe



Figure F11 (continued). (Continued on next page.)

**SITE: 1384A      Core 7      11/10/11      0600**

7H-1	0-10	A Syringe
	10-20	
	20-30	
	30-40	
	40-50	
	50-60	
	60-70	
	70-80	
	80-90	
	90-100	
	100-110	Paytan - 80
	110-120	Wang - 4
	120-130	Wang - 40
	130-140	Mills - 80
	140-150	Edwards - 80

7H-2	0-10	B Syringe
	10-20	
	20-30	
	30-40	
	40-50	
	50-60	
	60-70	
	70-80	
	80-90	Russell - 4
	90-100	Wang - 4
	100-110	Mamatha - 20
	110-120	Mills - 80
	120-130	Edwards - 80
	130-140	Geochem
	140-150	Geochem

7H-3	0-10	A Syringe
	10-20	
	20-30	
	30-40	
	40-50	
	50-60	
	60-70	
	70-80	
	80-90	Zeibis - 4
	90-100	Wang - 4
	100-110	Wang - 40
	110-120	Mills - 80
	120-130	Edwards - 80
	130-140	Geochem
	140-150	Geochem

7H-4	0-10	C Syringe
	10-20	
	20-30	
	30-40	
	40-50	
	50-60	
	60-70	
	70-80	
	80-90	Hirayama - 4
	90-100	Wang - 4
	100-110	Russell - 4
	110-120	Mills - 80
	120-130	Edwards - 80
	130-140	Geochem
	140-150	Geochem

7H-5	0-10	A Syringe
	10-20	
	20-30	
	30-40	
	40-50	
	50-60	
	60-70	Wang - 4
	70-80	Russell - 4
	80-90	Mills - 4
	90-100	Mills - 80
	100-110	Edwards - 80
	110-120	Geochem
	120-130	Geochem
	130-140	Geochem
	140-150	Geochem

7H-6	0-10	B Syringe
	10-20	
	20-30	
	30-40	
	40-50	
	50-60	
	60-70	
	70-80	Geochem
	80-90	Geochem
	90-100	Geochem
	100-110	Geochem
	110-120	
	120-130	
	130-140	
	140-150	

Cracked tube, only Geochem and Syringes collected



Figure F11 (continued). (Continued on next page.)

**SITE: 1384A**      **Core 8**      **11/10/11**      **0430**

0-10	B Syringe
10-20	
20-30	
30-40	
40-50	
50-60	
60-70	
70-80	
80-90	
90-100	
100-110	
110-120	
120-130	
130-140	
140-150	

0-10	A Syringe
10-20	
20-30	
30-40	
40-50	
50-60	
60-70	
70-80	
80-90	
90-100	
100-110	
110-120	
120-130	
130-140	
140-150	

0-10	B Syringe
10-20	
20-30	
30-40	
40-50	
50-60	
60-70	
70-80	
80-90	
90-100	
100-110	
110-120	
120-130	
130-140	
140-150	

0-10	
10-20	
20-30	
30-40	
40-50	
50-60	
60-70	Hirayama - 4
70-80	Wang - 4
80-90	Russell - 4
90-100	Mills - 80
100-110	Edwards - 80
110-120	Geochem
120-130	Geochem
130-140	Geochem
140-150	Geochem

0-10	A Syringe
10-20	
20-30	
30-40	
40-50	
50-60	
60-70	Wang - 4
70-80	Russell - 4
80-90	Mills - 4
90-100	Mills - 80
100-110	Edwards - 80
110-120	Geochem
120-130	Geochem
130-140	Geochem
140-150	Geochem

0-10	B Syringe
10-20	
20-30	
30-40	
40-50	
50-60	
60-70	Wang - 4
70-80	Wang - 40
80-90	Russell - 4
90-100	Mills - 80
100-110	Edwards - 80
110-120	Geochem
120-130	Geochem
130-140	Geochem
140-150	Geochem

B Syringe



Figure F11 (continued). (Continued on next page.)

SITE: 1384A Core 9 11/10/11

0-10	
10-20	
20-30	
30-40	
40-50	
50-60	
60-70	
70-80	
80-90	
90-100	
100-110	
110-120	
120-130	
130-140	
140-150	

Not sampled

0-10	B Syringe
10-20	
20-30	
30-40	
40-50	
50-60	
60-70	Russell - 4
70-80	Wang - 4
80-90	Mamatha - 20
90-100	Mills - 80
100-110	Edwards - 80
110-120	Geochem
120-130	Geochem
130-140	Geochem
140-150	Geochem

0-10	A Syringe
10-20	
20-30	
30-40	
40-50	
50-60	
60-70	Zeibis - 4
70-80	Wang - 4
80-90	Wang - 40
90-100	Mills - 80
100-110	Edwards - 80
110-120	Geochem
120-130	Geochem
130-140	Geochem
140-150	Geochem

0-10	C Syringe
10-20	
20-30	
30-40	
40-50	
50-60	
60-70	Hirayama - 4
70-80	Wang - 4
80-90	Russell - 4
90-100	Mills - 80
100-110	Edwards - 80
110-120	Geochem
120-130	Geochem
130-140	Geochem
140-150	Geochem

0-10	A Syringe
10-20	
20-30	
30-40	
40-50	
50-60	
60-70	Wang - 4
70-80	Russell - 4
80-90	Mills - 4
90-100	Mills - 80
100-110	Edwards - 80
110-120	Geochem
120-130	Geochem
130-140	Geochem
140-150	Geochem

0-10	B Syringe
10-20	
20-30	
30-40	
40-50	
50-60	
60-70	Wang - 4
70-80	Wang - 40
80-90	Russell - 4
90-100	Mills - 80
100-110	Edwards - 80
110-120	Geochem
120-130	Geochem
130-140	Geochem
140-150	Geochem

B Syringe



Figure F11 (continued).

**SITE: 1384A**      Core 11      11/10/11

11H-1 = Not sampled

11H-2	0-10	C Syringe
	10-20	
	20-30	
	30-40	
	40-50	
	50-60	
	60-70	Hirayama - 4
	70-80	Wang - 4
	80-90	Russell - 4
	90-100	Mills - 80
	100-110	Edwards - 80
	110-120	Geochem
	120-130	Geochem
	130-140	Geochem
	140-150	Geochem

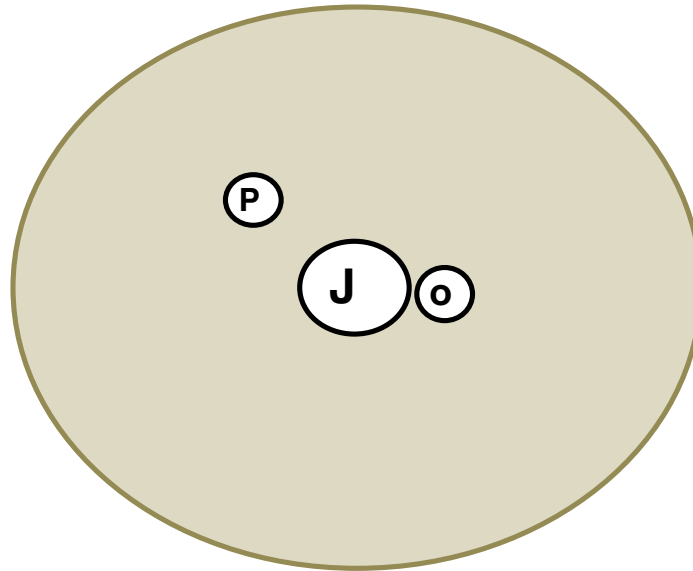
11H-3	0-10	A Syringe
	10-20	
	20-30	
	30-40	
	40-50	
	50-60	
	60-70	Wang - 4
	70-80	Russell - 4
	80-90	Mills - 4
	90-100	Mills - 80
	100-110	Edwards - 80
	110-120	Geochem
	120-130	Geochem
	130-140	Geochem
	140-150	Geochem

11H-4	0-10	B Syringe
	10-20	
	20-30	
	30-40	
	40-50	
	50-60	Mills - 80
	60-70	Wang - 4
	70-80	Wang - 40
	80-90	Russell - 4
	90-100	
	100-110	Edwards - 80
	110-120	Geochem
	120-130	Geochem
	130-140	Geochem
	140-150	Geochem

90-100 water washed out

**Figure F12.** Sampling profile for syringes, Expedition 336. Syringe locations are presented in relation to the open end of a core section. Syringe samples were collected according to the sampling profile for each core. J = Jorgensen, O = Orcutt, P = Paytan. PBS = phosphate-buffered saline.

### Syringes



#### Toothpick

Orcutt - Interior/exterior

- Place into tube w/PBS; 4°C

#### Syringes

Jorg - 10 mL, -80°C all sections

Orcutt - 1 x 3 mL - interior

- Only in section with Edwards

- 2 mL for methane

Paytan - 5 mL - Section 4, 4°C

#### Syringe profiles

Syringe A = Jorg, Orcutt, Toothpick

Syringe B = Jorg

Syringe C = Jorg and Paytan

**Figure F13.** Hard rock core flow for physical properties measurements, Expedition 336. Approximate time steps are given per core section. WR = whole-round sample, MBIO = microbiology, GRA = gamma ray attenuation, MS = magnetic susceptibility, NGR = natural gamma radiation, MAD = moisture and density, A = archive half, W = working half.

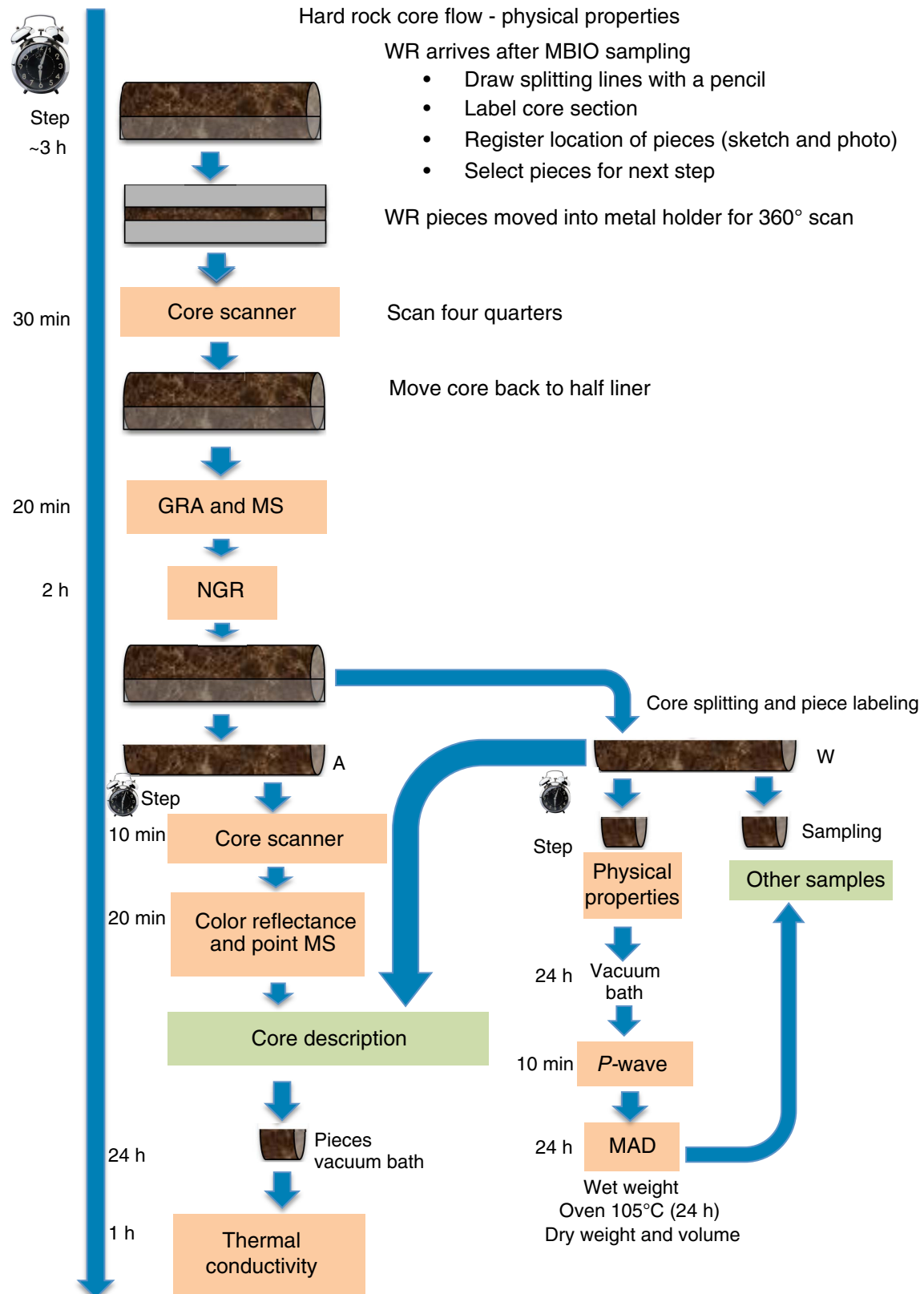


**Figure F14.** Sediment core flow for physical properties measurements, Expedition 336. Approximate time steps are given per core section. WR = whole-round sample, MBIO = microbiology, GRA = gamma ray attenuation, MS = magnetic susceptibility, NGR = natural gamma radiation, MAD = moisture and density, A = archive half, W = working half.

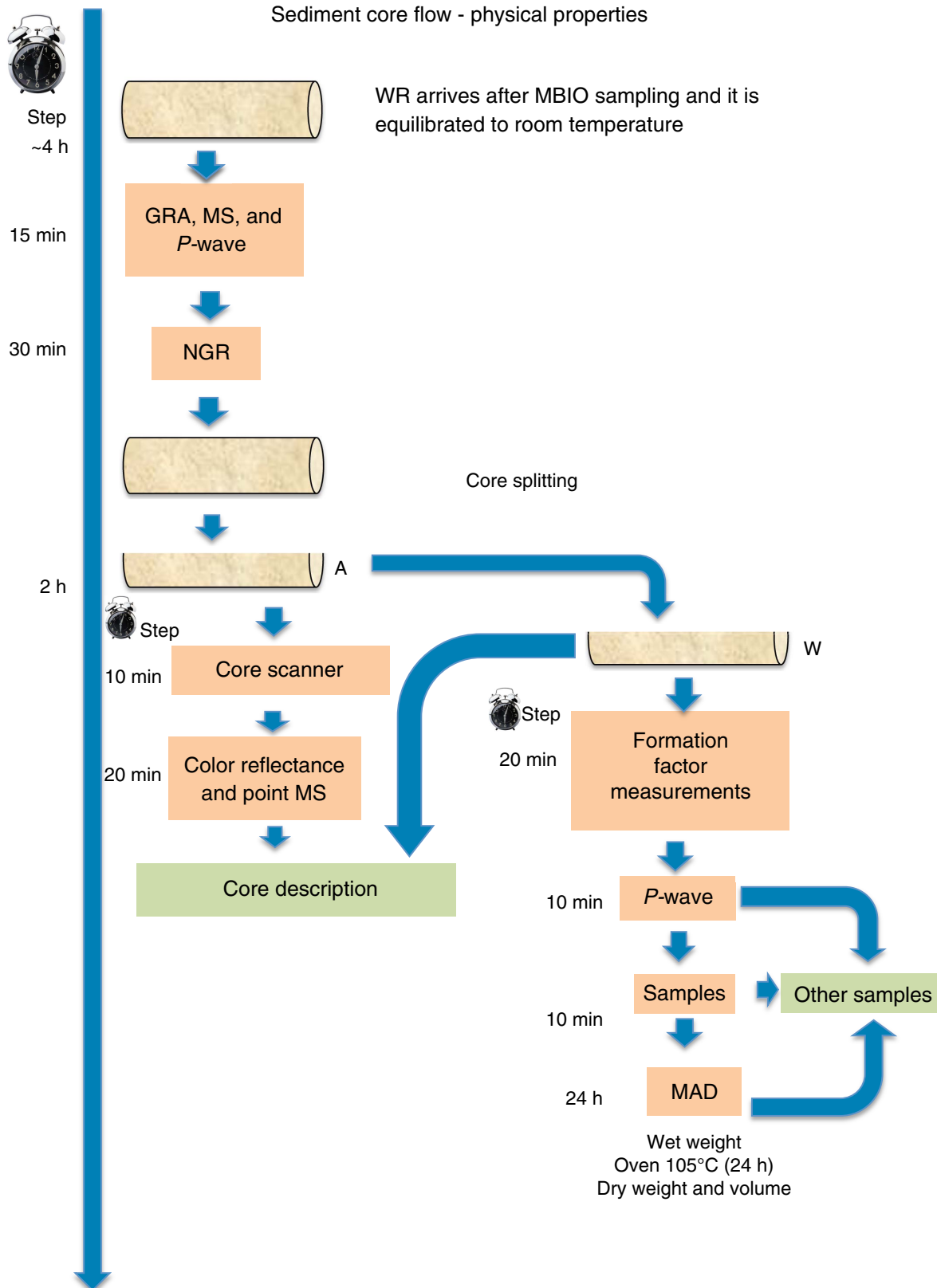




**Figure F15.** Wireline tool strings used during Expedition 336. LEH-MT = logging equipment head-mud temperature, EDTC = Enhanced Digital Telemetry Cartridge, HNGS = Hostile Environment Natural Gamma Ray Sonde, GPIT = General Purpose Inclinerometry Tool, MTT = Modular Temperature Tool, ELIC = EFTB-Lamont Interface Cartridge, MFTM = Multifunction Telemetry Module, DEBI-t = Deep Exploration Biosphere Investigative tool, HLDS = Hostile Environment Litho-Density Sonde, HRLA = High-Resolution Laterolog Array, FMS = Formation MicroScanner, LEH-QT = logging equipment head-q tension, DSI = Dipole Shear Sonic Imager.

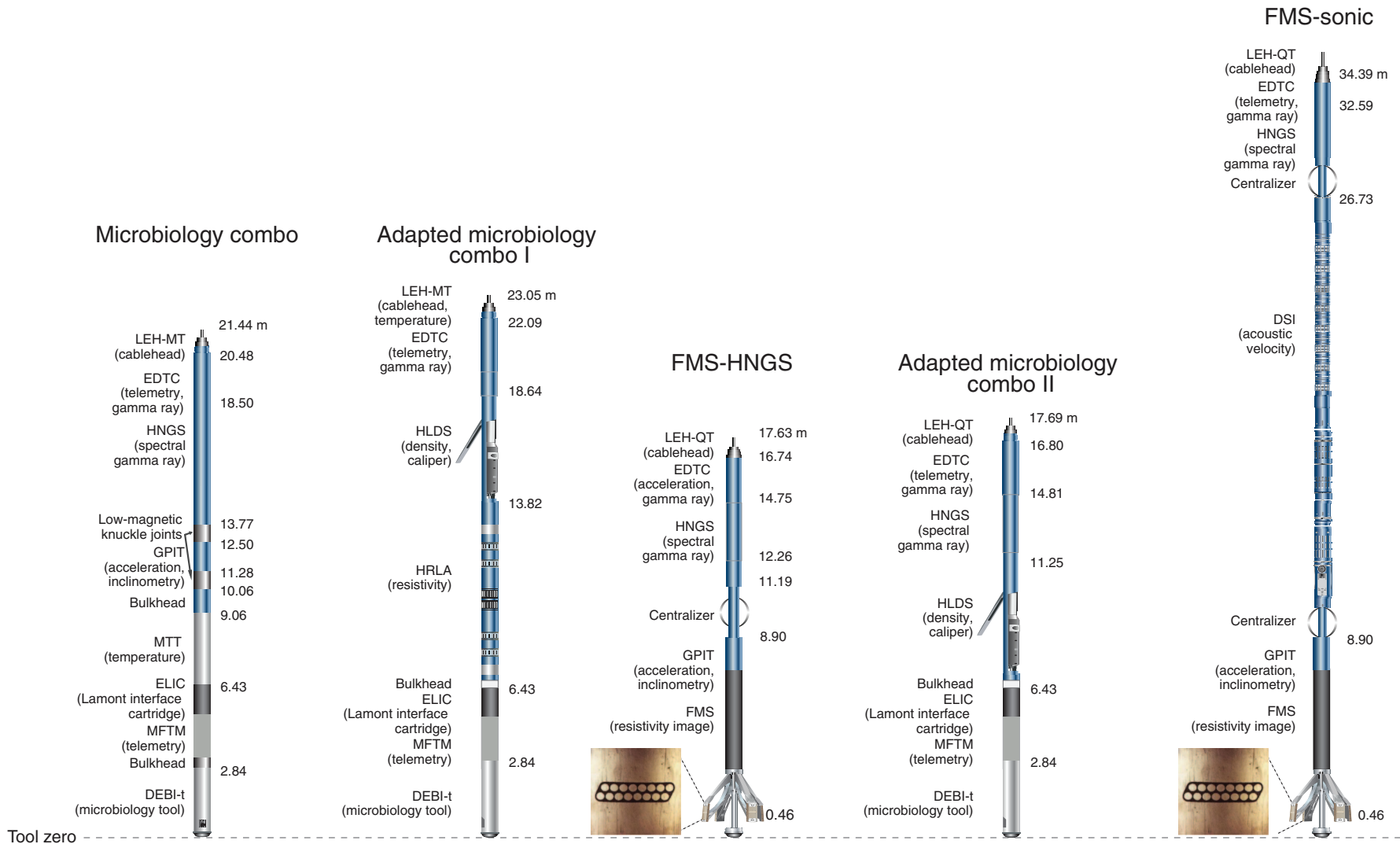


**Table T1.** IODP depth scale terminology (see IODP Depth Scales Terminology version 2 at [www.iodp.org/program-policies/](http://www.iodp.org/program-policies/)).

Depth scale	Acronym	Origin	Method description	Submethod	Unit	Previous name	Previous unit
Drillers depth scale: Drilling depth below rig floor	DRF	Drill floor	Add the lengths of all drill string components deployed beneath the rig floor, from bit to the point on the rig floor where the length of the deployed portion of the last string is measured	Describe submethod of measuring drill string component length and length deployed at rig floor.	m	Depth	mbrf
Drilling depth below seafloor	DSF	Seafloor	Subtract the distance between rig floor and sea level from an estimate of seafloor depth at the drilling depth below rig floor scale using one of the submethods	Specify submethod used: A. Tag seafloor B. Mudline core C. Visual control D. Inherit depth E. Other	m	Depth	mbsf
Core depth scale: Core depth (below seafloor)	CSF	Seafloor	Measure core sample or measurement offset below the core top and add it to the core top's drilling depth below seafloor; apply one of the submethods	Specify submethod used: A. Let overlap if long B. Scale if long C. Other	m	Depth	mbsf
Core composite depth	CCSF	Seafloor	Align cores from one hole or multiple adjacent holes based on one of the submethods. The result is a newly constructed depth scale.	Specify submethod used: A. Append if long B. Scale by factor C. Correlate features D. Splice E. Other	m	Depth	mcd
Wireline depth scale: Wireline log depth below rig floor	WRF	Drill floor	Measure length of wireline extended beneath the rig floor	Describe submethod	m	Depth	mbrf
Wireline log depth below seafloor	WSF	Seafloor	Subtract the distance between rig floor and sea level from an estimate of seafloor depth at the wireline depth below rig floor scale using one of three submethods	Specify submethod used: A. Seafloor signal B. Drilling depth C. Inherit depth D. Other	m	Depth	mbsf
Wireline log speed-corrected depth (below seafloor)	WSSF	Seafloor	Correction for irregular motion of the tool during logging using accelerometer data; used for high-resolution logs such as microresistivity (FMS)	Describe submethod if applicable	m	Depth	mbsf
Wireline log matched depth (below seafloor)	WMSF	Seafloor	Pick log data from one run as a reference and map other run data using several tie points	Describe reference log and number/type of tie points used	m	Depth	mbsf

**Table T2.** Analytical conditions for hard rock ICP-AES runs, Expedition 336.

Element	Wavelength (nm)	Integration time (s)	Power (kW)
Major:			
Si	251.611	30	1.2
Ti	337.280	30	1.2
Al	396.152	30	1.2
Fe	239.563	30	1.2
Mg	285.213	30	1.2
Ca	317.933	30	1.2
Na	588.995	30	1.2
K	766.491	30	1.2
P	214.914	30	1.2
Trace:			
Ba	233.527	30	1.2
Sr	407.771	30	1.2
Zr	339.198	30	1.2
Y	360.073	30	1.2
V	310.230	30	1.2
Sc	361.383	30	1.2
Cu	324.754	30	1.2
Zn	213.856	30	1.2
Co	228.615	30	1.2
Cr	267.716	30	1.2
Ni	231.604	30	1.2

The wavelength yielding the best calibration line was used. ICP-AES = inductively coupled plasma–atomic emission spectroscopy.

**Table T3.** Check-standard data for ICP-AES analyses, Expedition 336.

Element	BAS-140			MRG-1		
	Mean (N = 8)	RSD % (1 $\sigma$ )	Published	Mean (N = 8)	RSD % (1 $\sigma$ )	Published
Major (wt%):						
SiO <sub>2</sub>	50.81	0.7	50.5	38.9	0.7	39.6
TiO <sub>2</sub>	0.984	0.5	0.98	3.83	0.9	3.82
Al <sub>2</sub> O <sub>3</sub>	14.5	0.5	14.6	8.66	0.6	8.57
Fe <sub>2</sub> O <sub>3</sub> <sup>T</sup>	11.0	0.8	11.1	18.0	1.1	18.2
MnO	ND		0.19	ND		
MgO	8.21	1.0	8.15	13.4	0.7	13.7
CaO	12.4	0.5	12.4	14.7	0.8	14.9
Na <sub>2</sub> O	1.86	2.1	1.84	0.69	1.6	0.75
K <sub>2</sub> O	0.02	4.8	0.01	0.17	1.3	0.18
P <sub>2</sub> O <sub>5</sub>	0.08	18.9	0.08	0.09	18.5	0.08
Trace (ppm):						
Ba	3.0	20.0	2*	55.3	3.0	
Sr	31.9	8.5	44	275	2.3	270
Zr	48.3	3.0	49*	111	2.8	109
Y	27.5	2.9	24	13.5	4.1	14.2
V	335	0.7	333*	523	1.1	533
Sc	45.2	0.8	43	54.6	0.4	55.7
Cu	85.3	1.5	81	130	2.1	136
Zn	65.3 <sup>†</sup>	2.3 <sup>†</sup>	80	191 <sup>†</sup>	0.5 <sup>†</sup>	194
Co	49.4	1.4	55	88.0	2.3	88.1
Cr	185	1.2	186	445	0.5	436
Ni	82.5	2.8	85	191	3.4	196

\* = values reported by Expedition 309/312 Shipboard Scientific Party (2006). † = values calculated based on N = 4. ICP-AES = inductively coupled plasma–atomic emission spectroscopy. BAS-140 = values published by Sparks and Zuleger (1995). MRG-1 = values published by Govindaraju (1989). RSD = run-to-run relative standard deviation. Uncertainties are listed as RSD% (1 $\sigma$ ). Fe<sub>2</sub>O<sub>3</sub><sup>T</sup> = total iron calculated as ferric oxide. ND = not determined. BAS-140 is a laboratory standard.

**Table T4.** Composition of basic media for methanogens and other H<sub>2</sub>-oxidizers (per liter).

Component	Methanogens	Other H <sub>2</sub> -oxidizers
NaCl	20 g	20 g
K <sub>2</sub> HPO <sub>4</sub>	0.09 g	0.09 g
KH <sub>2</sub> PO <sub>4</sub>	0.07 g	0.07 g
CaCl <sub>2</sub>	0.8 g	0.8 g
MgSO <sub>4</sub> ·7H <sub>2</sub> O	6 g	3.4 g
MgCl <sub>2</sub> ·6H <sub>2</sub> O	1 g	4.2 g
KCl	0.33 g	0.33 g
FeSO <sub>4</sub>	0.05 g	0.02 g
Fe(NH <sub>4</sub> ) <sub>2</sub> (SO <sub>4</sub> ) <sub>2</sub> ·6H <sub>2</sub> O	0.01 g	—
NiCl <sub>2</sub> ·6H <sub>2</sub> O	5 mg	0.5 mg
Na <sub>2</sub> SeO <sub>3</sub> ·5H <sub>2</sub> O	5 mg	0.5 mg
Na <sub>2</sub> WO <sub>4</sub> ·2H <sub>2</sub> O	2 mg	0.5 mg
Trace mineral solution	10 mL	10 mL
Marine trace elements solution	30 mL	—

— = not applicable.

**Table T5.** Downhole measurements made by wireline tool strings, Expedition 336.

Tool string	Tool	Measurement	Sampling interval** (cm)	Approximate vertical resolution (cm)
Microbiology combo (Hole 395A)	LEH-MT*	Temperature	15	NA
	EDTC*	Total gamma ray	5 and 15	30
	HNGS*	Spectral gamma ray	15	51
	MTT	Borehole fluid temperature	15	NA
	DEBI-t	Biomass	0.15	NA
Adapted microbiology combo I (Hole U1382A)	LEH-MT*	Temperature	15	NA
	EDTC*	Total gamma ray	5 and 15	30
	HLDS*	Bulk density	2.5 and 15	38/46
	HRLA	Resistivity	15	30
	DEBI-t	Biomass	0.15	NA
FMS-HNGS (Hole U1382A)	LEH-QT*	Temperature	15	NA
	EDTC*	Total gamma ray	5 and 15	30
	HNGS*	Spectral gamma ray	15	51
	GPIT*	Tool orientation	0.25 and 15	NA
	FMS*	Microresistivity imaging	0.25	0.5
Adapted microbiology combo II (Hole U1383C)	LEH-QT*	Temperature	15	NA
	EDTC*	Total gamma ray	5 and 15	30
	HNGS*	Spectral gamma ray	15	51
	HLDS*	Bulk density	2.5 and 15	38/46
	DEBI	Biomass	0.15	NA
FMS-sonic* (Hole U1383C)	LEH-QT*	Temperature	15	NA
	EDTC*	Total gamma ray	5 and 15	30
	HNGS*	Spectral gamma ray	15	51
	DSI*	Acoustic velocity	15	107
	GPIT*	Tool orientation	0.25 and 15	NA
	FMS*	Microresistivity imaging	0.25	0.5

\* = all tool and tool string names are trademarks of Schlumberger. \*\* = Sampling interval based on optimal logging speed. For definitions and tool acronyms, see Table T6.

Table T6. Acronyms and units used for downhole wireline tools and measurements.

Tool	Output	Explanation	Unit
DEBI-t		Deep Exploration Biosphere Investigative tool	
	Ax, Ay, Az	Acceleration (three orthogonal components)	m/s <sup>2</sup>
	ADC	Analog-to-digital converted voltage of the detectors	counts
	TEMP	Internal tool temperature	°C
	VIDEO	Optical video (of borehole wall)	
DSI		Dipole Shear Sonic Imager	
	DTCO	Compressional wave delay time ( $\Delta_t$ )	ms/ft
	DTSM	Shear wave delay time ( $\Delta_t$ )	ms/ft
	DTST	Stoneley wave delay time ( $\Delta_t$ )	ms/ft
EDTC		Enhanced Digital Telemetry Cartridge	
	GR	Total gamma ray	gAPI
	ECGR	Environmentally corrected gamma ray	gAPI
	EHGR	High-resolution environmentally corrected gamma ray	gAPI
	MTEM	Borehole fluid temperature	°C
FMS		Formation MicroScanner	
	C1, C2	Orthogonal hole diameters	inch
	P1AZ	Pad 1 azimuth Spatially oriented resistivity images of borehole wall	degrees
GPIT		General Purpose Inclinometry Tool	
	DEVI	Hole deviation	degrees
	HAZI	Hole azimuth	degrees
	Fx, Fy, Fz	Earth's magnetic field (three orthogonal components)	Oe
	Ax, Ay, Az	Acceleration (three orthogonal components)	m/s <sup>2</sup>
HLDS		Hostile Environment Litho-Density Sonde	
	RHOM	Bulk density	g/cm <sup>3</sup>
	PEFL	Photoelectric effect	b/e <sup>-</sup>
	LCAL	Caliper (measure of borehole diameter)	inch
	DRH	Bulk density correction	g/cm <sup>3</sup>
HNCS		Hostile Environment Gamma Ray Sonde	
	HSGR	Standard (total) gamma ray	gAPI
	HCGR	Computed gamma ray (HSGR minus uranium contribution)	gAPI
	HFK	Potassium (K)	wt%
	HTHO	Thorium (Th)	ppm
	HURA	Uranium (U)	ppm
HRLA		High-Resolution Laterolog Array	
	RLAXXX	Apparent resistivity from computed focusing mode XXX	$\Omega$ m
	RT	True resistivity	$\Omega$ m
	MRES	Borehole fluid resistivity	$\Omega$ m
LEH-MT		Logging equipment head-mud temperature	
	MTEM	Borehole fluid temperature	°C
	TENS	Cablehead tension	lbf
LEH-QT		Logging environment head-q tension	
	TENS	Cablehead tension	lbf
MTT		Modular Temperature tool	
	WTPE	Borehole fluid temperature	°C

**Table T7.** Specifications for the Deep Exploration Biosphere Investigative tool (DEBI-t).

Item	Specification
Temperature rating (°C)	Up to 50
Pressure rating (psi)	10,000
Power requirements	24 VDC, 2A
Length (inches)	94
Weight (kg)	
Air	53.5
Internal components	6
Submerged	44.5
Detectors	
Type	Photomultiplier tubes (PMTs)
Number	7
Excitation source	224 nm HeAg laser (Photon Systems, Inc.)
Laser spot size	1 mm from instrument - 2 mm $\varnothing$
Video	High-definition pin-hole camera with micro-SD card capable of recording up to 8 h of continuous video
Maximum logging speed	275 m/h (900 ft/h)
Resolution at maximum logging speed	Data point every 15 mm
Sampling rate (Hz)	4
Cablehead connection	Schlumberger type